Antifouling and Smart Polymeric Ultrafiltration Membranes for Environmental and Biological Separations

Thesis submitted in partial fulfillment of the requirements

for the degree of

DOCTOR OF PHILOSOPHY

by

Randeep Singh

Roll No: 136107020

Department of Chemical Engineering

Indian Institute of Technology Guwahati

Guwahati-781039, India

Antifouling and Smart Polymeric Ultrafiltration Membranes for Environmental and Biological Separations

Randeep Singh

Dedicated to my Family,

Especially my Mother

Department of Chemical Engineering
Indian Institute of Technology Guwahati
Guwahati 781039, India

CERTIFICATE

It is certified that the work contained in the thesis entitled "**Antifouling and smart polymeric ultrafiltration membranes for environmental and biological separations**", by **Randeep Singh**, has been carried out under my supervision. The work documented in this thesis has not been submitted to any other University or Institute for the award of any degree or diploma.

Dr. Mihir Kumar Purkait

Professor

Department of Chemical Engineering

Indian Institute of Technology Guwahati

Guwahati 781039, India

Date:

Acknowledgements

First and foremost, I would like to express my gratitude to my thesis supervisor **Prof. Mihir Kumar Purkait** for his continuous guidance, help, support, and freedom he provided to me throughout this course. I am lucky enough to have such a down to earth, amicable, and humble person as my thesis supervisor with a great zeal and expertise in research. His trademark sessions regarding the planning and execution of this course were always marvellous and fruitful. The whole experience with **Prof. Purkait** was remarkable and his persona never let me feel the pressure of this course. The extent of freedom given by him in the course was incredible, which let me grow as a researcher. I highly appreciate his efforts and energy he put in this course and thank him for his omnipresence throughout this course. I am going to admire his persona throughout my career.

I am also thankful to my doctoral committee members, **Prof. Chandan Das**, **Prof. Subrata K. Majumder**, and **Prof. Pranab K. Ghosh** (Department of Civil Engineering) for their valuable remarks and contributions towards the research work. Their suggestions helped in the improvement of the research work. Furthermore, I feel very fortunate to have such a marvellous doctoral committee consisting of experienced and enthusiastic professors. Their interactions with me were always very harmonious and made me feel very close to them, which really boosted my confidence and interest in the course.

I must thank to the H.O.D and faculty members of the Department of Chemical Engineering for their encouragement and help at various stages during my stay in this department. In this regard, I would specially like to mention the name of **Prof. Vijay S. Moholkar**, **Prof. Pallab Ghosh, Prof. Kaustubha Mohanty**, **and Prof. G. Pugazhenthi**.

I must also thank to all the technical staffs of Department of Chemical Engineering, specially, **Mr. Lukumoni Borah**, **Mr. Debajit Borah**, and the Scientific Officers. The experimental works presented in this thesis would never have been possible without the help

of these proficient technicians. I am also very thankful to **Dr. Sidananda Sarma** (Scientific Officer, Department of Physics), who helped me in DRS and XRD analysis of my samples along with other benevolent and humanitarian works, we did together. I am also very grateful for the help and support provided by the Chemical Engineering Department Office and its staff, especially, **Mr. Sailen Das**, **Mr. Deep Jyoti Sinha**, **Mr. Bhagya Boro**, and **Mr. Jyotish** throughout my course.

I am thankful to the **Central Instruments Facility (commonly known as CIF)** of IIT Guwahati for allowing me to carry out characterizations of my samples with different characterization techniques available at the Centre, especially the **Field Emission Scanning Electron Microscopy** (FESEM) for which I was the operator throughout the course. I am grateful to the **CIF** Scientific Officers, especially **Dr. Kula Kamal Senapati** for providing me with the required suggestions and freedom for FESEM analysis of my samples. I also acknowledge the help provided by **Mr. Madhurjya Borah** and **Dr. Kh. Kesho Singh** throughout the course.

The suggestions and support provided by my seniors is also something which helped me to sail across the course. In this regard, I must thank **Dr. Manish Kumar Sinha** who played a crucial role in my course. His excellent advices and constructive criticism helped my research a lot. I owe a debt of gratitude to him for his constant presence in my life. I also thank **Dr. Snigdha Khuntia** Ma'm, **Mr. Supriyo Mondal**, **Dr. Jyoti Kumar Doley**, **Dr. Suman Saha**, **Dr. Vikranth Volli**, **Dr. V. Shyam K. Yadav**, **Dr. Saptak Rarotra**, and **Dr. Himadri Sahu** for their suggestions and support during the course. I also thank my lab juniors **Mr. Ravi Bhandari** and **Mr. Lokesh Lohani** for their help and support during the course.

The colleagues who require special mentions are **Mr. Babul Prasad**, **Mr. Atanu**, **Dr. Kibrom Alebel Gebru**, **Mr. Abdisa Jabesa**, **Dr. Melaku Tesfaye**, **Dr. Ali Shemsedin Reshad**, **Mr. Shailesh Varade**, **Mr. Pankaj Jha**, **Dr. Anand Bharti**, **Dr. Maneesh Poddar**,

Mr. Tusharkanta Sahu(Chemistry), **Mr. Suhaib Alam Ansari** (Chemistry), **Mr. Adil Rathar** (Chemistry), **Mr. Ardhendu** (Civil), **Dr. Vinay Kulkarni** (Civil), and **Mr. Anil Kumar**, **Mr. Anil Bidkar**, **Mr. Muthu**, **Mr. Krishna**, **Mr. Arun** and **Mr. Vicky** from BSBE department.

I am also very fortunate to have a bunch of colleagues who became outstanding friends cum brothers around me during the course, namely **Narendren soundararajan**, **Vinoth Kumar Raja**, **Md. Adil Afroz**, **Kamal Kumar Paul**, and, **Md. Shaad Ansari**. Their presence and cooperation comforted me in many ways. I could never have achieved my goal without their help and support. They always helped and encouraged me to be strong enough to surpass all my difficulties, conquests, and uncertainties. Their support, suggestions, and concern made my stay jovial at IITG.

I also thank my hostel friends, namely **Ali Bhai**, **Safikul**, **Sultan**, **Bajrangi**, **Gautam**, **Manoj Chettri**, **Anil**, **Michael**, **Raja**, and **Bahadur** who all made my hostel life easy, enriching, and joyful.

I would also thank **Dr. Kumar Pallav**, **Dr. Amrita Ranjan**, **Dr. T. Sivasankar**, **Dr. Machiavelli Singh**, and **Dr. Amit Jaiswal** for their love and guidance throughout the course.

Also, I would like to give my appreciation and love to my cousins, namely **Rajeev Bhatia**, **Soni**, **Vikas Bhatia**, **Mohit Bhatia**, **Gaurav Bhatia** and my friends **Mr. Ajay Singh Chauhan, Mr. Abhishek Jain,** and **Mr. Narender Sharma**.

Last but not the least, I would like to thank my father **JWO. Karnail Singh Chaudhary (IAF)**, my mother, **Smt. Kamlesh Chaudhary**, my sisters, **Ms. Anju Chaudhary** and **Ms. Rita Chaudhary** for supporting me to do my PhD with confidence. I am grateful to my parents, especially my mother that they stood firmly with me throughout this course. Also, I really appreciate the role played my sisters in my absence at home. I will be indebted to them throughout my life for their contributions and protagonist behaviour. The love, affection,

blessings, and sacrifices of my family made me stronger to overcome my huddles and achieve my target.

I have no words to thank **Kheda Badshah**, **Mata Bala Sundari**, **Maa Kamakhya Devi, Bhole Baba, Jahar Veer Googa Peer**, and **Laala Wala Peer**, the core of my strength and wisdom.

"नभः स्पृशं दीप्तम्"

Abstract

The main objective of this work is to prepare asymmetric polymeric membranes with antifouling properties with environmental and biological applications. In general, there are three well known methods that can be used to prepare antifouling membranes, first by increasing the hydrophilicity of membrane surface, second by electrostatic repulsion, and third by steric repulsion. This work taken into account of these methods and prepared modified polymeric membranes by using different types of additives. All the additives used in this thesis, helps in increasing the hydrophilicity of the modified membranes compared to nascent membranes. Additionally, synthesized additive poly(N-vinylcaprolactam-TiO_2-acrylic acid) (VCL-TiO_2-AA) provides the electrostatic repulsive property to the modified membranes and provides steric repulsion to the membrane surface. Phase inversion method was used for the synthesis of all of the membranes. Also, in all of the membranes polyethylene glycol (PEG) and N-methyl-2-pyrrolidone (NMP) were used as pore former and solvent, respectively.

First of all flat sheet antifouling and hydrophilic asymmetric polymeric membranes were prepared from homogeneous solution of polysulfone (PSF). The effects of the additive poly(2-acrylamido-2-methyl-1-propanesulfonic acid) (AMPS) on membrane properties were examined. Different wt % of AMPS was used to prepare polysulfone membranes by phase inversion method. The role of AMPS on the porosity, pore size distribution, hydrophilicity, and antifouling nature was investigated and analysed in detail using a batch cell of 350 mL capacity. Aqueous solutions of bovine serum albumin (BSA) and humic acid (HA) were used to study the protein separation performance of the membranes. Characterization techniques like FESEM, AFM, and imageJ software were used to characterize the morphology of prepared membranes. There is positive effect of the additive addition on all the membrane parameters like Pure water flux (101.76 L/m^2 h (MR0) to 464.06 L/m^2 h (MR4)), hydraulic permeability (0.65 L/m^2 h kPa (MR0) to 2.01 L/m^2 h kPa (MR4)), equilibrium water content (21.74 % (MR0)

to 71.45 % (MR4)), and porosity (0.024 (MR0) to 0.58 (MR4)). Response surface methodology was used for the optimization of BSA flux and rejection. The results of the morphological as well as permeation studies depicted that permeate flux and antifouling nature were increased with the amount of AMPS present in the membrane matrix. The antifouling study of the prepared membranes was undertaken by using bovine serum albumin (BSA) solution of 1000 mgL^{-1}. Positive results were seen with the increase in amount of AMPS, since, the total membrane resistance has been decreased from 0.95 (MR0) to 0.74 (MR4). Separation of humic acid (HA) from aqueous medium was also performed with the best performing membrane (MR4, having the highest amount of AMPS). Separation efficiency of 100% and 94% were obtained using 10 mgL^{-1} and 50 mgL^{-1} of HA.

Subsequently, keeping hydrophilicity as the key factor for anti-fouling nature of the polymeric membranes, flat sheet asymmetric polymeric membranes were prepared from homogeneous solution of PVDF-co-HFP (Poly(vinylidene fluoride-co-hexafluoropropylene)) flat sheet membranes were prepared by using methoxy poly(ethylene glycol) (mPEG) of three different molecular weights (550 Da, 2000 Da, and 5000 Da) to improve hydrophilicity and antifouling characteristics of the membranes. The improvements in the membrane attributes were studied under two categories viz. morphological and permeation. Field emission scanning electron microscopy (FESEM) and atomic force microscopy (AFM) were used to study the morphological properties of the prepared membranes. Presence and stability of the additive (mPEG) in the prepared membranes were confirmed by using the Fourier transform infrared spectroscopy (FTIR). Permeation studies of the prepared membranes were done in the form of pure water flux (PWF) and hydraulic permeability (P_m). Equilibrium water content (EWC) and static water contact angle of the prepared membranes were calculated to analyse the increase in hydrophilicity of the prepared membranes. Antifouling studies on the prepared membranes were done by using bovine serum albumin (BSA) and humic acid (HA) as model protein and

foulant, respectively. The modified PVDF-co-HFP membranes have shown a 50% increase in the PWF with an increase in the molecular weight of mPEG from 550 Da to 5000 Da. The increase in hydrophilicity and antifouling nature leads to an increased EWC, from 36.17 to 62.62. The water contact angle also decreases from 71.32° to 59.45° with an increase in the molecular weight of mPEG. Antifouling study with BSA and HA further confirms the increased antifouling nature of the prepared membranes, due to the presence of mPEG in the membranes. The proof of the same is presented in the form of flux recovery ratio, which increases from 73.07 to 87.47. The prepared membranes have shown good rejection profiles for both BSA and HA at 95% and 99%, respectively.

Further, novel flyash carbon nanotubes (CNTs) modified polysulfone (PSF) ultrafiltration membranes with antifouing nature were prepared. The flyash CNTs were synthesized and directly blended in the membrane casting solution to prepare the asymmetric membranes by phase inversion method. The membranes were characterized in terms of pure water flux (PWF), hydraulic permeability and hydrophilicity. The PWF of the membranes decreases with the addition of the additive, for example it is highest for membrane CM_0 at 473.90 L/m^2h and least for membrane CM_5 at 111.84 L/m^2h. However, water contact angle decreased from 76˚ (CM_0) to 58˚ (CM_9) with the addition of the additive in the membranes. Additionally, a significant increase in BSA flux and decrease in membrane fouling was observed in the membranes.

Also, asymmetric mixed matrix PSF membranes with photocatalytic properties were synthesized by using Cu_2O photocatalyst, which was synthesized by using electrodeposition method. Characterization techniques, such as XRD, FTIR, FESEM, FESEM-EDX, and AFM were used to characterize the photocatalyst and blended membranes so as to analyse their structural and functional attributes. Further, the membranes were analysed by using permeation techniques to analyse their flux profiles. Similarly, antifouling nature and hydrophilicity of the

membranes were studied by permeating aqueous BSA solutions and measuring the static water contact angle (SWCA), respectively. The pharmaceutical removal studies were carried out using ibuprofen (IBP). The additive improves the membrane attributes, such as flux improved from 34.24 Lm^{-2} h^{-1} to 179.54 Lm^{-2} h^{-1} deciphering improved porosity and pore size distribution; SWCA decreased from 71.5° to 45.3° showing increase in the hydrophilicity of the membranes; BSA adsorption decreased from 56 μg cm^{-2} to 27 μg cm^{-2}; and successful removal of IBP at 86% was achieved under visible light conditions with a removal rate of 32.63×10^{-3} min^{-1}.

Lastly, stimuli responsive pH and thermo-responsive mixed matrix polysulfone ultrafiltration membrane for photocatalytic dye removal were prepared. Stimuli responsive VCL-TiO_2-AA polymer nanocomposite was synthesized and directly blended to the membrane casting solutions. The stimuli responsive polymer nanocomposite makes the membrane antifouling, pH and thermos-responsive, and photocatalytic in nature. The membranes were characterized by using various standard characterization techniques, such as FESEM, FESEM-EDX, FTIR, Furthermore, the effect of the synthesized stimuli responsive VCL-TiO_2-AA polymer nanocomposite was analysed on the membrane performance in terms of fouling, temperature and pH responsiveness, and photocatalytic removal of MB dye under dark and UV light conditions at different pH values. Improvements were seen in the PWF and P_m of the membranes as the PWF changes from 214.54 L/m^2 h (RM0) to 597.78 L/m^2 h (RM34) and P_m of the modified membranes changes from 0.88 L/m^2 h kPa (RM0) to 2.49 L/m^2 h kPa (RM34). Also, the modified membranes indicates both pH and temperature sensitivity compared to nascent membrane. Similar to other modified membranes, membrane RM34 shows significant change in the PWF from 133.50 to 197.59 L/m^2 h on change in pH from 11 to 2. Similarly, like other modified membranes membrane RM34 shows increase in PWF from 167.07 L/m^2 h to 199.59 L/m^2 h with temperature change from 25°C to 40°C.

Research Publications

Books:

- M. K. Purkait and **R. Singh**, Membrane technology in separation science, first edition, CRC Press, 2017-18 (ISBN 9781138626263).
- M. K. Purkait, M. K. Sinha, P. Mondal, and **R. Singh**, Stimuli responsive polymeric membranes: smart polymeric membranes, first edition, Elsevier, 2018 (ISBN 9780128139622).
- M. K. Purkait and **R. Singh**, Thermal induced membrane separation processes, Elsevier, (**Under preparation**).

Book chapters:

- **R. Singh** and M. K. Purkait, Chapter: Microfiltration membranes, Book: Membrane separation principles and applications, first edition, Elsevier, 2019, Chapter 4, Pages 111-146 (ISBN: 9780128128152).
- B. K. Nandi, M. Rahaman, **R. Singh**, and M. K. Purkait, Chapter: Microfiltration membranes fabrication and application, Book: Membrane technology an approach towards sustainable solutions in water, health, energy and the environment, first edition, CRC Press, 2018, Chapter 9, Pages 190-209 (ISBN: 9781138095427).

Journal articles:

1. **R. Singh**, V.S.K. Yadav, and M. K. Purkait, Cu_2O photocatalyst modified antifouling polysulfone mixed matrix membrane for ultrafiltration of protein and visible light driven photocatalytic pharmaceutical removal, Separation and Purification Technology 212 (2019) 191–204.

2. **R. Singh** and M. K. Purkait, Role of poly(2-acrylamido-2-methyl-1-propanesulfonic acid) in the modification of polysulfone membranes for ultrafiltration, Journal of Applied Polymer Science 2017 (DOI: 10.1002/App.45290).
3. **R. Singh** and M. K. Purkait, Evaluation of mPEG effect on the hydrophilicity and antifouling nature of the PVDF-co-HFP flat sheet polymeric membranes for humic acid removal, Journal of Water Process Engineering 14 (2016) 9–18.
4. A. Dey, **R. Singh**, and M. K. Purkait, Cobalt ferrite nanoparticles aggregated schwertmannite: a novel adsorbent for the efficient removal of arsenic, Journal of Water Process Engineering 3 (2014) 1–9.
5. **R. Singh** and M. K. Purkait, Fly ash based carbon nanotubes modified hydrophilic and antifouling ultrafiltration polysulfone membranes, (**Under preparation**).
6. **R. Singh**, M. K. Sinha, and M. K. Purkait, pH and thermo-responsive mixed matrix polysulfone ultrafiltration membrane for photocatalytic dye removal, (**Under preparation**).

International conferences:

1. M. K. Purkait and **R. Singh**, Fouling free hydrophilic polysulfone ultrafiltration membranes, (AIChE Annual Meeting, 2018), 28 October-02 November, 2018, David L. Lawrence Convention Center, Pittsburgh, USA.
2. **R. Singh** and M. K. Purkait, Thermoresponsive nanocomposite modified hydrophilic and antifouling polymeric ultrafiltration membranes, (ICSIMR-2017), 30 June-01 July, 2017, IIT Guwahati.
3. **R. Singh** and M. K. Purkait, Polymer nanocomposite modified polysulfone ultrafiltration membranes with enhanced hydrophilicity and antifouling properties, (ICETNMST-2017), 04-06 January, 2017, NIT Nagaland.

4. **R. Singh** and M. K. Purkait, Polymer nanocomposite based hydrophilic and antifouling polysulfone ultrafiltration membranes, (CHEMCON-2016), 27-30 December, 2016, Anna University, IIT Madras, CLRI Chennai.
5. **R. Singh** and M. K. Purkait, Preparation, characterization and analysis of fouling mechanisms for blended PSF and PVDF-co-HFP ultrafiltration membranes, (CHEMCON-2016), 27-30 December, 2016, Anna University, IIT Madras, CLRI Chennai.
6. **R. Singh** and M. K. Purkait, Promising low fouling PVDF-co-HFP ultrafiltration membranes for water treatment, (FCASI-2016), 25-26 April, 2016, University of Rajasthan.
7. **R. Singh** and M. K. Purkait, Novel antifouling and hydrophilic ultrafiltration membrane for humic acid removal, (RECYCLE-2016), 01-02 April, 2016, IIT Guwahati.
8. **R. Singh** and M. K. Purkait, Effect of mPEG on PVDF-HFP membranes hydrophilicity and antifouling properties, (CHEMCON-2015), 27-30 December, 2015, IIT Guwahati.
9. **R. Singh** and M. K. Purkait, Modified PSF membranes with increased hydrophilicity and antifouling properties, (CHEMCON-2015), 27-30 December, 2015, IIT Guwahati.
10. **R. Singh**, L. Lohani and M. K. Purkait, Preparation of fly ash based mixed matrix ultrafiltration membrane using polysulfone as base polymer, (ISC-2015), 08-09 December, 2015, Tribhuvan University, Kathmandu, Nepal. (**Young Scientist Award**)
11. S. Saravanan, **R. Singh**, and T. Sivasankar, Degradation of Basic Blue 3 dye by using novel Fenton's reagent in assistance with Ultrasound, International Conference on Recent Advancements in Chemical, Environmental and Energy Engineering (RACEEE-14), February 27-28, 2014, SSN College of Engineering, Chennai, (India).

12. **R. Singh** and T. Sivasankar, Ultrasound assisted adsorptive removal of Reactive Black 5 dye using activated carbon prepared from Mangosteen fruit peel, Bright International Conference and Events (BIOFEST 2012), December 12-13, 2012, Hyderabad, (India).

National conferences:

1. **R. Singh** and M. K. Purkait, TiO_2-AMPS nanocomposite based hydrophilic and antibacterial polysulfone ultrafiltration membranes, Research Conclave, 08-11 March, 2018, IIT Guwahati (**Best Poster Award).**
2. **R. Singh** and M. K. Purkait, TiO_2-AMPS nanocomposite based PSF mixed matrix ultrafiltration membranes with better flux and rejection profiles, Research Conclave, 16-19 March, 2017, IIT Guwahati.
3. **R. Singh** and M. K. Purkait, Polymer nanocomposite based low fouling polysulfone mixed matrix membranes, (ACEE'16), 22-23 April, 2016, NIT Jalandhar.

Symposium:

1. **R. Singh** and M. K. Purkait, Modified flat sheet polymeric membranes for humic acid removal, (RAER-2017), 05 June, 2017, IIT Guwahati.
2. **R. Singh** and M. K. Purkait, Role of a high molecular weight hydrophilic additive in the betterment of hydrophilicity, antifouling and flux profiles of a polymeric membrane, 24-26 March, 2017, IIT Guwahati.

CONTENTS

CONTENTS

LIST OF FIGURES

LIST OF FIGURES

LIST OF TABLES

Nomenclature

Notations

A	effective membrane area
A_t	total area
C_f	concentration in the feed
C_p	concentration in permeate
J_{HA}/F_{HA}	HA aqueous solution flux
F_{ir}	irreversible fouling
F_r	reversible fouling
F_t	total fouling
h	hour
J_p	BSA aqueous solution flux
J_w	pure water flux
$J_{w1}/ J_1/ F_{W1}$	initial water flux
$J_{w2}/ J_2/ F_{W2}$	water flux in second run
L	length of pore in equations
P	pressure
P_m	hydraulic permeability
ΔP	transmembrane pressure in equations
Q	volume of water permeated
r	radius of pores
r_m	mean pore radius
V	volume of membrane in wet state
W_d	weight of dry membrane
W_w	weight of wet membrane

ε	porosity

Abbreviations

AA	poly(acrylic acid)
ATR	attenuated total reflectance
BSA	bovine serum albumin
CF	compaction factor
Da	Dalton
EWC	equilibrium water content
FESEM	field emission scanning electron microscope
FTIR	Fourier transform infrared spectroscopy
HA	humic acid
HD	1, 6-hexanediol
IP	isoelectric point
LCST	lower critical solution temperature
LLDP	liquid-liquid displacement porosimetry
MBAA	N,N′-methylenebisacrylamide
NMP	N-methyl-2-pyrrolidone
PEG	polyethylene glycol
mPEG	methoxy poly ethylene glycol
VCL	poly(N-vinyl caprolactam)
PVDF-co-HFP	poly(vinylidene fluoride-*co*-hexafluoropropylene)
PWF	pure water flux
UF	ultrafiltration
SWCA	static water contact angle

Chapter 1
Introduction to membranes

This chapter is dedicated to the introduction of the field of membranes and gives detailed insight about the field of membrane science, covering parts from membranes history to recent developments, significant membrane materials, and various membrane fouling mechanisms. The chapter also covers the state-of-the art in polymeric membranes, their applications, and the background of the problem chosen for this work, specifically, the problem of polymeric membrane fouling. Also, it discusses the different methods to abstain fouling. Further, the chapter comprises of the literature review that explains the basis of two major problems associated with polymeric membranes in applications, i.e., membrane fouling and membrane wetting. Moreover, the hydrophilic and antifouling modification methods are comprehended extensively towards the end of the chapter. Lastly, the objectives of the present work are highlighted.

1.1. An overview of separation processes

The word membrane is derived from the Latin word membrana, which means "skin." Membrane is a sort of barrier that separates things and allows materials to be passed selectively [1]. There are many definitions available for a membrane. A general definition could be: A membrane is a thin barrier, placed between two phases, or mediums, which allow one or more constituents to selectively pass from one medium to the other in the presence of an appropriate driving force while retaining the rest [2]. This definition is based on a macroscopic level, but it should be taken care that the separation is at the microscopic level. Accordingly, it can be said that a membrane process is a combination of both mass and momentum transfer. A membrane can be homogeneous or heterogeneous, symmetric or asymmetric, solid or liquid; it can carry a positive or negative charge or be neutral or

bipolar. Transport through a membrane can be affected by convection or by diffusion of individual molecules, induced by an electric field or concentration, pressure, or temperature gradient. The membrane thickness may vary from as small as 100 microns to several millimetres.

Membranes and membrane processes were first introduced as an analytical tool in chemical and biomedical laboratories. However, their industrial importance increased quite rapidly with significant technical and commercial impact [3]. Membranes now find wide applications in the food/beverage industry; in desalination processes; in the medical industry for the purification of body fluids, antibiotics, and so on; and in separation of industrial effluents, among other processes. This increase in the use of membranes in industry has been attributed to the various advantages associated with membrane processes, such as good product quality, better energy efficiency than conventional separation methods, simple operation, no chemical alteration of constituents, easy scale up, and better environment suitability. Although the rise in membrane usage has been observed only recently, the membrane phenomenon has been long studied. However, there are major drawbacks associated with membrane separation processes because of membrane fouling and concentration polarization, namely low membrane life time and low selectivity or flux.

Procedures are explored and applied to membranes for reducing membrane fouling and concentration polarization, so that the limitations cold be avoided. Nowadays, membrane technology is successfully applied and used for various applications in different industries, such as food and beverages, metallurgy, pulp and paper, textile, pharmaceutical, automotive, dairy, biotechnology, chemical industries, etc. [3].

1.1.1. Principle of membrane separation

There exists different mechanisms of separation for different membranes; membranes can also be classified based on the mechanisms. Porous membranes separate the feed from permeate on the basis of size and nonporous membranes on the basis of affinities between the feed components and membrane materials. The physical and chemical interactions between the feed components and membrane material also control the rate of mass transfer, that is, the flux in common terms. In general, the membrane flux can be given as

$$\text{Flux} = \frac{\text{Membrane permeability}}{\text{Membrane thickness}} \times \text{Driving force} \qquad (1.1)$$

Expression 1.1 shows that the membrane flux is proportional to the membrane permeability and driving force. The driving force differs for different membrane processes. It can be pressure, concentration, chemical, electrical, or thermal potential. The membrane flux is inversely proportional to the membrane thickness, which means the lesser the membrane thickness, the higher will be the membrane flux, and vice versa. Further, the membrane transport can be of three types, namely, passive, active, and facilitated or carrier mediated. In a passive system, the transport will be totally under the influence of the driving force and is not energy intensive. The transport usually takes place from a higher potential region to a lower potential region. The transport takes place until equilibrium is reached between the feed and permeate side for the driving force to be neutral. Active transport is totally opposite to passive transport as it is an energy-intensive process. Active transport is energy intensive because here the transport is opposite to the conventional transport that requires energy. The transport will be from a lower potential to a higher potential, and to carry out transport in this way energy is required. The process like osmosis is an example of passive transport and, on the other hand, reverse osmosis is an example of active transport. Facilitated or carrier-mediated transport accomplishes transport with the help of a carrier

that interacts with the feed components and carries them across the membrane. The carrier works as a boat for passengers in a stream of water. Similar to a boat, it carries the feed components across the membrane and comes back again after dissociating the previously attached components to the feed side. The carrier undergoes no changes and can be retrieved after the completion of the membrane process. Facilitated or carrier-mediated transport is mainly used in liquid membrane processes.

In a membrane separation process, the membrane allows selective passage of feed components to the permeate side. The feed components passed through the membrane are known as permeates or filtrates, and the feed components that remain on the membrane surface are known as retentates or filtrates. Figure 1.1 shows the membrane separation process with process variables and entities clearly in two common configurations modes: (a) dead-end filtration and (b) cross-flow filtration.

Some of the common terminologies used in membrane separation processes are mentioned next.

Flux: The permeate flux of a membrane is a very important parameter. It can be defined as the permeate volume (or mass) through the membrane per unit of membrane area. The permeate flux or simply the flux, F, of a membrane is given by the general relation [1]

$$F = \frac{1}{A}\frac{dV}{dt} \qquad (1.2)$$

where

F = flux (L/m^{2}h); V = permeate volume (L); t = time (h); A = membrane area (m^2)

***TMP*:** The pressure difference between the feed side and permeate side across the membrane is known as the transmembrane pressure (TMP). The relationship between *J* and TMP can be given by modified form of Darcy's law as [4]:

$$F = \frac{\Delta P}{\mu R_t} \quad (1.3)$$

where

ΔP = pressure difference (kPa); μ = viscosity (kPa.s);

and R_t = total resistance (m^{-1})

Rejection: An important feature of a membrane is its rejection, which is a measure of membrane selectivity [1]. Selectivity can be expressed in terms of rejection (or retention), *R*, which expresses the extent to which a solute is retained by the membrane and is defined as:

$$R = 1 - \frac{C_p}{C_f} \quad (1.4)$$

where

R = retention; C_p = concentration in the permeate (mgL^{-1});

and C_f = concentration in the feed (mgL^{-1})

In case of total retention of the feed components by the membrane, the *R* will be unity.

1.1.2. Classification of membranes

In general, membranes are barriers which selectively separates two phases. There are different types of membranes available, they may be solid or liquid, charged or neutral, homogeneous (uniform in composition and structure) or heterogeneous (non-uniform mainly structure wise). Further, membranes can also be classified on the basis of their nature, structure, or mechanism of separation. Nature wise the membranes may be biological or synthetic, which further subdivided as living and non-living in case of biological membranes and organic (polymeric or liquid) and inorganic (ceramic or metal)

in case of synthetic membranes. On the basis of structure or morphology the membranes are categorized under two categories viz. symmetric (isotropic) and asymmetric (anisotropic). The symmetric membranes are divided into porous, non-porous (dense), and charged membranes. The symmetric membranes are firm with voided structures and interconnected pores. The size exclusion mechanism is apt to explain the separation mechanism of porous membranes. That means the feed components are separated on the basis of their size, microfiltration and ultrafiltration are the most common examples. On the other hand, non-porous membranes separates the feed components on the basis of diffusion driven by the driving force of pressure, concentration, thermal, or electrical potential gradient, for example, nanofiltration and gas separation. The separation efficiency of two or more feed components depends upon their transport rate through the membrane, which further depends upon their diffusivity and solubility in the membrane material, for instance, pervaporation. The charged membranes carries a fixed positive or negative charge and may be porous or non-porous. The separation is based on the diffusivity and selectivity of the ions across the membrane, such as, electrodialysis.

In case of asymmetric membranes there are two layers of membranes with different thickness, pore sizes and porosity. A dense top layer, also known as skin layer, with thickness of 0.1 - 0.5 µm is present on a porous sub-layer of thickness around 50 - 150 µm. The asymmetric membranes with its top and sub-layer can be prepared in a single step, like in phase separation method, or separately, like in coating method. The membrane layers when prepared with different polymers are known as composite membranes. Here, both the layers can be optimized individually. The function of the dense top layer is to provide selectivity to the membrane and the porous sub-layer to provide mechanical strength. This type of membranes are the most famous and well established commercially.

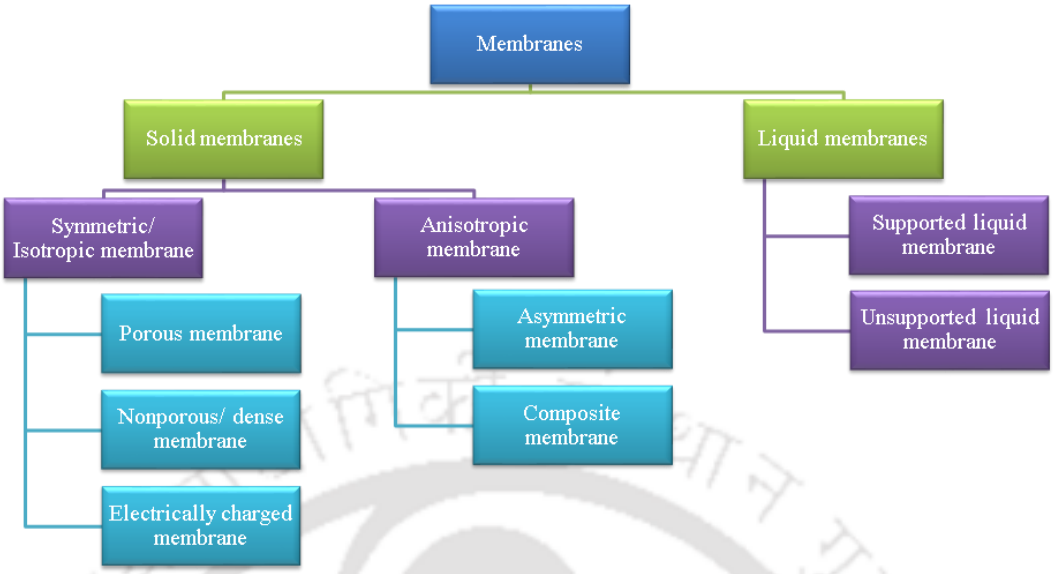

Figure 1.1. Membrane classifications according to morphology [5]

The liquid membranes are also of two type viz., supported liquid membranes and emulsion liquid membranes. In case of supported liquid membranes a porous structure is used as a support for the membrane phase (liquid). The membrane phase is supported by the porous structure in its pores. The porous structure provides the needed mechanical strength and the membrane phase the needed selectivity for the process. The separation process takes place under the influence of the concentration or chemical potential gradient from the feed phase to the permeate phase via the membrane phase, where the membrane phase acts like a connecting channel for the feed components. In case of emulsion liquid membranes, the membrane phase is stabilized with help of an emulsifier between the feed and permeate phase. Figure 1.1 presents the classification of membranes based on morphological aspects.

1.1.3. Classification of membrane separation processes

Membrane acts as a barrier between two phases and the filtration technique is called as separation process [1]. There are two parts of feed solution in separation process i.e. a) filtrate or permeate- which can easily pass through membrane and b) concentrate or

retentate – the portion that cannot pass through membrane. A simple schematic representation of a membrane process in two commonly used configurations, namely dead end filtration and cross flow filtration is shown in Figure 1.2.

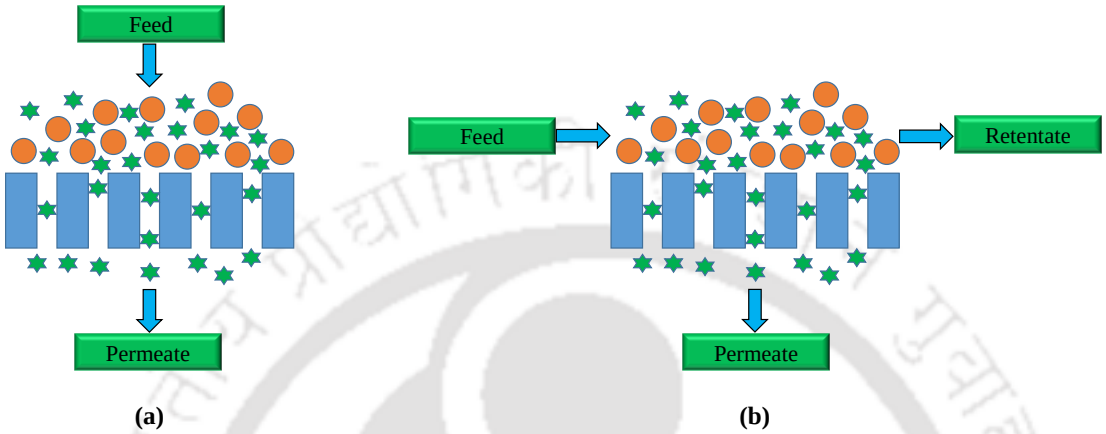

Figure 1.2. Schematics of a membrane process in two common configurations (a) Dead end, and (b) Cross flow [1]

The wide variety of membrane separation processes differ from one another in type and configuration of membrane; the mechanism of transport for various feed components; the nature of the process driving force; and pore sizes.

As a result of a driving force components are transported towards the membrane surface, where some components pass the membrane and others are retained at the membrane surface. Membrane processes are available for numerous applications, each with its own driving force and separation characteristics. Table 1.1 provides further information on these processes, such as membrane type, method of separation and range of applications.

Pressure driven membrane separation processes differ mainly in the pore size of their membranes, in which specific range of impurities can be removed only. In pressure driven membrane systems, due to the pressure of feed solution major portion of solution can pass through semi-permeable membrane.

- Reverse osmosis- Only iconic species can be removed because it has the smallest membrane pore size.
- Nanofiltration - It can remove divalent ions and low molecular weight contaminants whereas monovalent ions can pass through these membranes, sometimes these are referred to as 'loose reverse osmosis'
- Ultrafiltration- In this macromolecules such as proteins and small colloids can be removed easily, but allow ionic species to pass through.
- Microfiltration- It can remove particulates, bacteria, and other larger colloids.

Table 1.1: Distinctive membrane separation processes: Operating principles, driving force, and applications [1]

Separation process	Driving force	Separation mechanism	Range of application	Pre size (nm)
Micro filtration	Pressure difference (ΔP)	Sieving	Sterile filtration clarification	100-10000
Ultra filtration	Pressure difference (ΔP)	Sieving	Separation of macromolecular solutions	10-100
Nano filtration	Pressure difference (ΔP)	Solution diffusion	Separation of divalent ions from solutions	0.5-5
Reverse osmosis	Pressure difference (ΔP)	Solution diffusion	Separation of salts and micro solutes from solutions	<1
Dialysis	Concentration difference (ΔC)	Diffusion	Separation of salts and micro solutes from macro molecular solutions	<1
Electro dialysis	Electric potential difference (ΔE)	Selective transport of ions or molecules according to electric charge	Desalting of ionic solutions	<1

Supported liquid membrane	Concentration difference (ΔC)	Solution diffusion	Separation and concentration of metal ions and biological species	<1
Membrane distillation	Temperature difference (ΔT)	Vapor transport	Ultrapure water concentration of solutions	1-10
Pervaporatio	Concentration difference (ΔC)	Solution diffusion	Separation of organics	<1

Table 1.2 reports a summary of the main characteristics of the pressure driven processes in terms of pressure, pore size, and removable components.

Table 1.2: Characteristics of the pressure driven membrane processes [1]

Membrane processes	Transmembrane pressure (bar)	Pore size (nm)	Removable components
Microfiltration	1 - 2	100 - 1000	Bacteria, Suspended solids
Ultrafiltration	2 - 10	1 - 100	Proteins, Macromolecules, viruses
Nanofiltration	10 - 30	0.5 - 5	Bivalent ions, Micro pollutants,
Reverse osmosis	35 - 100	< 1	Monovalent ions, hardness

1.2. Materials for polymeric membranes

The most important and primarily used material for membranes is commercial thermoplastics and cellulose for large scale production. The class of material which is primarily famous for the preparation of membranes are the polymers due to their unique physical and chemical properties, such as supporting sub-structure, good mechanical

properties, reasonable degree of flexibility, good chemical resistance, tolerance limit of a wide pH range, and resistance to high chlorine concentrations (enabling rigorous cleaning). In addition, a high thermal resistance is required, so that membrane properties or life cannot be affected while using solutions with moderately elevated temperatures. Considering these parameters, polymeric material should be identified on the basis characteristics like molecular weight, chain flexibility, chain interaction, change in pH, change in temperature, density, melting point, glass transition temperature, and compressibility [2].

Recent advances in properties of non-cellulosic membrane are more durable, less susceptible to biodegradation and perform well within pH and temperature ranges as compared with the initial development of first asymmetric cellulose acetate membrane. The UF membrane are produced by phase inversion method by using materials such as cellulose acetate (CA), aromatic Polyamide (PA), polysulfone (PSF), polyethersulfone (PES), polyvinylidene fluoride (PVDF), polyacrylonitrile (PAN), polypropylene (PP), and polyethylene (PE) [6].

Figure 1.3 compares the common polymers in terms of strength and flexibility [2]. PES has similar mechanical properties to those of PSF. It shows that PSF and PVDF are the strongest polymers, whilst PVDF is more flexible. Of the polymers discussed above, the PSF/PES family has the widest chemical resistance, and can tolerate a pH range from 1.5 to 13, as well as moderate chlorine levels. PVDF tolerates acids, but is limited to pH 11 with caustic. However, its major advantage is a very high tolerance to chlorine, which makes it ideal for membrane reactors. Chlorine cleaning is preferred for PVDF membranes while PSF/PES may choose for caustic cleaning. PAN has similar pH tolerance to PVDF, combined with a moderate chlorine tolerance (almost similar to PSF/PES). CA is much more limited in its chemical resistance, since its natural hydrophilicity makes it susceptible

to hydrolysis in the presence of acids below pH 4 and alkalis above pH 8. It tolerates chlorine, but is biodegradable which makes it sensitive to bacterial attack. The polyolefin family, PP and PE, has good tolerance to acid and caustic, but low tolerance to chlorine, particularly in the case of PP. The lack of chlorine tolerance is a major limitation in the water industry, and this has limited the prospects for these membranes. Apart from this, solubility of PSF and PVDF makes them ideal candidate for polymer blend membranes since other polymer can be co-dissolved.

Presently, PSF and PVDF are widely used polymers because of their high chemical resistance, usability in a wide pH range, soluble in solvents like DMAc and NMP (making it easily applicable for the conventional phase inversion processes), high thermal stability, good mechanical strength and permeability, and ability to modify properties through blending with other polymers. These advantages make them preferred over other organic membrane materials [3].

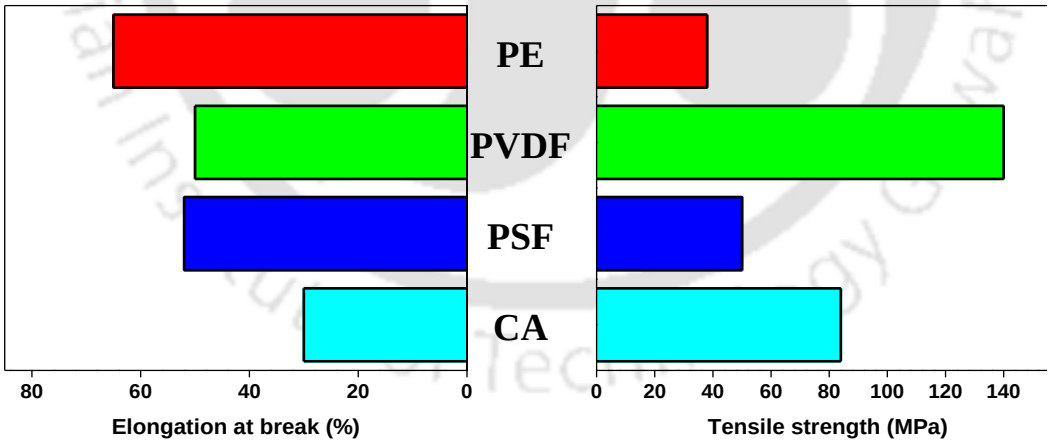

Figure 1.3. Comparison of physical stability of different membrane materials [5]

However, PSF and PVDF membrane exhibits drawback which can cause the adsorption and deposition of foulants (colloids, proteins, and particles) on inside the membrane pores and the surface of the membrane and it is mainly due to their hydrophobic nature and this leads to lower permeation flux and deterioration in performance. As to make

membranes more robust i.e. hydrophilic and less prone to fouling several methods are used such as surface coating by adsorption, free radical or radiation grafting of hydrophilic polymers, plasma treatment, chemical conversion of polymer side chains to hydrophilic groups, and the widely used is blending with hydrophilic polymers [3].

1.3. Membrane fouling

The biggest disadvantage of membrane processes is the phenomenon of concentration polarization and fouling. This is the consequence of the selective behaviour of the membranes as they allow specific feed components to pass through them and retain the remaining. This results in the accumulation of the retained feed components on the membrane surface in a mass transfer boundary layer. This accumulation of the feed components over the membrane surface gradually declines the membrane flux. The accumulated material give rise to a concentration gradient between the solution at the membrane surface and bulk, this results in the back transport by diffusion of the feed components accumulated over the membrane surface. This phenomenon is known as concentration polarization [1] and is shown in Fig. 1.4.

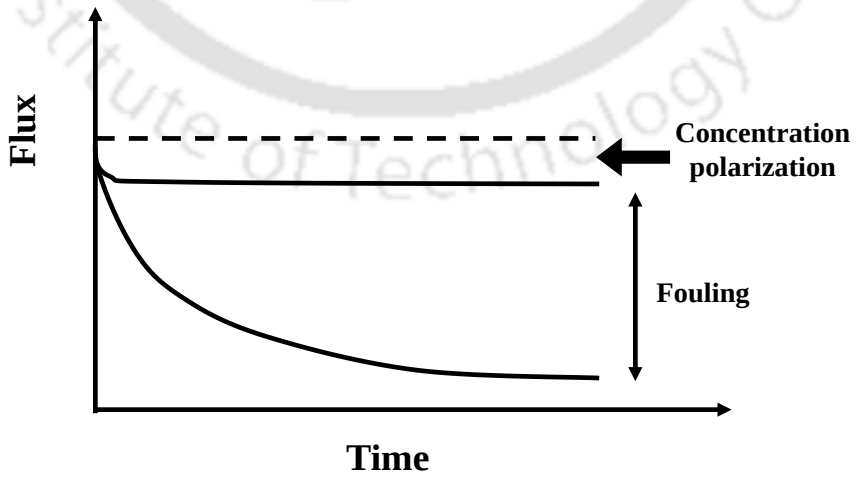

Figure 1.4. Schematic representation of the gradual decrease in membrane flux due to concentration polarization and fouling [1]

On the other hand fouling is the membrane phenomenon occurs due to the deposition of the retained feed components over the membrane surface or in the membrane pores. This results in the long term membrane flux decline and it depends upon the physicochemical nature of the membrane, feed, and system design. The common definition of membrane fouling is provided by the International Union for Pure and Applied Chemistry (IUPAC), which defined fouling as: '*Fouling is the process resulting in loss of performance of a membrane due to the deposition of suspended or dissolved substances on its external surfaces, at its pore openings, or within its pores*' [7]. The decrease in flux that is found during membrane filtration is schematically shown in Fig. 1.3.

1.4. Evaluation of membrane fouling

In general, flux of a membrane is taken as the measure of its performance. Therefore, any decline in flux means decline in the performance of a membrane. Thus, it is necessary to maintain an inclined flux over the period of a membrane process. In a membrane process, the first step towards membrane fouling are the pore plugging (R_p) and pore adsorption (R_a) resistances. These resistances arises either by the plugging of the feed components in the membrane pore, where the feed component size is equivalent to that of the membrane pore size or by the adsorption of the feed components in the membrane pores, where the membrane pore size is bigger than the feed component size. Afterwards, comes the continuous accumulation of feed components near the membrane surface. This is generally known as concentration polarization and represented as, R_{cp}, the resistance due to concentration polarization. This resistance reduces the mass transfer across the membrane and also reduces the membrane flux.

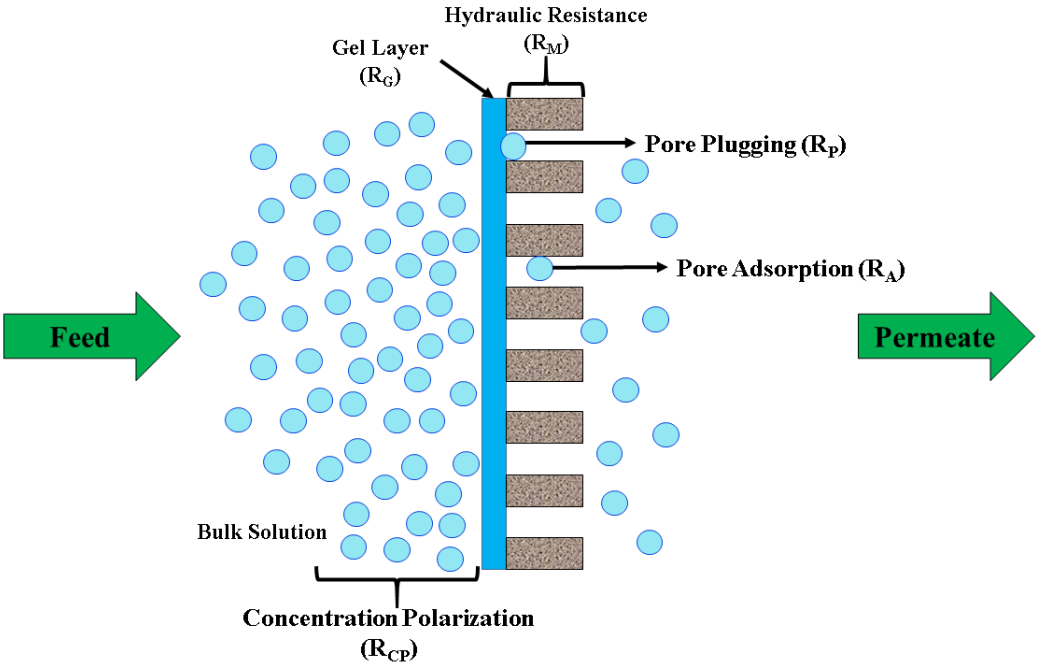

Figure 1.5. Schematic representation of concentration polarization and fouling in a membrane process [8]

Later, over the time a gel layer is formed by the continuous accumulation of feed components over the membrane surface. This gel layer also offers a resistance known as gel layer resistance, R_g, which hampers the membrane performance and play a vital role in flux decline of a membrane. The reasons for the resistances, such as concentration polarization, pore plugging, and pore adsorption is the membrane resistance (R_m). This is the innate resistance of a particular membrane and totally depends upon the properties of the membrane and membrane material, such as hydrophobicity, hydrophilicity, charge, and response to external stimulus. These all resistances combined together gives the total membrane process resistance, R_t. These resistances can be seen in Fig. 1.5.

The contribution of various resistances in the total membrane process resistance is different, some plays major role and some may not be present. These all depends upon the membrane properties and membrane process conditions. The resistances other than the membrane

resistance can be controlled by using some physical means, such as mode of operation (cross-flow), use of stirrer, and pre-treatments of the feed but the membrane resistance, which is the innate property of a membrane, cannot be controlled by these means. Therefore, in ideal conditions only membrane resistance involved in the decline of the membrane performance is the membrane resistance. Therefore, it is important to prepare membrane with the least of this resistance. This can be done by either using hydrophilic or hydrophobic materials or making the membranes hydrophilic or hydrophobic as the situation demands. The membranes can be made hydrophilic or hydrophobic by coating, grafting, or blending hydrophilic or hydrophobic materials with the membranes. A lot of research is going on in this direction and have lots of scope for the membrane enthusiasts to come up with better membranes and membrane materials.

1.5. Methods to abstain fouling

The problem of fouling makes it difficult for the membranes to be used for important industrial applications. Therefore, it is important to tackle this problem of membrane fouling. Generally, membranes are modified in such a way that the feed components repel themselves from the membrane surface. There are two ways to do so, first, the membrane is made hydrophilic in case of hydrophobic feed components by using hydrophilic components as membrane materials. These materials are either grafted/coated or directly blended within the membranes to impart hydrophilicity to the membranes. This leads to increase in the antifouling nature of the membranes. Second, charge can be imparted on membranes so that the feed components will not attract towards the membrane surface and thus fouling of the membrane could be reduced. The two methods are shown in Fig. 1.6. These methods are described in the following subsections.

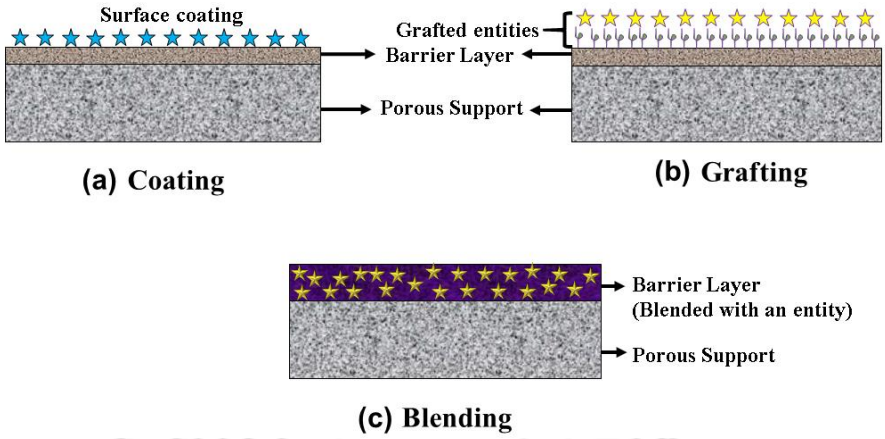

Figure 1.6. Schematic representation of (a) coating, (b) grafting, and (c) blending of (hydrophilic or responsive) components [8]

Increase in the hydrophilicity of the membranes by blending method

In this method, the hydrophilic membrane materials are directly blended with membranes during the membrane preparation process. Hydrophilic polymers, charged polymers, organic acids, and surfactants are some of the examples of commonly used hydrophilic components for the modification of membranes to reduce overall membrane fouling. Nowadays, materials such as co-polymers and stimuli responsive materials are also commonly used. In addition to the hydrophilic organic components there are some inorganic components which are used for the enhancement of the antifouling nature of the membranes, such as metallic nanoparticles, carbon nanotubes, etc. Therefore, this method is prominent, easy to use, and result oriented.

Antifouling membranes by surface modification

The prepared membranes are also modified by modifying their surface. Generally, a hydrophilic component is either coated or grafted over the membrane surface to achieve

the goal of antifouling. There are two methods to do the surface modification of the membranes viz. physical method and chemical method.

Physical Modification

In this method, the hydrophilic components are coated on the membrane surface with physical interactions and without any covalent bonding. In simple words the chemical composition of the membrane remains unchanged even after the surface modification. However, a chemical reaction might be needed during the process of membrane modification. The membranes are either directly coated with the hydrophilic component or they are first dipped in a solution containing chemically active monomers. Later, the monomers are immobilized on the membrane surface by cross linking or polymerization without the chemical participation of the base membrane. Commonly used hydrophilic materials for this purpose are poly vinyl alcohol, chitosan, poly ethylene glycol, etc.

Chemical modification

In this method, the membranes are modified by covalent bonding interaction. Firstly, the membrane base polymer chains are activated chemically or by irradiation. Then the hydrophilic components are coated or grafted over the active membrane surface. In this method too, the basic membrane properties are not changed. The advantage of this method is that due to the presence of covalent bonding between the hydrophilic component and membrane surface the membrane modifying agent will remain intact over the membrane surface for a longer period of time.

1.6. State of the art

This section covers the literature review of the contemporary research, explaining their outcomes which helps in identifying potential areas of research that requires to be addressed

in this thesis. The state of the art has been presented for the antifouling polymeric ultrafiltration membranes for various environmental and biological applications.

1.6.1. Modification of polymeric membranes with non-solvent soluble additives

Literature survey

Researchers across the globe have used various techniques to overcome the fouling issue, like effective cleaning of membranes, maintaining effective pore sizes, increasing the hydrophilicity and antifouling properties of the membranes. The later techniques are now a day's very much prominent among the membrane enthusiasts. The emphasis is given to increase the hydrophilicity of the membranes as fouling occurs due to the hydrophobicity of the membrane polymer [9,10]. The uses of hydrophilic polymers, surfactants and polymers having charges on them induce hydrophilicity and antifouling properties to the membranes. Hydrophilicity helps to reduce fouling, which hinders the attachment of different solutes from the feed to the membrane surface and thus reduces fouling.

The two most widely used techniques for making the membranes more hydrophilic and antifouling are, deposition of the hydrophilic substances onto the membrane surface by various means of coating and grafting [11-13] or blending of these hydrophilic substances [14,15] into the membrane. These techniques are easy and effective as compared to other techniques like use of nanoparticles [16] or other types of hydrophilic and antifouling additives [17,18]. The drawback of using a coating or grafting additives to the membrane is that this alters the pore sizes, pore size distribution of a membrane and also blocks the pores. By this there may be an increase in hydrophilicity of a membrane, but the final flux which is the sole criteria for a membrane to be called good or excellent will be

compromised. There are also chances of removal of the coated or grafted material from the membrane while in operation. Thus, blending is a good option to opt for. It is easy to get compatible hydrophilic polymers for getting a good hydrophilic and antifouling membrane with desired characteristics. Many researchers [19-21] have used this technique of blending hydrophilic polymers with the membrane. They have used polymers like PEG, PVP, and PEGME, respectively; of different molecular weights to get increased hydrophilicity as well as antifouling nature of the membranes.

Blending, by far, is the most handy and popular technique. Jung et al., investigated the role of molecular weight of PVP in PAN membranes, with DMSO as solvent. In the study it was seen that, with the increase in molecular weight of additive PVP, the top layer became thicker and the structure of the membrane changed. Amount of PVP in the membrane also affects the flux of the membrane, higher the amount lower will be the flux and vice versa [21]. Boom et al., concluded that a minimum molecular weight of the additive PVP is required to be added to the polymer solution of PES and NMP to suppress macrovoid formation and that, molecular weight is an important factor for optimization of membrane performance [22]. Sinha et al., found that by increasing the molecular weight of the additive PEGME in PSF membranes, the hydrophilicity and porosity increases. The contact angle decreased from 59^0 to 47^0 on increasing the molecular weight from 550 Da to 5000 Da and the porosity increased from 0.44 to 0.57 [23]. Hence, it is clear from the literature that additives play a major role in shaping the morphological and permeation properties of polymeric membranes. In most cases, for the synthesis of the membranes, phase inversion technique using immersion precipitation is employed. The process requires a solution of the polymer, for which any organic solvent can be employed. NMP and DMSO are popular solvents for polymers. That is why NMP which is far better as a solvent than DMSO is used

in the present study as the solvent. Water is generally employed as the non-solvent because polymers are generally insoluble in it. Moreover, it is easily available and environmentally suitable. In other systems, polymeric additives, among which PVP is the well-known, are commonly used with PSF or PVDF [24,25].

Possible scope for further research

From the above literatures, it can be accounted that use of a good hydrophilic agent can impart good hydrophilicity and antifouling properties to UF membranes. Hydrogels which are hydrophilic in nature [26] are proven as good agents for imparting hydrophilic and antifouling properties to an UF membrane. Many researchers had been used hydrogels for the same purpose [27]. AMPS is a good agent for this purpose because of the presence of sulfonate groups.

Till now the direct blending of AMPS in a membrane is not reported. In this work different wt% of AMPS were blended with PSF casting solutions. The effect of different wt% of AMPS hydrogel on the prepared UF membranes was studied, in order to analyze the effect of different weight by weight percentages of the hydrogel on the membrane structure, flux, hydrophilicity, and antifouling properties. Various characterization techniques were employed so as to confirm the authenticity of the hydrogel in the prepared membranes. The separation of BSA and HA was studied competently and RSM was applied for the study of BSA flux and rejection response at various time and pressure values. The objective of the study is to maximize the membrane flux and rejection of the model proteins and pollutants from the feed.

Furthermore, the thesis reports the use of mPEG in a PVDF-co-HFP/NMP system and explains the effects of the additive on the system. The effect of different molecular weights of the additive mPEG on prepared PVDF-co-HFP membranes morphology and

performance, using NMP as solvent and water as non-solvent were studied. The reforming effects of mPEG as an additive on the PVDF-co-HFP membranes are positive in nature in terms of membranes hydrophilicity and antifouling nature. mPEG is found to be suitable for the enhancement of both hydrophilic as well as the antifouling nature of the PVDF-co-HFP membranes as it is a neutral hydrophilic polymer. This neutral hydrophilic characteristic of mPEG ends up the membranes to be hydrophilic and antifouling in nature. A systematic study regarding the effect of mPEG on the membranes morphological and permeation parameters was carried out. For the analysis of the effect of mPEG on the structure of the prepared membranes FESEM was used. FTIR analysis was used to confirm the presence and stability of the mPEG and other compounds in the prepared membranes. Hydrophilicity of the membrane surface was determined by measuring the contact angle. The membranes were studied with foulants like BSA and HA for the analysis of the antifouling nature of the membranes. The retentate contains HA in case of HA study. The disposal of which is again a point of question. Therefore, for the disposal of HA it is proposed that the separated HA can be used for brick manufacturing for common construction purposes, as HA helps in increasing the plasticity of the bricks [28].

1.6.2. Fabrication of polymeric membranes with carbon nanotubes synthesised from fly ash

Literature survey

Carbon nanotubes are the stronger and stiff materials in terms of tensile strength and elastic modulus respectively. This strength results from the covalent sp^2 bonds formed between the individual carbon atoms. CNTs name was derived from their long, hollow structure with the walls formed by one atom-thick sheets of carbon, called graphene. Individual

nanotubes naturally align themselves into "ropes" held together by van-der waals forces, more specifically pi stacking. The chemical bonding of nanotubes is composed entirely of sp^2 bonds, similar to those of graphite.

Coal fired boilers have major share in total electricity production across the globe. The dominant residue of these coal fired boilers is flyash. Flyash contains fine particles are powder in nature moves along with the flue gas produced during combustion. Generally, gas solid contactors like cyclone separators, bag houses and electrostatic precipitator are employed for the collection of flyash but its storage and disposal is the major concern for industries and other environmental protecting bodies. A big chunk of this flyash residue is used for filling lagoons, dams, lands yet a huge amount is still unused and causes shortage of land, unnecessary money and manpower investment and other serious environmental impacts. One solution can be to search the application of flyash in value addition. Extensive research has been done in the field of value addition, some dominating fields are cement and bricks production, adsorbent, for removal of organic compounds and metals, and zeolites synthesis [29].

Use of waste material in the production of carbon nanotube is a promising application of flyash, not only the reduction in disposal problem but also conversion in a commodity having marketable existence. Carbon nanotubes have diversified applications, viz. composites having conductive and high strength, devices for energy conversion, probes, sensors, displays, and semiconductor devices [30].

Possible scope for further research

The amount of research done on carbon nanotubes in the past one decade provides a wealth of information on their electronic, mechanical, thermal, optical and other physical properties, it becomes possible to attach things outside and to put things inside of CNTs.

Manipulation of CNTs into defined arrangement and their further incorporation into polymeric, ceramic or metal matrices increase the projection of their application. Therefore, CNTs synthesized from flyash are potential additive for the modification of polymeric ultrafiltration membranes.

Polymeric membranes with CNTs as additives were synthesized and characterized. The effect of CNTs on the performance of polymeric membranes is studied and its role on various membrane parameters like number of pores, pores area, porosity, permeability, and contact angle. Furthermore, the synthesized membranes were analysed for the separation of BSA protein from its aqueous solution. This helps in the assessment of the antifouling nature of the membranes.

1.6.3. Preparation of mixed matrix polymeric ultrafiltration membrane with Cu_2O photocatalyst

Literature survey

Photocatalysis is a potential technology for the treatment of organic pollutants present in the aquatic ecosystems. Researchers around the world used various photocatalysts for water treatment, such as TiO_2 [31], ZnO [32], CuO [33], and α-Fe_2O_3 [34], etc. Cuprous oxide (Cu_2O) is an antiferromagnetic p-type semiconductor used in this study as a photocatalyst due to its low direct band gap (2.17 eV) [35], which makes it a very effective and efficient photocatalyst compared to other commonly used photocatalysts. Due to its high catalytic activity, low growth temperature, and better electrical conductivity it is widely used in sensors [36], solar cells [37], semiconductor devices [38], polymer memory devices [39], as an electrocatalyst [40], and photocatalyst [41]. The major problems associated with the use of powder photocatalysts is their meagre dispersion and regeneration from an aquatic

phase. The scant dispersion results in their agglomeration and devouring of the active sites required for effective and efficient photocatalysis. Therefore, in this study the Cu_2O photocatalyst is embedded in polysulfone (PSF) polymeric membranes in the form of mixed matrix membranes (MMM). This inhibits the problem of agglomeration and make available the active sites for photocatalysis. Also, this helps in the development of commercially acceptable membrane based photocatalyst. As discussed earlier, it is well versed now that the use of membranes is augmented in various applications, such as water treatment, desalination, food processing, and biotechnology due to their cost effectiveness, stability, and efficiency [1]. The combine system of photocatalyst and membrane will mask the disadvantages of each other and will provide synergistic effect in the removal of pharmaceuticals from the wastewaters.

Possible scope for further research

Ibuprofen (IBP) is a pharmaceutical under nonsteroidal anti-inflammatory drug (NSAID) class, which is commonly used for the treatment of pain, fever, and inflammation. The team of Steward Adams at Boots Group discovered and patented it in the year 1961. The low toxicity, stable profile, higher efficiency, insignificant side effects with fruitful results make it an over the counter drug, which makes it easily available in pharmacies, retail stores, and supermarkets worldwide [42]. This leads to its excess usage and develops pseudo persistent phenomenon over the years. Thereby, inflicting damage to flora and fauna in aquatic ecosystems [43,44]. IBP and several other pharmaceuticals, such as naproxen, iopromide, and sulfamethoxazole reportedly escapes primary treatment and show resistance to their complete removal in an ensuing biological treatment [45]. These outputs makes IBP an emerging organic micropollutant. This demands sound methodology for the elimination of IBP from the aquatic ecosystems.

In this study, PSF MMM membranes were prepared by using Cu_2O as a photocatalyst for the removal of IBP from aqueous solutions. Furthermore, the other photocatalysts, like TiO_2 requires UV light for the activation of their catalytic properties but in this study visible light is used for the photocatalysis, which further decreases the overall energy impact and makes the process safe and secure.

1.6.4. Synthesis of polymeric ultrafiltration membrane using stimuli responsive polymer nanocomposite

Literature survey

Recently, stimuli responsive membranes are gaining importance for their smart functionalities that is their response to an external response, such as temperature, pH, light, electrical, or magnetic for different membrane separation processes [1]. The smart membranes possesses great potential for their use in various applications related to separation science. Membranes can be made stimuli responsive either by grafting or by blending responsive materials. These responsive materials have specific properties to respond to a particular external stimuli. This responsiveness of the material to an external response changes the physical properties, such as pore size of the membranes. Further, these changes makes the membranes self-cleaning with high permeability and selectivity. Therefore, it can be said responsive membranes are capable of bringing a mammoth change and opportunities for the field of membrane science.

Blending is the most effective and efficient method for the modification of membranes. Since, it assures the stable and proficient addition of the desired property into the membranes. Some of the commonly used hydrophilic materials used for membrane modifications are polymers with hydrophilic groups like polyethylene glycol,

polyvinylpyrrolidone and nanoparticles, such as TiO_2, ZnO [23,46]. The use of inorganic nanoparticles is proposed because in addition to hydrophilicity they also help in enhancing the membrane strength [47]. Also, the use of nanoparticles such as TiO_2 is advocated as it can act as a photocatalyst [31]. Furthermore, the functionality of the membranes could be improved if stimuli responsive materials are used to modify the membranes [9]. Therefore, the modification of inorganic TiO_2 nanoparticles are with responsive polymers before blending it with polymeric membranes is a good approach for making the membrane antifouling and suitable for various applications. Furthermore, this will help the membrane to perform better in terms of its selectivity, permeability, and antifouling behaviour.

Possible scope for further research

Based on the literature review it can be stated that modification of polymeric membranes with stimuli responsive polymeric nanocomposites will be a novel work for the fabrication of antifouling polymeric membranes. Therefore, in this section of the thesis, stimuli responsive poly(N-vinylcaprolactam-TiO_2-acrylic acid) (VCL-TiO_2-AA) polymer nanocomposites were synthesized in various ratios and blended with PSF membranes so as to make them hydrophilic and stimuli responsive. The effect of the synthesized VCL-TiO_2-AA polymer nanocomposite was analysed on the membrane performance in terms of fouling, temperature and pH responsiveness, and photocatalytic removal of MB dye. Furthermore, the photocatalytic dye removal was carried out under dark and visible light conditions at different pH values.

1.7. Objectives and scope of work

The present PhD thesis, based on the above state of the art, includes the following main objectives

- To investigate the role of poly(2-acrylamido-2-methyl-1-propanesulfonic acid) in the modification of polysulfone membranes for ultrafiltration.
- To evaluate the mPEG effect on the hydrophilicity and antifouling nature of the PVDF-co-HFP flat sheet polymeric membranes for humic acid removal.
- To investigate flyash based carbon nanotubes modified polysulfone ultrafiltration membranes for their hydrophilic and antifouling nature.
- To investigate Cu_2O photocatalyst modified antifouling polysulfone mixed matrix membrane for ultrafiltration of protein and visible light driven photocatalytic pharmaceutical removal.
- To investigate the stimuli responsive polymer nanocomposite modified mixed matrix polysulfone ultrafiltration membrane for dye removal.

1.8. Organization of the thesis

Chapter 1 covers the context of the problem associated with the fouling tendency of polymeric UF membranes. In addition to this the chapter also covers the objectives of the present work. **Chapter 2** discusses about the experimentation involved in the preparation and characterization of polymeric membranes. The phase inversion method used for the membrane preparation is explained in detail along with different membrane characterisation techniques, such as microscopic techniques like field emission electron microscopy (FESEM), Fourier transform infrared spectroscopy (FTIR), liquid-liquid displacement porosimetry (LLDP) method, etc. **Chapter 3** describes the Role of poly(2-acrylamido-2-methyl-1-propanesulfonic acid) in the modification of polysulfone membranes for ultrafiltration. The effect of different wt% of AMPS hydrogel on the prepared ultrafiltration membranes was studied, in order to analyse the effect of different weight by weight percentages of the polymer on the membrane structure, flux,

hydrophilicity, and antifouling properties. **Chapter 4** presents the results obtained from the addition of different molecular wt. of methoxy poly(ethylene glycol) in the PVDF-co-HFP membranes morphology and performance, using NMP as solvent and water as non-solvent. **Chapter 5** explains the fabrication and characterization of fly ash based carbon nanotubes modified hydrophilic and antifouling ultrafiltration polysulfone membranes for protein separation. **Chapter 6** explains the preparation of Cu_2O modified PSF MMM by using phase inversion technique and characterization using Field emission electron microscopy (FESEM), atomic force microscopy (AFM), Fourier transform infrared spectroscopy (FTIR), and FESEM-EDX. Also, the analysis of their flux profile and photocatalytic removal of IBP under dark and visible conditions is carried out. Additionally, the hydrophilicity and antifouling performance is also analysed by measuring membranes water contact angle (WCA) and BSA permeation. **Chapter 7** discusses the synthesis of stimuli responsive VCL-TiO_2-AA polymer nanocomposites and their role in the modification of polysulfone ultrafiltration membranes. The effect of the synthesized VCL-TiO_2-AA polymer nanocomposite was analysed on the membrane performance in terms of fouling, temperature and pH responsiveness, and photocatalytic removal of methylene blue (MB) dye. **Chapter 8** concludes this work with appropriate suggestions concerning future research in the field.

Chapter 2
Membrane preparation and characterization techniques

This chapter explains different membrane preparation methods explaining the fabrication of various kinds of polymeric membranes. The importance of various materials along with their role in different membranes is explained in detail. The fast growth in the strategies and methods for the design and fabrication of membranes with required properties of selectivity, permeability, functionalities, and physico-chemical nature established them in the commercial membrane market. Therefore, functions of membrane precursors and various fabrication methods are discussed here. In addition, various characterization instruments, such as FTIR, ATR-FTIR, FESEM, AFM, UV-VIS spectrophotometer, FESEM-EDX, and XRD are also discussed. Furthermore, the chapter explains various membrane permeation techniques elaborating the pure water flux (PWF), compaction factor (CF), equilibrium water content (EWC), hydraulic permeability (P_m), pH sensitivity, thermo sensitivity, water contact angle, hydration capacity, BSA adsorption, flux, and separation capabilities of the synthesized membranes. The synthesis of specific membranes is described in section 1.6. Additionally, the subsequent chapters reports the conditions required for various experiments.

2.1. Materials

Polysulfone (PSF) is used as the base polymer for all of the membranes except Chapter 4, where PVDF-co-HFP was used as base polymer. The solvent NMP was used for the preparation of all of the membranes. In this work as explained in Chapter 1, different sort of additives were used for the modification of polymeric membranes. Some additives were used directly like AMPS and mPEG; where as other additives were synthesized for specific membrane properties like hydrophilic, pH responsive, and thermo responsive. Table 2.1 presents the various chemicals utilized for the membrane preparation and modification. All of the chemicals used

for additive synthesis were of analytical grade and rest were of lab grade. Also, all of the chemicals were used as purchased without any purification. The deionized (DI) water obtained from a Millipore system (Millipore, France) was used as a non- solvent in the phase inversion process as well as for all other needs.

Table 2.1. Chemicals used in this work

Sr. No.	Chemicals (specification)	Brand
1.	Polysulfone (average molecular weight 30000 Da)	Sigma-Aldrich Co. USA
2.	1-methyl-2-pyrrolidone (reagent grade)	LOBA Chemie, India
3.	Methoxy poly(ethylene glycol) (average molecular weight 550 Da, 2000 Da and 5000 Da)	Sigma-Aldrich Co. USA
4.	Bovine serum albumin (68,000 Da)	Otto Chemie, India
5.	Poly(vinylidene fluoride-*co*-hexafluoropropylene) (average molecular weight 400000 Da)	Sigma-Aldrich Co. USA
6.	Polyethylene glycol 6000 (synthesis grade)	Merck, India
7.	Methanol (synthesis grade)	Merck, India
8.	Ethanol (synthesis grade)	Merck, India
9.	Propanol (synthesis grade)	Merck, India
10.	Butanol (synthesis grade)	Merck, India
11.	Potassium bromide (FTIR grade)	LOBA Chemie, India
12.	N- vinylcaprolactam	Sigma-Aldrich Co. USA
13.	Acrylic acid (synthesis grade)	Merck, India
14.	Azobisisobutyronitrile	Otto Chemie, India
15.	N, N′-methylenebisacrylamide (average molecular weight 500 Da)	Sigma-Aldrich Co. USA
16.	Flyash (F type)	NTPC, Visakhapatnam, India
17.	Sodium hydroxide	Fischer Scientific Pvt. Ltd
18.	Ibuprofen	Sigma-Aldrich Co. USA
19.	N, O-Bis-(Trimethylsilyl) Acetamide (BSA)	Otto Chemie, India
20.	Humic acid	Otto Chemie, India

2.2. Membrane preparation technique

The asymmetric membranes were prepared in the flat sheet configuration using the phase inversion technique by immersion precipitation. The casting solutions were stirred on magnetic stirrers for 12 h at a speed of 200 rpm at required temperature. The clear polymer solutions were left for degassing up to 12 h at room temperature. Following the degassing period, the polymer solutions were casted on clean glass plates using a casting knife. The casted polymeric films along with the glass plates were immediately immersed in a DI water bath. Water, being a non-solvent to the polymer, results in the coagulation and immediate precipitation of the polymeric films. This changes the film colour to white and the membranes formed, separates out from the glass plates immediately. The formed membranes were kept immersed in fresh DI water for another 12 h for removal of any residual solvent. Finally, the membranes were dried in air at room temperature. Membrane sheets were finally air dried at room temperature thereafter [48,49].

2.3. Membrane characterization techniques

The structure of a membrane is as important as its application. Since, all the virtues of membranes mainly depends on the morphology, therefore, it is very necessary to analyse its structure. The characterization of the structure and membrane in particular helps to get better performance out of a membrane indirectly. Indirectly, because the performance of a membrane is directly proportional to its structure. Different applications have wide ranges of membrane requirements that mainly depend upon their structure. Therefore, membrane characterization techniques provide the best solution for applying specific membranes for exact applications. These techniques also help in identifying appropriate membrane structure for a specific application.

The characterization techniques are also important so as to make sure the membranes are defect free and have proper structural and functional properties intact, since a single defect can lead to a total loss of membrane performance. The characterization techniques are also the tools to make sure the consistency in the membranes produced over batches. The membranes should be checked for the presence of any defect or to establish a specific protocol for the preparation of particular membranes. The characterization techniques are also important in relating the membrane parameters like pore size, pore size distribution, porosity, and permeability to the area of application stated. Since, different membrane applications requires different membrane properties, characterization of membranes makes it easier for the user to select more appropriate membrane for a specific application.

In this chapter, the membrane characterization techniques are basically presented under two categories, first based on morphological aspects of the membranes, microscopy techniques and another based on the permeation factors, the permeation techniques. Though sometimes it is difficult to relate the two as the pore size and shape are inconsistent in nature and in some characterization technique several assumptions are made regarding the two. Figure 2.1 is the representation of the fact regarding the pore size and shape (actual and model). Therefore, conclusive interpretations ought to be made after employing combination of morphological and permeation characterization techniques. Other techniques are also available to characterize the membrane materials and other physical properties of the membranes. Techniques like Fourier transform infrared spectroscopy and X-ray diffraction, are also covered in this chapter. These techniques help in analysing the components present in the membranes. These techniques also reveal almost everything about the physical properties of the membranes like stability, performance, different conditions of pH, temperature, and pressure.

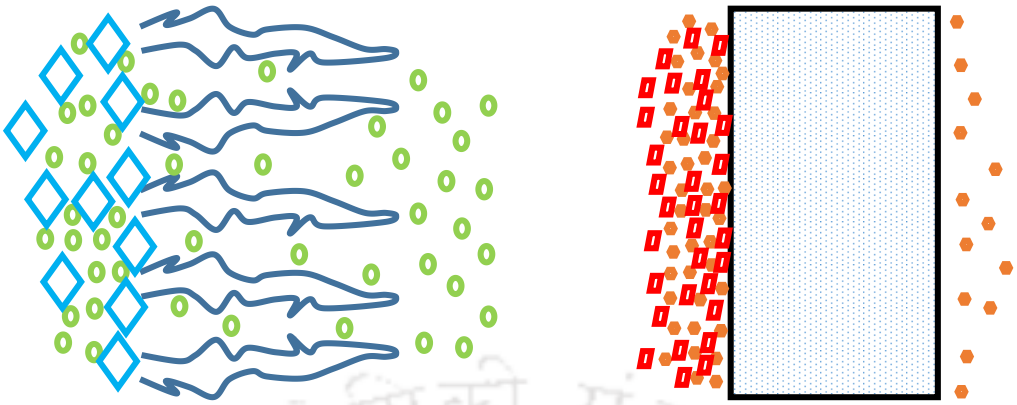

Figure 2.1. Schematic representation of (a) porous and (b) non-porous membranes [1]

2.3.1. Microscopic techniques

Microscopic observation was done by field emission scanning electron microscope (FESEM, Make: Zeiss LSM 510 Meta) after the samples were coated with thin gold layer. Erwin Wilhelm Muller invented FESEM in the year 1936, which was having resolution of 2 nm. He was the first person to observe atoms experimentally because of this invention. FESEM is a higher version of SEM in terms of magnification and resolution. The basic working principle and mode of working is same as SEM. The main difference, which is also the main reason for other differences among SEM and FESEM, is the electron gun used. In FESEM a field emission gun is used as compared to thermionic gun in case of SEM. The field emission gun electron beam is the most intense; also it is brighter than the thermionic gun. The electron beam is narrower as compared to SEM and thus results into a better image quality and higher magnification. The FESEM has near atomic resolution (0.2 – 0.6 nm). In FESEM also the common mode of operation is the detection of SE. BSE and X-rays are also detected and used in elemental analysis of the samples. There are fewer chances of sample burning and charging in case of FESEM as compared to SEM due to the use of low operating voltage (0.5-10 kV). Still, the samples are sputter coated with conductive materials as in the case of SEM for extra protection

and better image acquisition. The high resolution, magnification and the resultant better image quality are the reasons, the top surface images of the membrane samples are preferred to be taken by FESEM. The greater in depth and better image quality makes it easy to analyse the morphology and structure of the membrane samples. The pores and their geometry can be seen very easily and clearly, which further helps in the calculation of pore size, pore size distribution and porosity of the membranes.

The membrane pore size as well as membrane thickness were measured by using of imageJ software. The FESEM micrographs clearly provides the top layer as well as cross sectional morphological information of the membranes. A number of FESEM micrographs of the membranes were taken at different magnifications so as to perfectly analyse both the top surface and cross section of the prepared membranes.

2.3.2. Liquid-liquid displacement (LLDP) porosimetry method

The liquid-liquid displacement (LLDP) method is mainly used in case of ultrafiltration and nanofiltration membranes. LLDP is a combination of bubble point and solvent permeability [50] methods. This method also helps in the calculation of membrane pore size, pore size distribution, and pore number [51,52]. The pore radius can be calculated by using the Cantor's equation given below as the pressure value is known [50].

$$P = \frac{2\gamma}{r} cos\theta \qquad 2.1$$

where, P represents the pressure (Pa), r the pore radius (m), and γ the surface tension at the liquid/air interface (N/m).

In this method firstly, the membrane is wetted with a wetting liquid. Assuming that all the pores are filled with the wetting liquid, the membrane is secondly bring in contact with another liquid which is non-wetting for the membrane and also immiscible with the wetting

liquid. This non-wetting liquid is permeated through the membrane with an applied pressure, displacing the wetting liquid occupying the membrane pores. Since, the liquids are immiscible an interfacial tension arises between the two liquids at their subsequent boundaries. The non-wetting liquid is only able to displace the wetting liquid when the applied pressure value attains the value given Eqn. 2.1. The mechanism of this method is based on the assumption that at low pressures the largest pores are invaded and at high pressures the smallest pores by the non-wetting liquid.

Here, an assumption has made that at pressure P_i the non-wetting liquid permeates only through the pores of radius $r \geq r_i$ ($\approx 2\gamma/P_i$). The smaller radius pores r_k become permeable at pressure P_k ($>P_i$). Therefore, it is feasible to get a flux vs pressure plot. Where, flux J_i represents the pores for which $r \geq r_i$, flux J_k to the pores for which $r \geq r_k$. Thus, the flux $J_{i,k}$ at pressure $P_{i,k}$ is the result of pores with radii between r_i and r_k. The flux will keep on increasing until the pressure P_n is not reached. This point is reached when all the pores are occupied by the non-wetting liquid. If the pressure P_n is crossed than the membrane flux, J; becomes directly proportional to the applied pressure.

Since, P_n depends on both the pore radius as well as interfacial tension between the wetting and non-wetting liquid. It is important to select liquids with low interfacial tensions, γ, so that the smallest pores can also be measured without applying very high pressures. Generally, a water-isobutanol-methanol (25:15:7 v/v) mixture was used as the wetting liquid and deionized water as non-wetting liquid. The interfacial tension between these two liquids is low (0.35 mPa.m (dyne/cm)) at 20°C [9].

The data of variation of the flux with respect to pressure yields the pore size distribution of the membrane by using following equations:

$$L_n = \Sigma L_{i,k} = \Sigma \frac{J_{i,k}}{P_{i,k}} \quad 2.2$$

where $J_{i,k}$ represents the flux at pressure $P_{i,k}$, and $L_{i,k}$ the partial permeability coefficient of the pores with radius between r_r and r_k at pressure $P_{i,k}$. This corresponds to a mean radius:

$$r_{i,k} = \frac{r_i + r_k}{2} \quad 2.3$$

Combining Eqns. 2.1 and 2.2, the permeability vs pore radius curve may be obtained from flux vs pressure data. Also, from the following equations pore number vs pore radius and pore area vs pore radius curves can be obtained:

$$N_{i,k} = \frac{d\eta}{2\pi\sigma^4} P_{i,k}^{\ 3} J_{i,k} \quad 2.4$$

and

$$A_{i,k} = \pi r_{i,k}^{\ 2} N_{i,k} \quad 2.5$$

where $N_{i,k}$ represents the pore density i.e., the number of pores having radii between r_i and r_k per unit membrane surface area, d the length of the pore, and η the viscosity of the wetting liquid. $A_{i,k}$ represents the pore area having radii between r_i and r_k. Eqns. 2.4 and 2.5 are obtained from Cantor's equation (Eqn. 2.1) and Hagen Poiseuille's permeation equation (Eqn. 2.6) assuming cylindrical pores and laminar flow as given below [4,52,53]:

$$J_{i,k} = \frac{\pi N_{i,k} r_{i,k}^{\ 4} P_{i,k}}{8d\eta} \quad 2.6$$

The total pore area $A_{t,p}$ and the total number of pores per unit area of membrane N_t can be calculated as:

$$A_{t,p} = \Sigma A_{i,k} \quad 2.7$$

$$N_t = \Sigma N_{i,k} \quad 2.8$$

The mean pore radius r_m can be calculated as [23]:

$$r_m = \frac{\Sigma N_{i,k} r_{i,k}}{\Sigma N_{i,k}} \quad 2.9$$

The limitation of LLDP is that the calculated values of pore size and pore size distribution comes out to be marginally different from actual values. This might be due to the assumptions made during the analysis regarding pores viz., the pores are cylindrical in nature and membrane thickness is uniform throughout the membrane. However, the information comes handy while comparing different membranes.

2.3.3. Atomic force microscopy (AFM)

Atomic force microscope (AFM) is used for the analysis of top surface of materials especially thin films. It was invented in the year 1982 by IBM scientists. Scanning tunnelling microscope was also invented by IBM scientists Gerd Bining and Heinrich Rohrer for which they were awarded 1986 Physics Nobel Prize. In this technique a cantilever is used with a probe, this sharp probe scans the surface of the samples. The tip of the probe scans the sample surface in contact, non-contact, or tapping mode. The tip is deflected by the forces created according to Hooke's law [54], when the tip of the probe and sample surface is near or in contact with each other. This deflection of the cantilever in turn changes the reflection of a laser beam which was targeted on the top surface of the cantilever and detected by a detector. This variation in the laser beam is the measure of the applied forces.

In AFM analysis no pre-treatment of samples is required and samples can be observed under their native state. Also, since the AFM operates at very low forces it can be used to analyse soft samples as well. In this work, AFM is used to analyse the top surface of the

membrane samples. This reveals about the extent of smoothness or roughness, pores, pore geometry, pore size as well as pore size distribution in membrane samples. The obtained 3D AFM micrographs were used to analyse the effect of different additives on the membrane surface roughness.

2.3.4. Permeation methods

In the preceding sections, the membranes are characterised with different microscopy methods. Those techniques revealed information about the membranes by the methods where it is visible to the eyes. The morphological and structural properties are pore size, pore geometry, pore size distribution and pore number. The techniques are superficial in the sense they can only analyse the membrane surface and not gives the in depth detail about the sample. The blind pores are also considered for calculations of pore size distribution and pore number. The instruments used for the analysis are very expensive and the methods of sample preparation are also not easy. There is also special requirement of operators for the analysis. These are some of the shortcomings of the characterization techniques discussed previously. Therefore, there is a need of techniques that are easy, cheap, and accurate.

There comes the permeation based characterization techniques for membrane characterization. These techniques first of all are non-destructive in nature, easy to use and thus require no special operator, cheap, and needs minimum special equipment. These technique uses either pure water or a gas for the analysis of a membrane and gives results like pore size, pore size distribution, pore number, and porosity of a membrane with maximum accuracy as the blind pores are not taken into account in this technique.

A stainless steel membrane cell with capacity of 350 ml was used to carry out the unstirred batch experiments. In the membrane cell, the membranes of circular shapes with diameter 3×10^{-2} m and effective membrane area of 7.065×10^{-4} m^2 were placed over a base

support. The membrane cell was filled with the feed solution and the cell was pressurized using a nitrogen cylinder. The permeating permeate was collected from the bottom of the cell. The schematic of batch experimental setup is shown in Figure 2.2 [23].

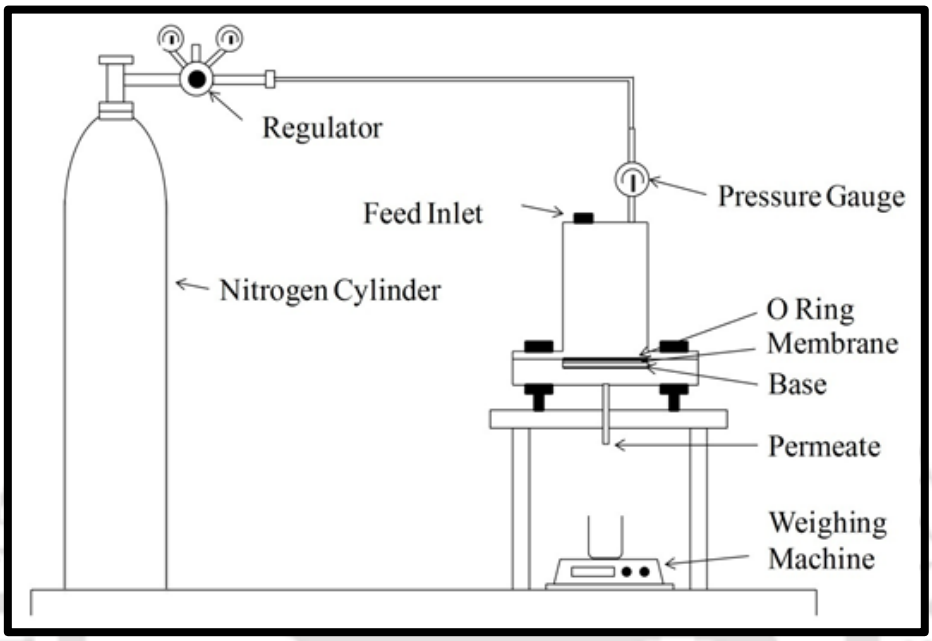

Figure 2.2. Schematic of experimental setup [23].

2.3.4.1. Membrane compaction and pure water flux (PWF) at constant pressure

Water permeation is the base of all the membrane applications and is measured in terms of a membranes flux (L/m^2h). Therefore, a membrane with better flux profile is considered as the best. To analyse membranes permeation profile pure water is used as feed. Since, there are no impurities present, the membrane process is free from any kind of anomaly and will give defect free results for the membrane. The membrane flux is further based on other membrane measures like membrane pure water flux (PWF), compaction factor (CF), permeability (P_m), and hydrophilicity. In this work, the prepared membranes were first compacted with DI water at 240-300 kPa transmembrane pressure for 2 h. The transmembrane pressure was always higher than the maximum operating pressure used in this work. The PWF was calculated by

measuring the membrane flux at regular time interval after attaining stabilized flow across the membrane.

The PWF was calculated by using the following equation:

$$J_W = \frac{Q}{A\Delta t} \quad 2.10$$

where J_W represents the PWF (L/m^{2}h), Q the total volume of water permeated (L), A the total effective area (m^2), and Δt the permeation time (h).

Furthermore, the CF can be calculated as a ratio of the initial PWF and steady state PWF. Given by Eqn. 2.11:

$$CF = \frac{PWF_{initial\ state}}{PWF_{steady\ state}} \quad 2.11$$

2.3.4.2. Hydraulic permeability (P_m)

Hydraulic permeability (P_m) also known as permeability defines a membranes permeation property. P_m is directly proportional to the porosity of a membrane. Therefore, a membrane with high permeability results into higher flux and vice versa. The P_m (L/m^{2}hkPa) can be determined by the slope of the curve between PWF and transmembrane pressure. It can also be calculated as:

$$P_m = \frac{J_W}{\Delta P} \quad 2.12$$

where, P_m stands for the hydraulic permeability (L/m^{2}h kPa) and ΔP for transmembrane pressure (kPa).

2.3.5. Equilibrium water content (EWC), porosity and hydrophilicity

Equilibrium water content (EWC) is important in case of membrane studies as it is directly related to the porosity of a membrane and indirectly deciphers the extent of hydrophilicity or

hydrophobicity of a membrane [1,48]. For calculation of EWC, a membrane token is taken and soaked in DI water for overnight. After mopping with tissue paper they are weighed on a weighing balance and then dried in a vacuum oven for 24 h at 60°C. The membranes are again weighed in the dry state. Following relation is used to calculate EWC at room temperature [1]:

$$EWC\ (\%) = \frac{W_w - W_d}{W_w} \qquad 2.13$$

where W_w represents the weight of a wet membrane (g) and W_d the weight of a dry membrane (g).

Membrane porosity

Porosity is the property of a membrane which tells about its permeation and separation quality. A good membrane is always having a good porosity with well-defined pores. It can be calculated with the help of following relation [1]:

$$Porosity = \frac{W_w - W_d}{\rho_w \times V} \qquad 2.14$$

where ρ_w represents the density (Kg/m^3) of pure water at room temperature and V the volume of the membrane (m^3). Cross-sectional images of the membranes are used to get the membrane thickness for membrane volume calculations. The error found in the membrane thickness calculations was within 2-3 %.

Membrane hydrophilicity

The extent of membranes hydrophilicity is measured in terms of membrane static contact angle, lesser the membrane static contact angle higher the hydrophilicity of the membrane and vice-versa [49,55]. A drop of DI water is to be placed on the membrane surface with the help of a micropipette, at room temperature, then the images of the drop is to be taken with the help of a digital instrument and the membrane static contact angle can be deciphered.

2.3.6. BSA adsorption on membranes surface

BSA adsorption over the membrane surface was carried out by using 10 mg L^{-1} aqueous BSA solution. Membrane samples of 2 × 2 cm were taken and immersed into 10 ml of aqueous BSA solution for 12 h at STP conditions. Thereafter, the solution was analyzed by using UV Visible spectrophotometer (Perkin-Elmer Precisel, Lambda-35) to estimate the BSA concentration remaining in the solution. The difference between the initial and final BSA concentrations (i.e., before and after BSA adsorption) gives the amount of BSA adsorbed over the membrane surface.

2.3.7. ATR-FTIR of modified membranes

Fourier transform infrared (FTIR) analysis was done by using ATR-8200 HA (Shimadzu, Japan) attached to the FTIR spectrometer (Make: IRAffinity-1, Shimadzu, Japan). The membrane samples were clamped appropriately to the surface of the attenuated total reflectance (ATR) crystal and analysed at room temperature. The number of scans was fixed at 30 and apparatus resolution was set at 4.

2.3.8. Ultrafiltration experiment and fouling studies

The membrane cell explained in the preceding section was used for the membrane ultrafiltration experiments throughout the work. The membrane ultrafiltration experiments were carried out with BSA and HA aqueous solutions of 1000 mg L^{-1} concentration. In this work, the membranes were first compacted at 300 kPa pressure and then operated at 150 kPa transmembrane pressure. Firstly, the membrane was permeated with DI water to get pure water flux (F_{W1}) of the membrane. Secondly, the membrane cell was filled with the prepared aqueous solution of BSA or HA and the resulting membrane flux (F_{BSA} or F_{HA}) was measured. Lastly,

the membranes were cleaned under normal tap water and again the membrane pure water flux (F_{W2}) was measured.

Membranes practical aspects viz. fouling, separation, and permeate flux were analyzed by using BSA and HA. Aqueous solutions of BSA and HA were prepared with 1000 mg L^{-1} concentration in DI water, while keeping the solution pH 7 by using 0.1 M NaOH and 0.1 M HCl. The experiments of this ultrafiltration study of the membranes were similar to PWF study, where the membranes were compacted for 1 h at 240-300 kPa and then water flux was measured at 150-200 kPa (J_{w1} or F_1, in case of BSA and HA, respectively) by permeating DI water for 1 h duration through the membranes. The membrane cell was filled with the model solution (BSA or HA) after the completion of the first run of 1 h with DI water. The pressure and duration of this second run with the model solution was same. The model solution flux (J_p in case of BSA solution and F_{HA} for HA solution) was measured during this second run. The second run also helps in calculating the % rejection of BSA or HA. The following relation was used to calculate the % rejection of the BSA or HA concentration from the feed solution:

$$R(\%) = \left(1 - \frac{C_p}{C_f}\right) \times 100 \qquad 2.15$$

where, C_p and C_f are concentrations of BSA and HA in the permeate and feed (mg/L), respectively. The membrane cell as well the membrane was cleaned, after the completion of the second run, with running tap water. The third and the final run (J_{w2} or F_2 in case of BSA and HA, respectively), was similar to the first run of the experiment in every aspect. DI water was used as the feed for the final run and the DI water was permeated for 1 h through the membranes. By using J_{w1} or F_1 and J_{w2} or F_2, flux recovery ratio (F_{RR}) of the membranes was calculated by using the following relation:

$$F_{RR}(\%) = \frac{J_{w2}}{J_{w1}} \times 100 \qquad 2.16$$

The cleaning efficiency (CE) of the prepared membranes was calculated by using the following relation:

$$CE(\%) = ((J_{W2} - J_P) \times (J_{W1} - J_P)) \times 100 \quad 2.17$$

The BSA concentration in permeate was determined by using UV-Vis spectrophotometer (Make: Perkin-Elmer Precisel, Lamda-35) at a wavelength of 280 nm with a scan speed of 240 nm/min. The HA concentration in permeate was calculated at 254 nm wavelength by keeping other instrumental parameters same.

Membrane fouling on a broad scale is usually of two types viz. reversible and irreversible fouling. Reversible fouling is the fouling caused by reversible adsorption of the foulant on the membrane, which can be reduced or removed with simple hydraulic cleaning of the membrane. On the other hand, irreversible fouling is irreversible in nature and is difficult to remove or reduce. The sum of both reversible as well as irreversible fouling gives total fouling of the membranes. In the present study fouling process of the membranes was calculated by using the following relations:

Total fouling ratio, $F_t = 1 - \left(\frac{J_p}{J_{w1}}\right)$ 2.18

Reversible fouling, $F_r = \left(\frac{J_{w2} - J_p}{J_{w1}}\right)$ 2.19

Irreversible fouling, $F_{ir} = \left(\frac{J_{w1} - J_p}{J_{w1}}\right)$ 2.20

The BSA and HA concentration values were plotted against corresponding values of absorbance. The relation between absorbance versus concentration was found to be a linear one with R^2 = 0.9995. This relation was used for measuring concentration of unknown sample i.e. permeate. The calibration curve for BSA is shown in Fig. 2.3.

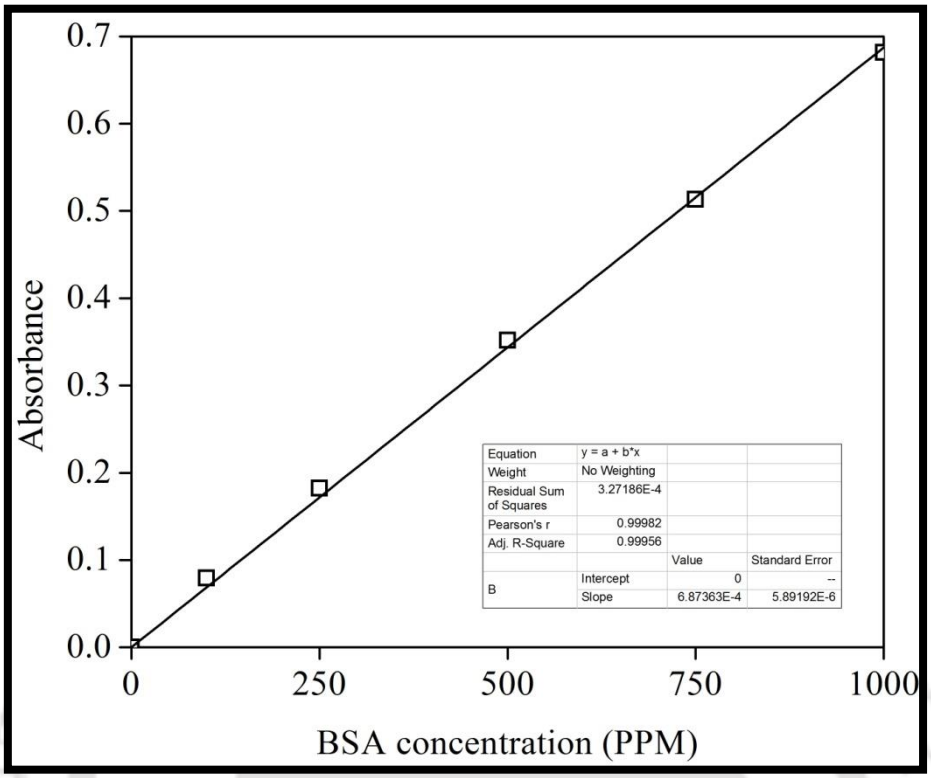

Figure 2.3. Calibration plot of BSA solution.

2.4. Characterization of synthesized additives

The chapter 1 of this thesis explains that some of the membranes were made antifouling by using different additives, which were synthesized and directly blended with the membrane casting solution. One of the example of such additive is the N-vinylcaprolactam-TiO_2-acrylic acid (VCL-TiO_2-AA) polymer nanocomposite having pH, temperature, and photocatalytic responsiveness. It is important to ensure that the responsiveness of such additives is intact and they are ready to be used for the modification of the membranes. Therefore, various characterization techniques were used to analyse their characteristic features. These characterization techniques are discussed in the subsequent subsections of the chapter.

2.4.1. Field emission scanning electron microscopy- Energy dispersive x-ray spectroscopy (FESEM-EDX)

FESEM has different modes of operation and detection of secondary electrons is the most common. Other modes are like detection of back scattered electrons (BSE) and X-rays. To detect these different electrons or x-rays different detectors are employed and SE detector is the standard detector present in all the FESEM machines. BSE are the electrons that are emitted from the sample by elastic scattering. Unlike SE these are emitted from the depth of the sample. Thus carries less energy and results into poorer images as compared to SE images in terms of resolution. Due to their source of origin and relevance to the sample atomic number they are used for the elemental analysis along with sample characteristic X-rays. Thus, the BSE images can provide details of the elemental distribution in a sample. The characteristic X-rays are emitted from a sample when an inner shell electron is emitted by the PE, which results in fill up of the vacancy by a higher energy electron and release of energy in the form of X-rays. The detection of these sample characteristic X-rays is used in elemental analysis of the sample, which provide information about the composition and number of elements present in a sample. This is known as Energy dispersive X-ray spectroscopy (EDS or EDX) technique of sample analysis and FESEM-EDX when the cause of origin of X-rays is FESEM or in simple words when FESEM is combined with EDS.

In the present work, the compositional studies of the additives as well as prepared membranes were carried out by using FESEM-EDX analysis. The gold coated additives and membrane samples fixed on carbon tape pasted stubs were analysed by using FESEM-EDX analysis for the elements present in the prepared membranes.

2.4.2. X-ray diffractometry

X-ray diffractometry (XRD) is a material characterization technique. It is mainly used for the analysis of crystal structures of powder samples from its inception, therefore, named as XRD. In XRD, single wavelength X-ray beam is used for the analysis. The X-ray beam incident angle is continuously changed during the analysis so as to get a spectrum of diffraction intensity vs angle (angle between the incident and diffracted beam). The crystal structure and quality of the sample can be analysed by comparing the obtained data with XRD database available. The database contains over 60,000 diffraction spectrums of known crystalline materials.

In order to confirm the structure, phase, and crystallinity XRD analysis, using D8 Advance, Bruker instrument in the range of 20–80° 2θ with a scan rate of 3°/min, of the additives as well as fresh and used membranes was carried out.

2.4.3. Thermogravimetric Analysis (TGA)

Thermogravimetric analysis (TGA) is a thermal analysis technique that measures mass change in a material as a function of temperature. The thermal events in a material can bring change to its properties like structure, mass, phase, and stability.

A microbalance is the heart of the TGA instrument as it measures the mass change, which is the base of this technique. The null point type microbalance, the Cahn microbalance, is a common type of microbalance used in most TGA instruments based on its property to keep the sample in a vertical position when its mass change occurs. In the TGA instrument the sample is located in the center of the furnace over a microbalance. The furnace is cylindrical in shape with heating elements present in its walls. A thermocouple is present under the sample holder with a gap in between. This arrangement eliminates any possibility of a temperature gradient to occur between the thermocouple and heating elements and helps them to reach

thermal equilibrium swiftly. Generally, nitrogen gas is used to fill the furnace to maintain an inert atmosphere.

In TGA, mass change is monitored with respect to increase in temperature. TGA is mainly used to analyze a material's decomposition and stability as a function of temperature in a scanning mode or as a function of time in isothermal mode by means of mass change. TGA curves can be plotted as percent mass change versus temperature or time.

In the present work, samples were analysed from 20°C up to 650°C with a 10°C/min heating rate so as to analyse the thermal stability of the membranes with respect to the additive used to modify the membranes. Additives like high molecular weight polymers, metallic nanoparticles, and zeolites are reported for increasing the stability of a membrane by using TGA as the technique of analysis [1].

Chapter 3
Role of poly(2-acrylamido-2-methyl-1-propanesulfonic acid) in the modification of polysulfone membranes for ultrafiltration

Antifouling nature and hydrophilicity are critical for a high performance membrane. In this chapter, the effect of the additive poly(2-acrylamido-2-methyl-1-propanesulfonic acid) (AMPS) on the antifouling and hydrophilic properties of polysulfone membranes were discussed. Different wt% of AMPS was used to prepare polysulfone membranes by phase inversion method. The role of AMPS on the porosity, pore size distribution, hydrophilicity, and antifouling nature was investigated and analyzed in detail. Characterization techniques like FESEM, AFM, and imageJ software were used to characterize the morphology of prepared membranes. Response surface methodology was used for the optimization of BSA flux and rejection. The antifouling study of the prepared membranes were undertaken by using bovine serum albumin (BSA) solution of 1000 mgL^{-1}.

3.1. Experimental

3.1.1. Materials

The membrane base material and additive used in this study were Polysulfone (PSF) (average molecular weight 30 kDa) and poly(2-acrylamido-2-methyl-1-propanesulfonic acid) (AMPS) (average molecular weight 2000 kDa), respectively. 1-methyl-2-pyrrolidone (NMP) and polyethylene glycol (PEG) (Molecular weight 6 kDa) were used as solvent and pore former, respectively. Bovine serum albumin (BSA) (Molecular weight 68 kDa) and humic acid (HA) were used as model protein and foulant, respectively. The complete details of all the chemicals is reported in Chapter 2 (Table 2.1).

Content of this chapter is published as below:

R. Singh and M. K. Purkait, Role of poly(2-acrylamido-2-methyl-1-propanesulfonic acid) in the modification of polysulfone membranes for ultrafiltration, Journal of Applied Polymer Science 134 (37) (2017) 45290.

3.1.2. Membrane preparation

Membranes of flat sheet configuration were prepared by the technique of non-solvent induced phase separation (NIPS). The amount of PSF and PEG were fixed at 12 wt% and 8 wt%, respectively. The amount of AMPS was varied from 1 - 4 wt% and rest was NMP. The membrane was prepared using phase inversion method, which is explained in section 2.2 of Chapter 2. The prepared membranes were named as MR0, MR1, MR2, MR3, and MR4 on the basis of increasing order of the AMPS content of 0 - 4 wt% and shown in Table 3.1.

Table 3.1. Constituents of the prepared membranes

Membrane	PSF (wt%)	PEG 6000 (wt%)	AMPS (wt%)	NMP (wt%)
MR0	12	8	0	80
MR1	12	8	1	79
MR2	12	8	2	78
MR3	12	8	3	77
MR4	12	8	4	76

3.2. Membrane characterization

3.2.1. Morphological and constituent studies

The morphological analysis of the membranes was carried out by using field emission scanning electron microscope (FESEM). These images directly provide the top layer visual information as well as cross sectional information of the membranes. Atomic force microscopy (Agilent, Model 5500 series) was used for measuring the surface roughness of

the prepared membranes. The details of the characterization techniques is mentioned in Chapter 2.

The presence and stability of the AMPS in the membrane was confirmed by Fourier transform infrared (FTIR) spectroscopy as explained in section 2.3.7 of Chapter 2. The stability check for the AMPS additive was carried out by taking 20 ml of DI water into 100 mL conical flasks to which membrane samples of 3 cm^2 area were added. These conical flasks were kept in an incubator cum shaker at STP conditions for 72 h at 150 rpm. On completion of the run the water from the conical flasks was taken and analyzed by using FTIR technique as mentioned previously.

3.2.2. Characterization by permeation experiments

3.2.2.1. Membrane compaction

As explained in Chapter 2, a membrane cell of 350 ml capacity was used to carry out the permeation experiments. The compaction of the prepared membranes was done at a pressure of 240 kPa for 2 h. The compaction factor was calculated by using Eqn. 2.11.

3.2.2.2. Pure water flux and hydraulic permeability (Pm)

The pure water flux (PWF) is one of the most important membrane traits, which talks about the membranes quality. The PWF of all the prepared membranes was calculated by using Eqn. 2.10. Hydraulic permeability is important for the pressure driven separation processes. It was calculated Eqn. 2.12.

3.2.2.3 Equilibrium water content (EWC)

Equilibrium water content is important in case of membrane characterization as it is directly related to the porosity of a membrane and indirectly deciphers the extent of hydrophilicity or hydrophobicity of a membrane [24]. For calculation of EWC of a membrane the

preocedure explained in Chapter 2 was followed. Briefly, a membrane with dimensions 3 × 3 cm is taken and soaked in DI water for overnight. After mopping with tissue paper the membranes were dried in a vacuum oven for 24 h at 60°C. EWC of the membranes was calculated by using Eqn. 2.13.

3.2.2.4 Membrane porosity

Porosity is the property of a membrane which depicts the permeation and separation quality. It was calculated by using Eqn. 2.14.

3.2.2.5 Membrane contact angle

Static water contact angle (SWCA) was measured to know the membrane hydrophilicity. Lesser the SWCA, higher will be the hydrophilicity of the membranes and vice-versa [55]. The procedure for SWCA measurement is given in chapter 2.

3.2.3. Ultrafiltration experiment

Solute separation and permeate flux ultrafiltration experiments were performed using the same batch cell as explained in section 2.3.8 of Chapter 2. The effect of AMPS on solute separation and permeate flux of the membrane was analysed in this study. The BSA and HA rejection was estimated by using Eqn. 2.15. The water flux (J_{w1} and J_{w2}) in L/m^{2}h were calculated using Eqn. 2.10 at 100 kPa after membrane compaction at 240 kPa using DI water for 1 h.

3.2.4. Antifouling Property

The membrane fouling causes flux loss (J_{w1} - J_p). This flux loss was caused by total fouling (F_t), reversible fouling (F_r), and irreversible fouling (F_{ir}). These fouling resistances were calculated by using Eqns. 2.18, 2.19 and 2.20, respectively.

3.2.4.1. Preparation of the HA Stock Solution

A stock solution of HA (1000 mgL^{-1}) was prepared by adding 1 g of HA into 0.1 M NaOH solution of 100 ml to accomplish HA removal study from the water with the help of the prepared membranes. After complete mixing of HA into the solution the total quantity was made to 1000 ml by adding 900 ml of DI water to the 100 ml solution. pH of the solution was made 7 immediately by using 4 M HCl. The final HA solution was again stirred for the next 4 h at STP conditions. After stirring Whatmann 41 filter paper was used to filter the solution. From this prepared stock solution known concentrations of 10 mgL^{-1} and 50 mgL^{-1} were made by diluting with DI water and were utilized to carry out the HA removal experiments.

3.2.4.2. HA Separation Experiment

The PWF and UF experiments with the BSA was depicted that the membrane MR4 gives a better antifouling and flux profile and thus used for the separation experiments for HA. After the successful preparation of two different HA solutions of concentration 10 mgL^{-1} and 50 mgL^{-1}, these solutions were permeated through the MR4 membrane. The fashion in which these experiments were carried out was similar to the experiments explained in Chapter 2. Firstly, DI water was permeated through the membranes. Secondly, HA solutions of 10 mgL^{-1} and 50 mgL^{-1} concentrations were permeated through the membranes. Finally, the membranes after completion of the HA solution permeations were cleaned with DI water and the second run of DI water was completed. The first, second and last run was named as J_1, J_{HA} (in case of the HA solution), and J_2, respectively. The equations and methods used for the calculations of flux and HA rejection by the membranes were same as explained in the case of BSA UF experiments. Concentration of HA was measured using UV-Vis spectrophotometer at 254 nm wavelength.

3.2.5. Response surface methodology

The response of BSA flux and rejection was systematically studied by using response surface methodology (RSM) for the prepared membranes. The software Design Expert 7.0.0, Stat-Ease, Inc., Minneapolis, USA was used to carry out the study. In RSM methodology, analysis can be done by assigning two values for the each concerned factor, which are -1 for minimum score (x_{min}) and +1 for maximum score (x_{max}). These transformed variables -1 and +1, of no particular units, are known as coded variables (Z). The relation used for the transformation of these coded values is:

$$Z = \frac{x - [\frac{x_{max} + x_{min}}{2}]}{[\frac{x_{max} - x_{min}}{2}]} \quad 3.1$$

The BSA flux and rejection were analyzed by using face centered central composite design (FC^3D). The variables time (min) and pressure (kPa) were used to find out the effects on the two factors under consideration viz. BSA flux and rejection. The experimental data was fitted in the FC^3D by using the following second order non-linear polynomial equation [56] and presented in Table 3.2.

$$Y = \beta_o + \sum_{i=1}^{n} \beta_i X_i + \sum_{i=1}^{n} \beta_{ii} X_i^2 + \sum_{i=1}^{n-1} \sum_{j=i+1}^{n} \beta_{ij} X_i X_j + \varepsilon \quad 3.2$$

where, Y represents the response (BSA flux (F) and rejection (R)), n represents the number of variables, β_o, β_i, β_{ii}, and β_{ij} represents the model intercept term, linear effect term, square effect term, and the interaction effect term, respectively. X_i and X_j represents the level of the independent variables and ε represents the random error.

Table 3.2. Analysis of variance based on the second order polynomial models as per the RSM-FC^3D experimental design

S. No.	Variable	Membrane	Flux	Rejection
1.	F-value	MR0	287.36	53.36

		MR1	114.27	27.46
		MR2	197.44	24.81
		MR3	685.44	25.80
		MR4	896.75	25.36
2.	Coefficient of variations (%)	MR0	4.17	0.68
		MR1	2.95	1.00
		MR2	3.36	1.03
		MR3	1.66	1.00
		MR4	0.99	1.04
3.	Determination coefficient (R^2)	MR0	0.9952	0.9744
		MR1	0.9879	0.9515
		MR2	0.9930	0.9466
		MR3	0.9980	0.9485
		MR4	0.9984	0.9477
4.	Adequate precision values	MR0	60.617	25.576
		MR1	38.750	18.071
		MR2	48.948	17.547
		MR3	85.678	17.920
		MR4	105.085	17.829
5.	Predicted error sum square	MR0	249.94	20.06
		MR1	589.03	51.68
		MR2	1773.96	55.18

		MR3	830.59	50.48
		MR4	610.23	56.84

This equation (Eqn. 3.1) will adequately provide the optimum set of operating conditions for BSA flux and rejection. The resulted responses were further optimized by using the Derringer's desirability function methodology [57]. The resulted responses were converted into individual desirability function d_i. The desirability function varies over a range of 0 to 1, where 0 and 1 represents complete undesirability and desirability, respectively. The overall desirability was determined as:

$$D = \left(\prod_{i=1}^{n} d_i\right)^{\frac{1}{n}} \quad 3.3$$

where, D represents overall desirability, d_i the individual desirability and n the number of responses. The criterion's used for individual desirability are mentioned below:

$$d = \begin{cases} 0, & y < L \\ \left(\dfrac{y-L}{U-L}\right)^{r}, & L \le y \le U \\ 1, & y > U \end{cases} \quad 3.4$$

where, L represents the lower response, U is the higher response, and r is the weight factor.

3.3. Results and discussion

3.3.1. Morphological and elemental analysis

3.3.1.1. Top surface and cross section

Figure 3.1a shows the top surface of the all prepared membranes (air side). It may be seen that the pores are uniformly formed and distributed throughout the membranes. The density of the pores is also high. PEG used in the membrane act as the source for pore formation as well as to induce hydrophilicity in the membranes in addition to AMPS. This is due to the fact of instantaneous demixing of solvent and non-solvent which results into a highly

porous membrane [58,59]. The gradual increase in the wt% of AMPS from 0 wt% to 4 wt% helps in the enhancement of the porosity in the membranes. This is also because of the fact that a high molecular weight additive considerably changes the morphological structure of the membrane [60]. Therefore, the membranes acquired high porosity, well interconnected pores, and less macrovoid formation. This was also corroborated with the flux behaviour discussed in subsequent sections.

Figure 3.1b shows the cross sectional images of all the prepared membranes. The images clearly show three regions viz. upper selective skin layer (air side), bottom sponge like layer (glass side) and a middle porous sub-layer containing finger like channels. The canals (the finger like structures) are starting from the top layer and going throughout the membrane up to the bottom layer showing the pores are continuous in nature. Function of the skin layer is to impart selectivity in the membrane and a porous sub-layer provides support to the membrane. The channel formation in the membrane is explained in preceding section while explaining the membrane top surface. The increase in the wt% of AMPS from 0 – 4 wt%, gradually increases and makes the membrane more porous. Results of BSA and HA rejection are in agreement with the phenomena and explained in the subsequent sections.

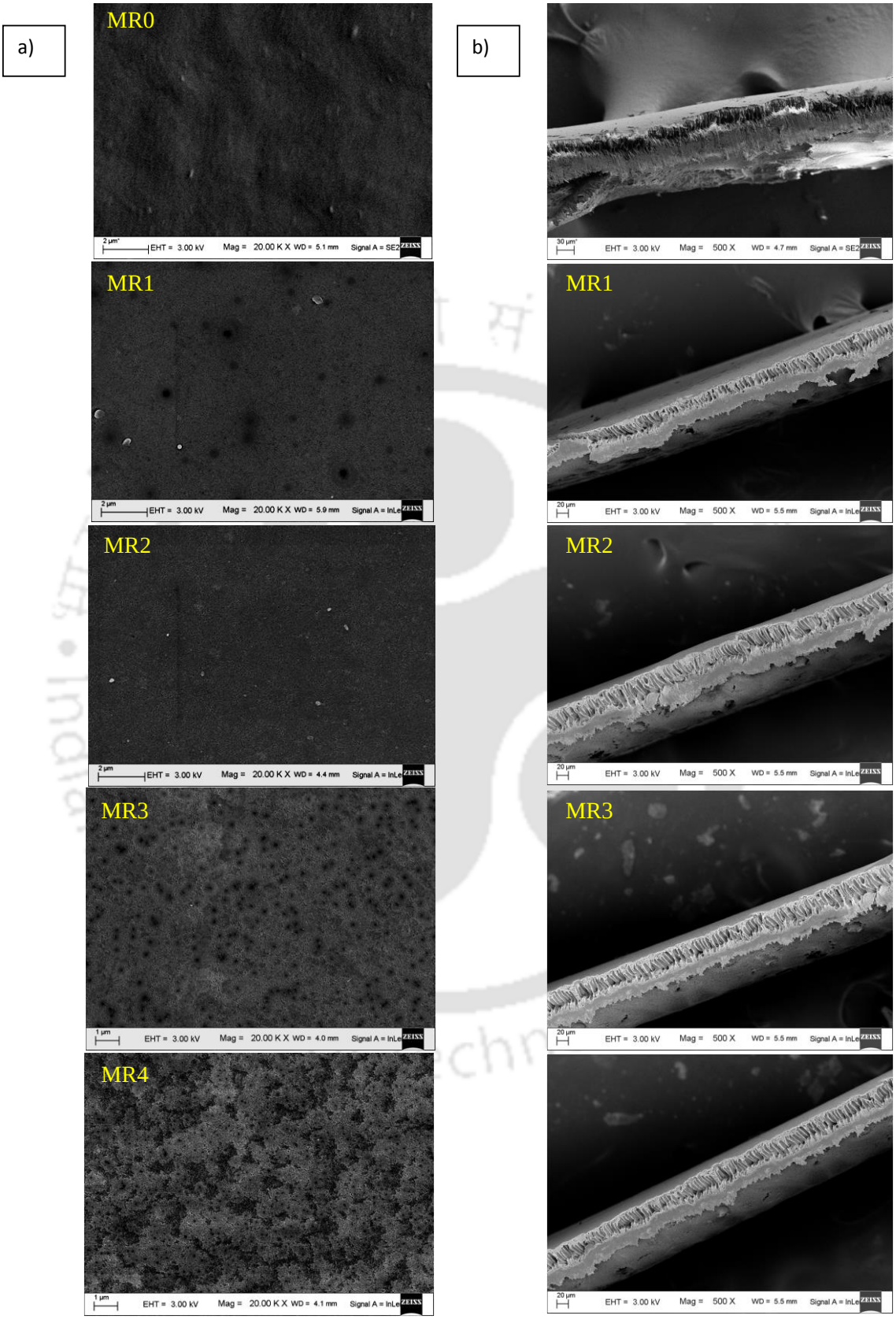

Figure 3.1. FESEM images of the membranes: a) Top surface b) Cross section

FESEM of top surface images were used for pore size analysis of 5 membranes by using ImageJ software as explained in Chapter 2 and shown in Fig. 3.2. The calculated pore sizes are 3.43 nm, 4.07 nm, 6.4 nm, 7.20 nm, and 8.48 nm for MR0, MR1, MR2, MR3, and MR4 membranes, respectively.

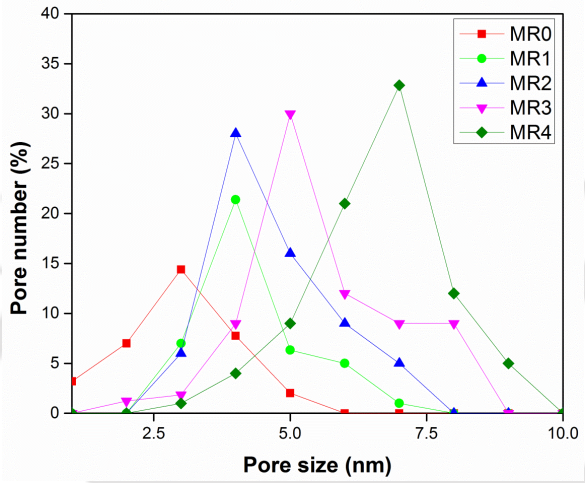

Figure 3.2. Pore size distribution of the membranes

3.3.1.2. AFM Analysis

AFM images of prepared membranes with different wt% of AMPS are presented in Fig. 3.3. It is observed from the topographical images of the prepared membranes that as the wt% of the additive (AMPS) increases from 0 – 4 wt% in the membrane their surface roughness also increases. Average roughness values for the prepared membranes are given in Table 3.3. The reason for this increase in the roughness of the membranes is the addition of hydrophilic AMPS. During the phase inversion process the hydrophilic end group comes to the surface and the long chain of the AMPS stays with the bulk PSF phase. This results in rougher membrane surfaces as the wt% of the AMPS varies from 0 – 4 wt% [15,61].

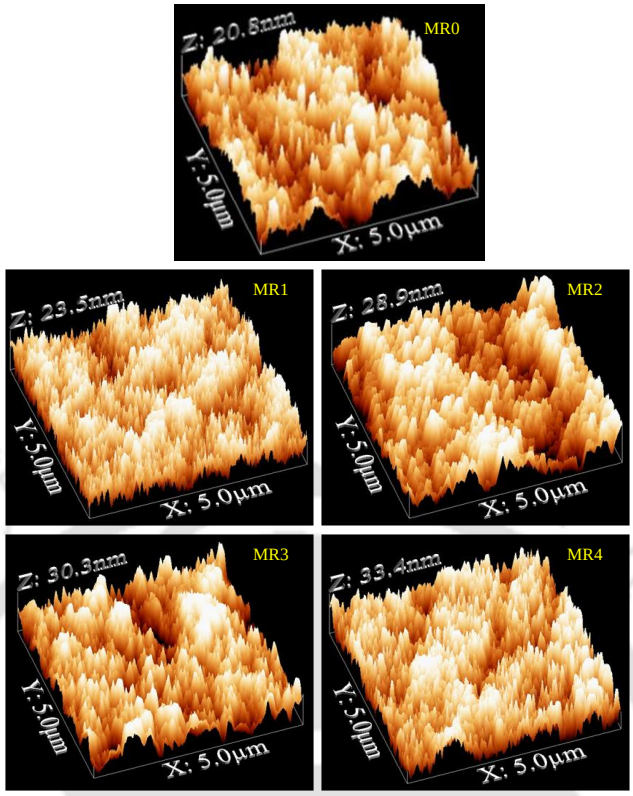

Figure 3.3 AFM 3D topographical images of the membranes

Table 3.3. Some of the characterization parameters of the prepared membranes

Membrane	Average Roughness (nm)	P_m (L m^{-2} h^{-1} kPa)	CF	EWC (%)	Porosity	Average Pore Size (nm)	SWCA (°)
MR0	5.30	0.65	8.11	21.74	0.024	3.43	68.23± 1.0
MR1	5.52	0.79	6.53	57.58	0.24	4.07	62.63 ± 2.0
MR2	5.64	1.10	4.77	62.5	0.33	6.4	57.28 ± 1.0
MR3	6.08	1.38	4.80	66.24	0.43	7.2	53.14 ± 1.5
MR4	6.42	2.01	4.55	71.45	0.58	8.4	49.83 ± 2.0

3.3.1.3. FTIR Analysis

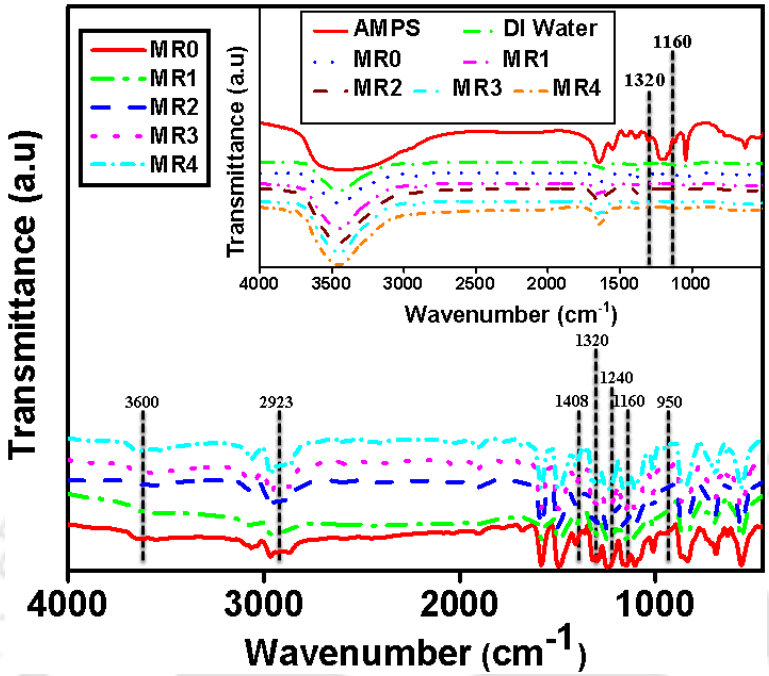

Figure 3.4. FTIR analysis of the membranes (MR0-MR4). Inset: The stability analysis of AMPS in the membranes

Figure 3.4 shows the FTIR analysis of the membranes. It is known that in the range of 1300 cm^{-1} – 1350 cm^{-1} both sulfones and aromatic secondary amines have strong adsorption bonds at 1320 cm^{-1} and 1160 cm^{-1}. This signifies the presence of both PSF and AMPS in the membrane matrix. Presence of PSF is also confirmed by the peaks at 1240 cm^{-1} for C-O-C vibrations and at 1408 cm^{-1} for the vibration of aromatic rings. Peak at 2923 cm^{-1} shows the C-H asymmetric stretch for the pore former which is somewhat vanished as it's not distinctively observable. This confirms that it is coming out of the casting solution by playing its role of a pore former. The peak at 950 cm^{-1} is also of the pore former and is not very prominent. This supports the presence of the pore former in the membrane, but in a recessive state. Sulfones also have an adsorption range from 1120 cm^{-1} to 1160 cm^{-1} which is faded in this case.

The inset of Fig. 3.4 shows the results for the stability analysis of AMPS in the membranes. The membrane results were compared with DI water and pure AMPS so as to depict removal of AMPS, if any. The curves for the membrane samples shows that there is no peak available matching with AMPS, which confirms that there is no removal of AMPS from the membranes even after long exposure. The additive AMPS is firmly embedded in the membranes, which further strengthens the discussion of the preceding sections that AMPS plays a role in the hydrophilicity and antifouling nature of the membranes. Thus membranes can be used for longer period of time.

3.3.2. Additive effect on membrane permeation

Compaction factor (CF), pure water flux (PWF), hydraulic permeability (P_m), equilibrium water content (EWC), porosity, hydrophilicity and protein (BSA) permeation studies were performed to observe the effect of additive (AMPS) on the membrane morphology.

3.3.2.1. Study of CF with increasing Wt % of AMPS in the membranes

CF of a membrane is the factor by which a membrane can be compacted and signifies the presence or absence of macrovoids in the membrane. More the number of macrovoids in the membrane higher will be the compaction factor or vice versa. The results of membrane compaction with time are shown in Fig. 3.5. This infers about the effect of increasing wt% of AMPS on the PWF of the membranes. The PWF declines drastically for first 45 min for all the membranes and attain steady state after 60 min. The reason behind this is the presence of channels and a reduction in the pore size of the prepared membranes. With time at an applied pressure the channels suppresses as the walls of the channels and pores come closer. This reduces the pore size of the membranes and by virtue of which the permeate flux reduces. The other reason for the decline in flux for first 40-60 min are the inherent properties of the additive. The additive AMPS is a hydrogel, which on contact with water

swells and thus even though the membranes are compacted but have shown a flux profile as in Fig. 3.5.

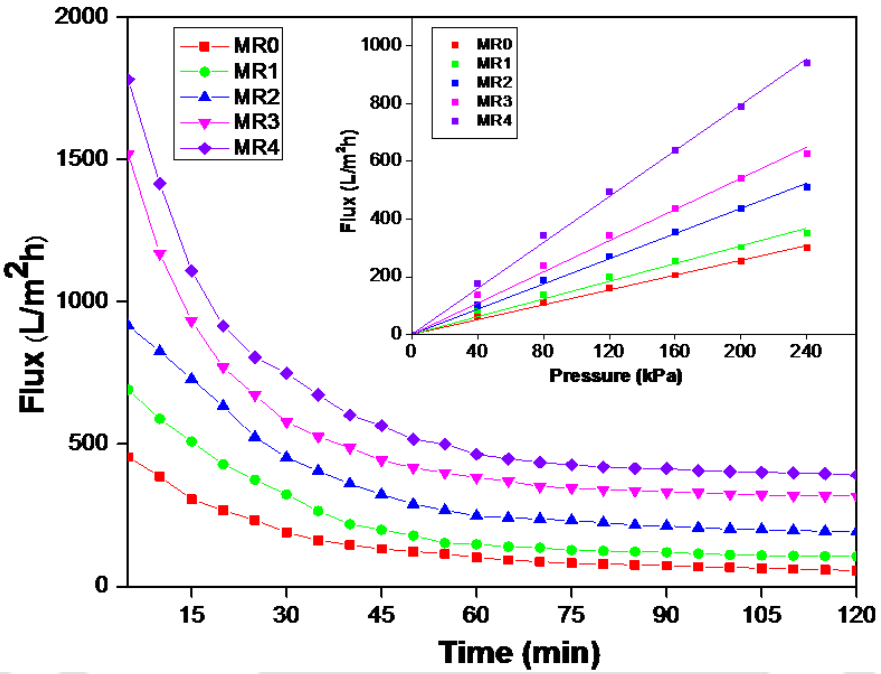

Fig. 3.5. Flux profile of the membranes during compaction with time and pressure (inset)

The figure depicts that the PWF increases with increase in AMPS. It can also be seen that the steady state flux increases from 101.76 L/m^{2}h (MR0) to 464.06 L/m^{2}h (MR4). All the flux values shown in this study are having an error value in the range of 1-2%. The flux decreases with time and attains steady state after 60 min of operation. This can be described by the fact that additives added to the membranes can increase or decrease the channel formation in the membranes. This also depends on the molecular weight and the amount of the additives used [24].

3.3.2.2. Study of PWF and hydraulic permeability

The flux profiles of the prepared membranes were analyzed by measuring PWF at various transmembrane pressures (0 kPa to 240 kPa) and shown in Fig. 3.5 (Inset). The results infer

that with the increased amount of AMPS, the PWF increases. For example, at 160 kPa PWF increases from 205.64 L/m^{2}h (MR0) to 638.45 L/m^{2}h (MR4). The results agree with that of CF study. Also the PWF increases linearly for all the membranes because of the increasing effective driving force (transmembrane pressure). Hydraulic permeability (P_m) of the prepared membranes was calculated by the slope of the graph (Inset of Fig. 3.5) using Eqn. 2.12 and shown in Table 3.3. The P_m of all the membranes has shown similar trends as that of CF and PWF. P_m increases from 0.65 L/m^{2}hkPa (MR0) to 2.01 L/m^{2}hkPa (MR4). The permeability result clearly shows that, in addition to AMPS, PEG 6000 also helps in pore formation as well as in increasing the hydrophilicity of the membranes. Fane et al. described the relation between pores and permeability for UF membranes [62]. More number of pores means more permeability of the membrane, which is applicable in this study also. Feng et al. justified the statement that the additives with high molecular weights if added to the membranes get accumulated inside the membrane because of their high molecular weight and make it quite difficult for the additives to get out of the membranes [63]. This higher molecular weight sustains the additives, in this case AMPS and PEG, in the prepared membranes and thus leads to the increase in hydrophilicity of the prepared membranes.

3.3.2.3. Study of EWC of the prepared membranes

EWC is in a closed relationship with PWF as both the entities depends upon the number of pores and cavities present in a membrane [33]. In this study, the EWC values are calculated by using Eqn. 2.13 and the values are shown in Table 3.3. The trend shown by the values is same as in the case of PWF. The values are increasing from 21.74% (MR0) to 71.45% (MR4). This confirms that with increased wt% of AMPS the number of pores increases in the membranes.

3.3.2.4. Study of porosity and hydrophilicity

High porosity and hydrophilicity are the required traits of a good membrane. In this study, porosity of the membranes was calculated by using Eqn. 2.14. Hydrophilicity was depicted by calculating the SWCA of the membranes. The values of both, porosity and SWCA are given in Table 3.3. It can be seen that the porosity is increased from 0.024 (MR0) to 0.58 (MR4). SWCA also decreases from 68.23° (MR0) to 49.83° (MR4), which shows that the hydrophilicity is higher for membranes having higher wt% of AMPS. The results are totally in agreement with the results of the PWF study of the membranes. The additive is added to the casting solution enhances the mixing of solvent and non-solvent and thus results into a highly porous membrane. On the other hand, after a limit the addition of an additive to the casting solution delays the mixing process of solvent and non-solvent and results in a less porous dense membrane [63]. AMPS and residual PEG 6000 in the membrane, result into increased hydrophilicity and antifouling nature of the prepared membranes. This is the reason for the decrease in SWCA of the membranes.

3.3.3. Protein permeation studies

Permeation studies were carried out to analyze the antifouling nature of the membranes using BSA (1000 mgL^{-1}) and HA (10 mgL^{-1} and 50 mgL^{-1}) as a model protein and pollutant, respectively. Flux and rejection behavior was observed and critically analyzed. The variation in rejection behavior and corresponding flux values are shown in Fig. 3.6. At first, water permeation results are shown (J_{w1} and J_1). BSA (J_P) (Fig. 3.6) and HA (J_{HA}) (Inset of Fig. 3.6) permeation results are shown thereafter. Followed by cleaning are shown water permeation experiments (J_{w2} and J_2). The extent of irreversible fouling was observed from the permeate flux declination of the second water permeation run. The values of flux,

rejection, reversible and irreversible fouling values are determined using Eqns. 2.10, 2.15, and 2.18-2.20. The outcomes are shown in Table 3.4.

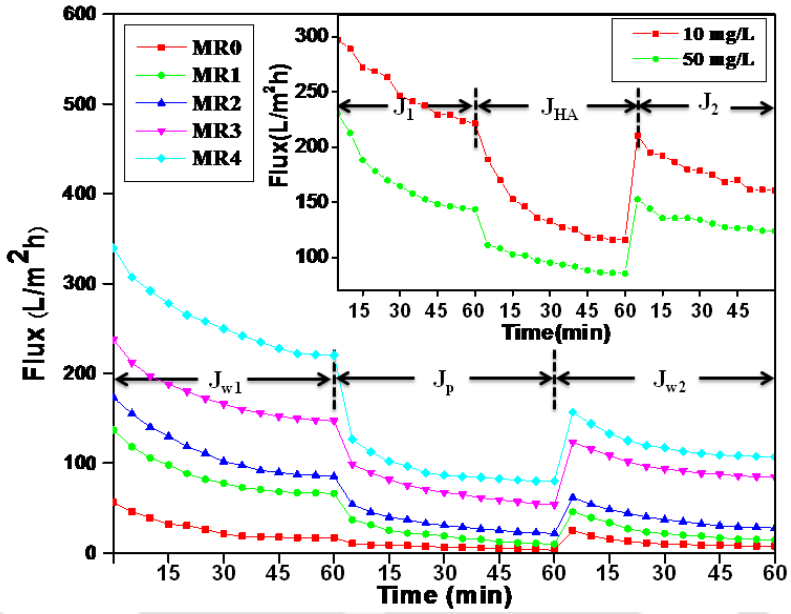

Figure 3.6. Ultrafiltration profile of the membranes with BSA (1000 mgL^{-1}) and HA (inset) 10 mgL^{-1} and 50 mgL^{-1}

Table 3.4. Flux based characterization parameters of the prepared membranes with BSA

Membrane	J_{w1} (L/m^2h)	J_p (L/m^2h)	J_{w2} (L/m^2h)	F_r $(\frac{J_{w2}-J_p}{J_{w1}})$	F_{ir} $(\frac{J_{w1}-J_{w2}}{J_{w1}})$	F_t $(1-\frac{J_p}{J_{w1}})$	$Flux_{RR}$ $(\frac{J_{w2}}{J_{w1}}\times 100)$
MR0	25	6.51	11.96	0.21	0.74	0.95	47.85
MR1	81.83	19.23	24.23	0.06	0.76	0.82	29.61
MR2	107.82	32.34	39.01	0.06	0.70	0.76	36.18
MR3	168.87	69.49	96.76	0.16	0.58	0.75	57.30
MR4	251.36	92.18	120.88	0.11	0.63	0.74	48.09

From the figure it may be seen that pure water flux (J_{w1}) changed moderately prior to the UF of BSA but initially there is a steep decrease in the flux when UF of BSA and

HA is done. This is because of the deposition or adsorption of proteins on the membrane surface, which reduces the pore size of the prepared membranes. This tendency of protein deposition or adsorption of a membrane depends on both the hydrophobicity of the membrane and electrostatic interactions between the protein molecules and membrane surface [64]. The initial decline in the BSA flux stabilizes at later stages and steady state flux (J_p) was obtained. The BSA and HA rejection studies are shown in Fig. 3.7.

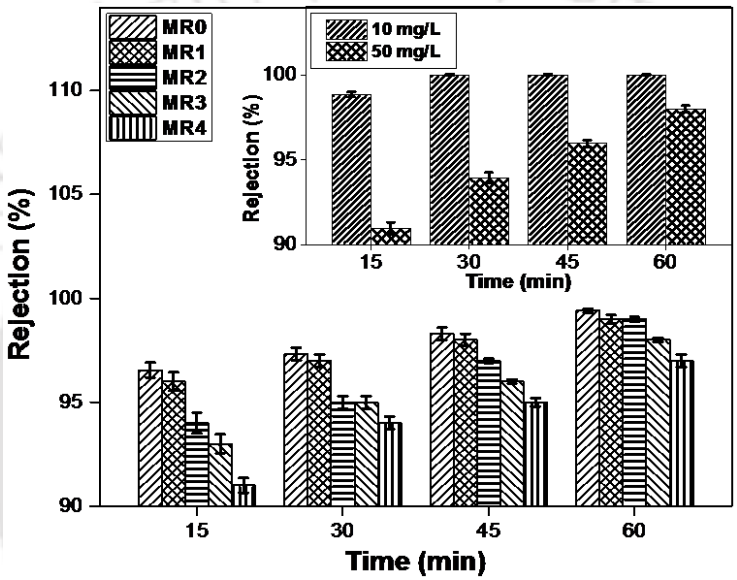

Figure 3.7. BSA and HA (inset) rejection profile of the membranes

It is evident from the figure that all the membranes show comparative BSA and HA rejection after a run of 1 h. Membrane MR0 shows highest rejection of 100 % and MR4 lowest i.e., 97% of BSA. The reasons for this have been explained in preceding sections based on membrane porosity. It is explicable that if the porosity of a membrane is low, then it will give highest rejection and vice versa. The permeated HA solutions were analyzed by using UV-Vis spectrophotometer at 254 nm and calculated percentage rejection or separation of the HA by the membrane. The % rejection of HA is shown in Inset of Fig. 3.7. The figure depicted that 100% rejection is obtained for the initial HA concentration of 10 mgL^{-1} after 15 min. whereas, 98% rejection was obtained for 50 mgL^{-1} of HA. This 2%

decrease in rejection value was due to the increased concentration polarization. This has also been reflected in the flux value discussed in preceding section. A comparative study on the efficacy of various membranes for the separation of HA is shown in Table 3.5. It may be concluded that the present membrane may be used as an alternative to other membrane for the separation of HA.

Table 3.5. Comparison of HA removal with present and past studies

Membrane material	Additive	Concentration (mgL^{-1})	pH	% Removal*	Reference
Regenerated Cellulose	-	50	-	90.00	65
PES	XA	10	7.0	94.00	66
PSF	PVA/ZnO	5	7.0	87.65	67
PES	DBA/GA	1000	7.0	~90.00	68
TiO_2/Fe_2O_3 Nanowires	-	200	-	98.00	69
PES	ZnO	10	7.7	97.98	70
CA	OMMt	-	-	95.05	71
CA	SMM	1000	6.9	96.00	72
PPSU	SPPSU/MgO	300	8.0	91.70	73
PPSU/PEI	PEG/AC	1400	6.7	80.00	74
PSF	**AMPS**	**10/50**	**7.0**	**99.00/98.00**	**Present work**

*Highest rejection reported in the study

Reversible fouling can be escaped by simple washing of the membrane with water and on the other side the irreversible fouling can be removed by either chemical cleaning or enzyme degradation. Higher total fouling value signifies flux decline, as a decrease in flux. This depends upon the membrane pore size as fouling either narrows or blocks the pores. Low total fouling values are desirable as it means less loss of the flux value. Figure 3.8 shows the positive effect of increasing wt% of AMPS in the hydrophilicity and the antifouling property of the membranes. It may be observed from Fig. 3.8 that the R_r decreases with amount (0 – 4 wt%) of AMPS in the membrane and the decreasing R_r values are 0.21 (MR0) to 0.16 (MR1), 0.12 (MR2), 0.10 (MR3) and 0.09 (MR4). Slight variation in the value of R_r for MR1 – MR4 was due to the presence of amount of AMPS. This value is also corroborated with the SWCA values of the membranes as shown in Table 3.2.

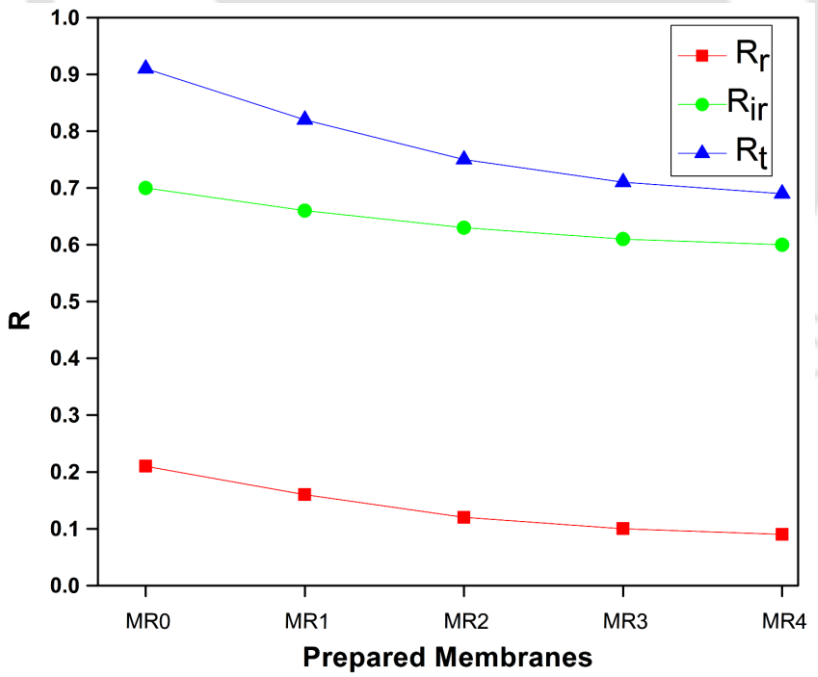

Figure 3.8. Reversible, irreversible and total resistances of the membranes MR0-MR4 with BSA

3.3.3.1. Protein permeation studies with varying pH values

Considering the PWF, MR4 was chosen for further permeation studies. BSA solutions (1000 mgL^{-1}) of different pH (4.7, 7 and 10) were used for the permeation experiments. The Isoelectric point (IP) of BSA is 4.7 at 25°C. The variation in permeate flux is shown in Fig. 3.9. It may be seen from the figure that the flux gradually decreases with time for all the three cases. However, at any time flux is less at pH 4.7. At 30 min the flux values are 15.4 L/m^2h, 25 L/m^2h and 36 L/m^2h for pH 4.7, 10 and 7, respectively. The reason behind these results can be explained on the basis of change in charge present on the membrane or BSA molecules. At IP the membrane has given the least flux as at this pH the BSA molecules doesn't contain any charge and thus remains in a compact structure and resulting concentration polarization over the membrane surface with time.

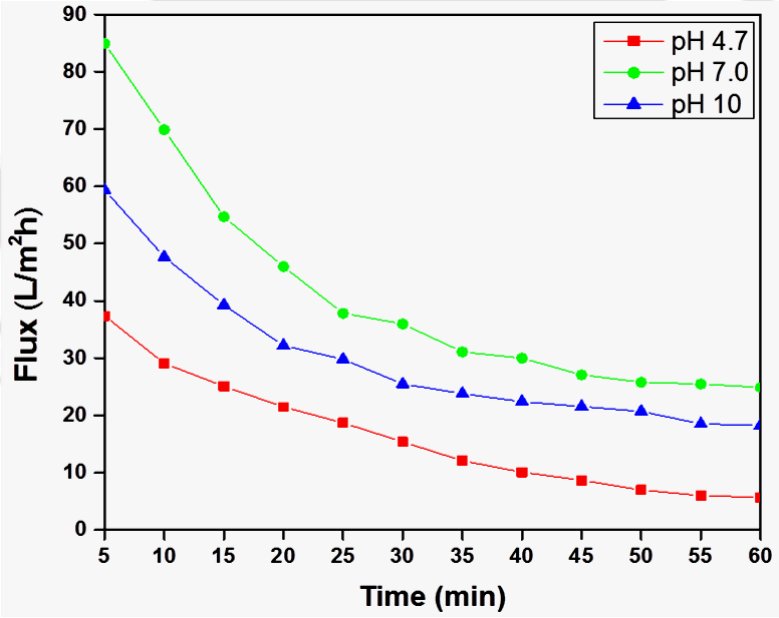

Figure 3.9. Ultrafiltration profile of the membranes with BSA solutions of different pH values

At pH 7, the BSA molecules remains negatively charged and thus the membrane gives a higher flux and higher rejection. The reason for this is the presence of charge on the BSA molecules which causes inter ionic repulsions and hinder the concentration polarization

over the membrane surface. The BSA molecules contain more negative charge at pH 10, this results in more rejection of BSA molecules and less flux by the membrane as compared to pH 7, which can be explained on the basis of coulombs law [41]. Thus, it can be said that the pH of the feed solution also plays a vital role irrespective of the membrane.

3.3.4. Response Surface Methodology

The time and pressure were taken in account for getting the best BSA flux and rejection profile by using RSM for the prepared membranes. The concentration and pH of the BSA solution was fixed at 1000 mgL^{-1} and 7, respectively. The experiments were carried out at different time and pressure values. The obtained data was fitted in the second order polynomial Eqn 3.1 for the BSA flux and rejection, respectively.

3.3.5. Model Accuracy Check

The verification of the developed model is requisite to confirm whether the model gives apt approximation of the experimental data or not. The reasonable fit confirms that the model is giving near to accurate results. The following sections discuss about various statistical parameters along with assorted diagnostic and influence plots to validate the accuracy of the model.

3.3.5.1. Statistical parameters for model accuracy

F-test for analysis of variance (ANOVA) was used for the statistical significance of individual interaction and quadratic terms of the model Eqn. 3.11. The quadratic models for the BSA flux and rejection for the prepared membranes were summoned in Table 3.6. The developed regression model has high significance as the model F-value for each response is high with a low probability value ($p < 0.001$).

The predicted models correlate well with the experimental data is confirmed by the F-value of lack of fit with the *p*-value greater than 0.05, which confirms that each response is not significantly relative to pure error. The previous statement is further backed up by the fact that each response has high R^2 (Determination coefficient) values, which also confirms a good correlation between the predicted and experimental values. The predicted R^2 and adjusted R^2 (Table 3.2) are in concurrence with the determination coefficient. This also point to a good fit of the models [42]. The signal to noise ratio tells about the adequate precision of the models. A value greater than 4 is desirable. In this study the adequate precision values for the responses F and R, are greater than 4 and successfully satisfy the criteria of a precise model. In addition to this, a low coefficient of variation advocates that the experiments are precise and consistent. Another factor, predicted error sum square (PRESS) analyses point fitting of a model in the design. For a better fitted model small values of PRESS are desirable. The PRESS values for F and R, are summarized in Table 3.2. It can be attributed from the PRESS values that the models are well fitted and can be used for the prediction of responses in a new experiment.

3.3.5.2. Diagnostic and influence plots

The diagnostic and influence plots for the best performing membrane in terms of hydrophilicity and antifouling nature were plotted in Figs. 3.10 and 3.11, respectively for membrane MR4. These plots communicates about the model adequacy. The residues (difference between the experimental and predicted values of response is the residual or random error) obtained were used to plot the diagnostic plots.

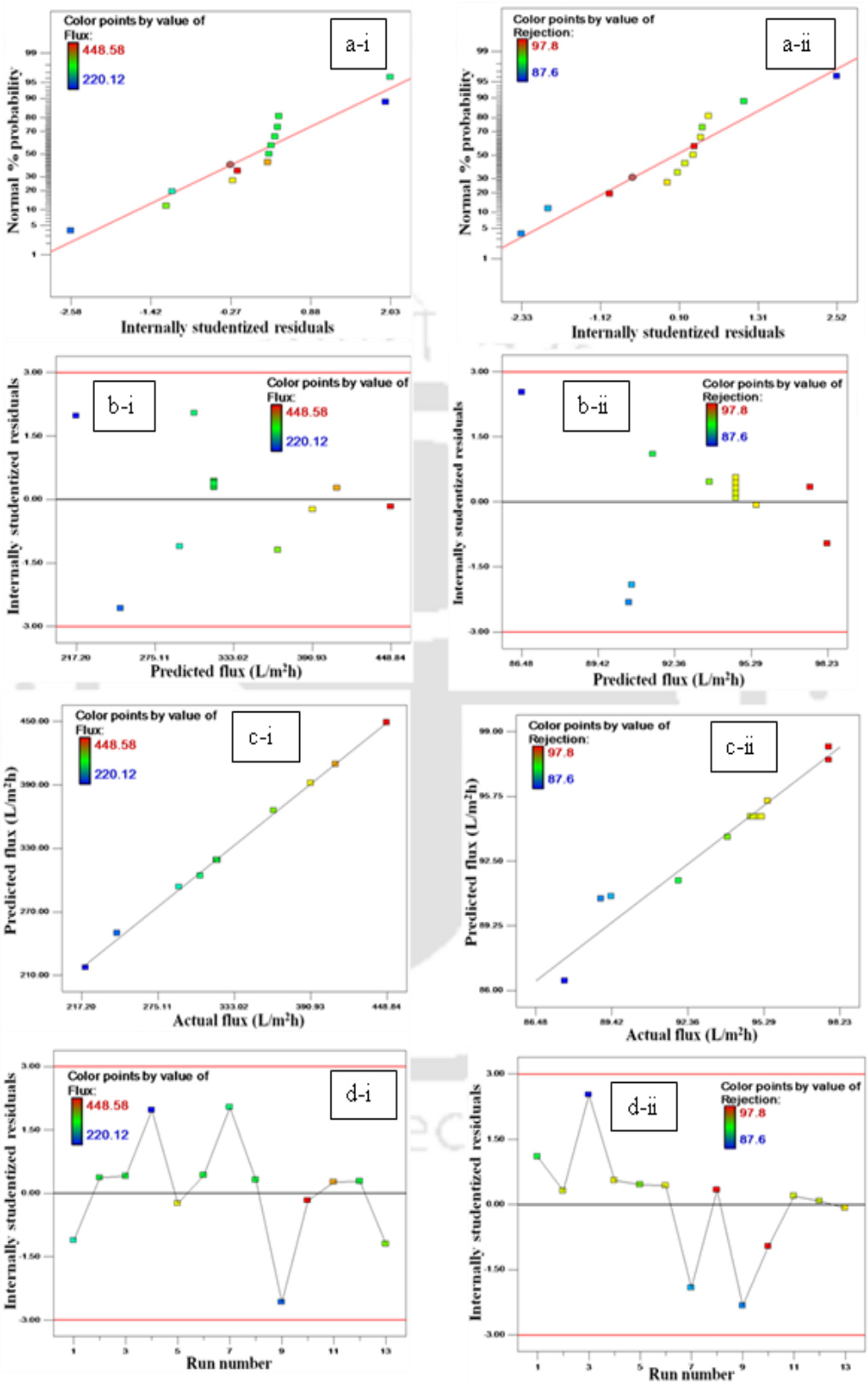

Figure 3.10. Diagnostic plots representing the adequacy of the predictive models for MR4 membrane

The normal probability plot for the studentized residual for the BSA flux and rejection is shown in Fig. 3.10 (a-i and a-ii). The residuals of the response being close to the straight line depicts that they are normally distributed. The residuals vs. the ascending predicted response values plot is shown in Fig. 3.10 (b-i and b-ii). The evidence of obvious patterns was not established in both the responses, in fact, the plots are random scatter. This indicates that there is no need for transformation. Fig. 3.10 (c-i and c-ii) explains the plot between the actual vs. predicted response values. The figure clearly depicts that the actual responses are very close to the predicted responses and the points for both lies very close to the 45° line. The results from the figures confirm that the developed models successfully confined the correlation between the process variables of the BSA flux and rejection. The plot of residuals vs. run number is shown in Fig. 3.10 (d-i and d-ii). The lurking variables, which may affect the dependent variables in the course of experimentation, were found out by using this plot. Accordingly, the data points should be scattered in the plot. It can be seen from the figure that the points are all scattered randomly and lies within the limit (±3). Thus, it can be said that the experimental data is satisfactory.

The plot of leverage vs. run number is shown in Fig. 11 (a). Leverage is the potential for design point, based on its position in the design space, to influence the fit of the model coefficients. Leverage, if equals to one point to a problem (unexpected error) with the data point and this unexpected error strongly affects the model. Since the leverage value is less than one for both the responses. Hence, there is no evidence of unexpected error and no outliers in the developed models in this study. The influence of each experimental run on each regression coefficient is measured by the variation in beta values (DFBETAS) plot (Fig 11 (b)). Larger the DFBETAS value larger is the influence of the specific observation on the particular regression coefficient. It can be seen from the DFBETAS plot (Fig 11 (b-

i and b-ii)) that there is no influence of any observation on any regression coefficient of the developed models for BSA flux and rejection.

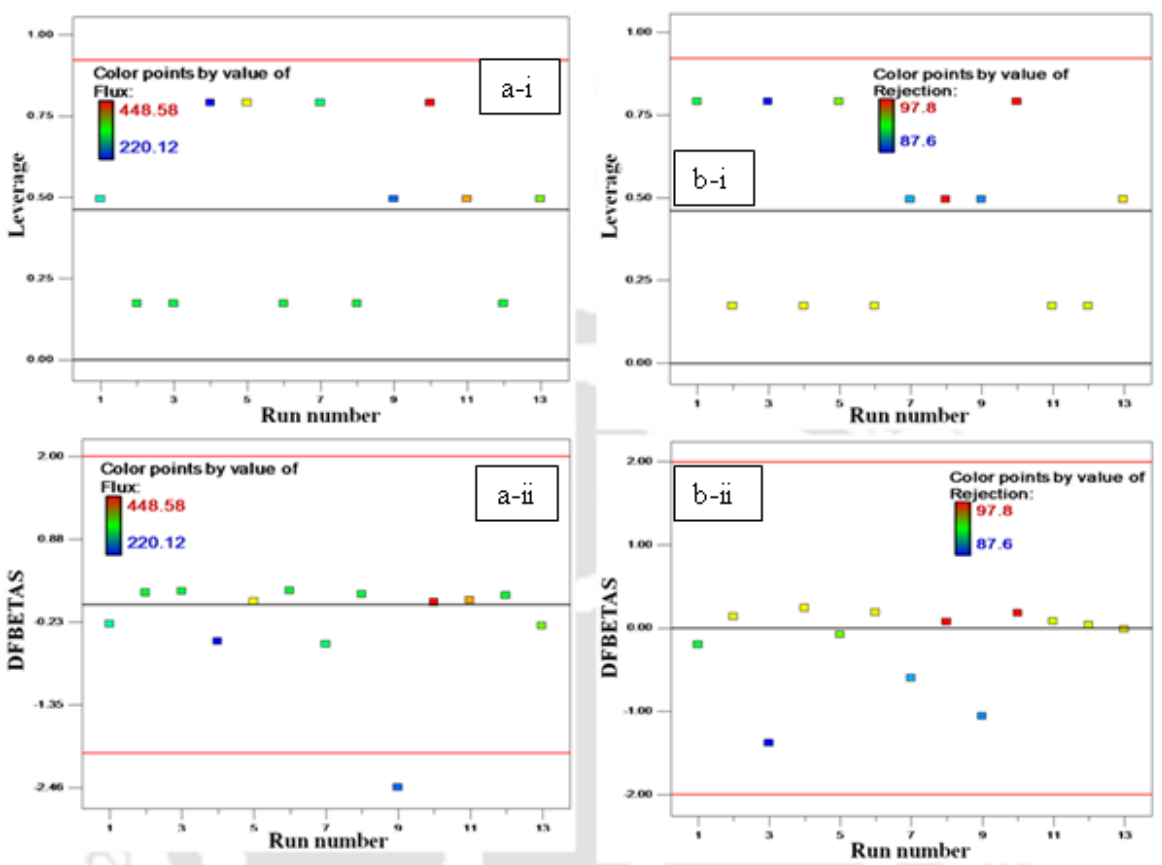

Figure 3.11. Influence plots representing the adequacy of the predictive models for MR4 membrane

3.3.5.3. Effect of the process variables on the BSA flux and rejection

The performance of the prepared membranes was evaluated on the basis of two important membrane parameters viz. BSA flux and rejection by considering the effect of time and pressure. The prepared membranes were investigated by using the FC^3D to analyze the performance of the membranes. The effects of the two variables on the selected parameters were shown in Figs. 3.12 and 3.13 and explained individually in the successive sections.

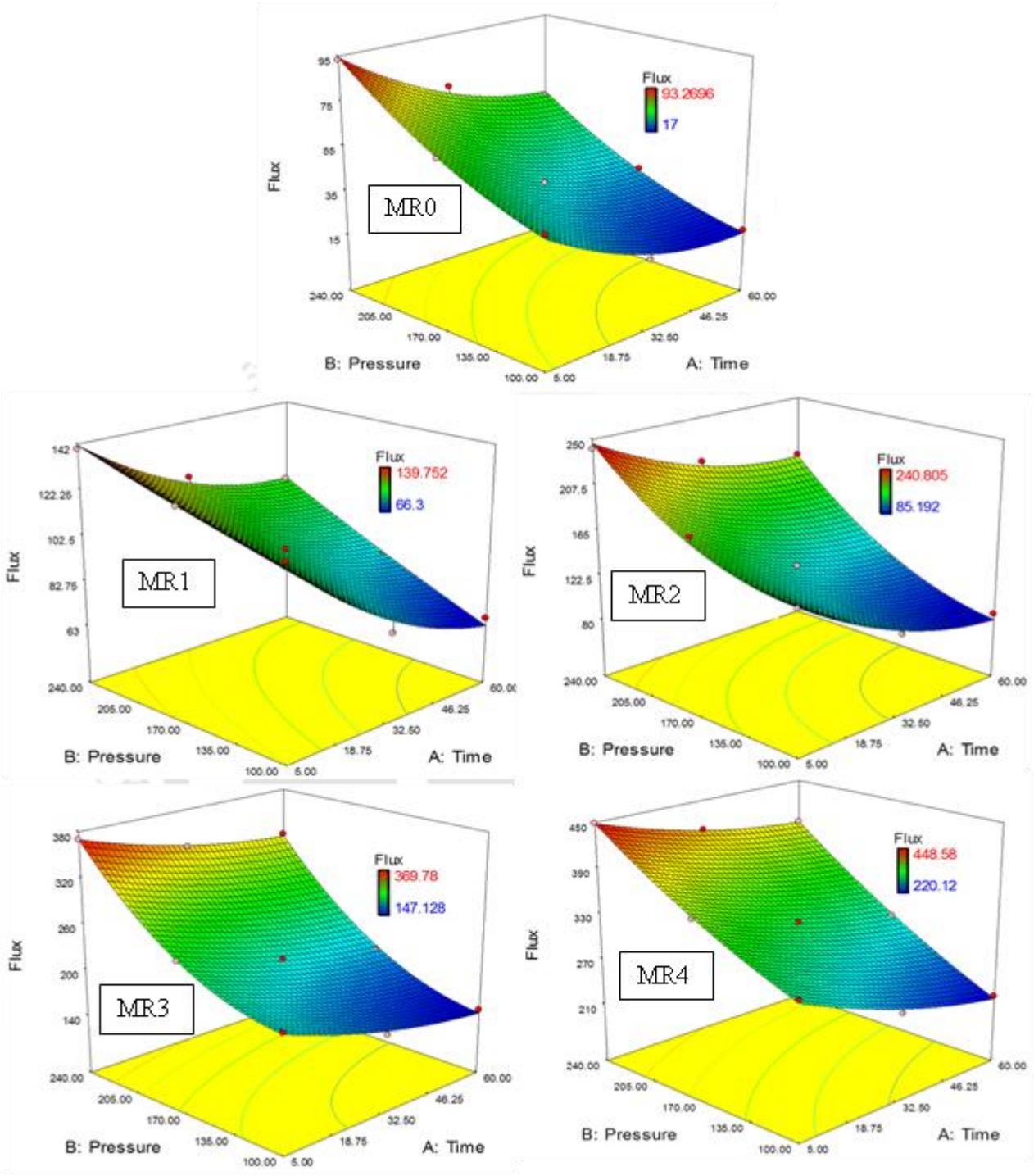

Figure 3.12. Response surface plot indicating the effect of time and pressure on the BSA flux for MR4 membrane

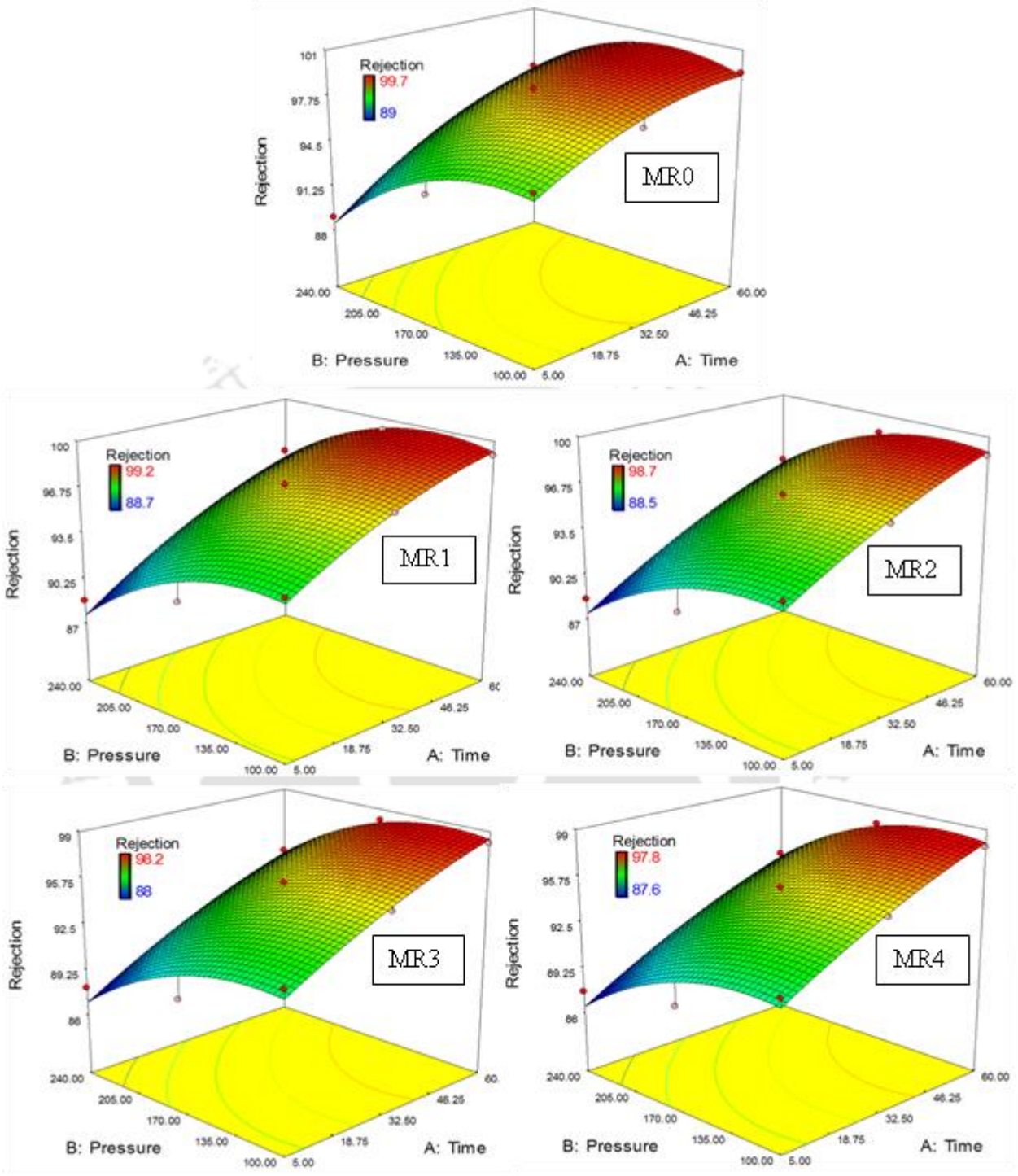

Figure 3.13. Response surface plot indicating the effect of time and pressure on the BSA rejection for MR4 membrane

3.3.5.4. BSA flux

In general, the BSA flux decreases with increasing time as discussed in the preceding sections. Similarly, here the BSA flux decreases with time. The BSA flux for the membranes is higher at lower time and higher pressure values and lower at increased time, where pressure has a little role to play. With time the flux decreases because of the deposition of BSA particles on the surface of the membrane. In case, the pressure is high then the deposition takes place at a higher rate as compared to lower pressures. Similarly, with more time of operation the deposition is high and vice versa. It can be seen from Figs. 3.12 and 3.13 that highest permeate flux (448.580 L/m^{2}h) is reported for the pressure and time 240 kPa and 5 min, respectively, for membrane MR4 and lowest (17 L/m^{2}h) for 100 kPa and 60 min for membrane MR0. The high and low flux values are the results of the high and low driving force. Though, it is clear from the Fig. 5 and Fig. 6 that the BSA flux values are lower than the pure water flux, reason being the presence of the BSA molecules in the feed. The BSA molecules create an additional resistance to the flow. It can be observed from the figures that the trend of flux and rejection are non-linear with the variation in the applied pressure. It can be said from this study that the applied pressure plays a role in the permeate flux but there are other factors which also contributes to the membrane separation process to a greater extent.

3.3.5.5. BSA rejection

The BSA rejection increases with time as the deposition layer increases with time on the membrane surface and act as a barrier for the BSA molecules to pass through. The applied pressure also plays a vital role in the rejection of BSA molecules. The rejection is lower at higher pressure for initial periods as there is a higher driving force which drives the BSA molecules through the membrane. Later in the membrane separation process due to the

deposition of BSA molecules on the membrane surface the BSA rejection increases. The interaction effects for BSA rejection on responses are shown in Fig. 3.13. The highest and lowest BSA rejections were reported for membrane MR0 (99.70 %) and MR4 (87.60 %), respectively. The predicted and experimental values of BSA rejection are significant and discussed well.

3.4 Summary

The additive AMPS was successfully used to increase the hydrophilicity and antifouling nature of the PSF flat sheet membranes. The incorporation of the additive in the membrane matrix shows a significant improvement in the flux profile as well as the antifouling behaviour of the membranes. There is an increment of 68% in the pure water flux of the membranes from MR0 to MR4. A decrease in the WCA from 68.238 (MR0) to 49.838 (MR4) was observed. Effect of additives were significantly found on the surface roughness, pore size, protein absorption resistance, EWC, Pm, and hydrophilicity of the membranes. Upon the addition of the additive the membranes surface roughness, EWC, Pm, and hydrophilicity was increased, whereas the protein (BSA) rejection was decreased. The prepared membrane was used for effective HA removal of 100% and 98% from the initial concentration of 10 mgL^{-1} and 50 mgL^{-1}, respectively. The response surface methodology was used successfully to define the parameters influencing the BSA flux and separation. The study was shown that all the individual, interaction and quadratic terms of variables influence the BSA flux and separation. The optimum conditions obtained were successfully validated experimentally. The comparison table has shown that the HA rejection was better than the earlier literature reported. This work would benefit the improved separation of proteins and pollutants on a larger scale

Chapter 4

Evaluation of mPEG effect on the hydrophilicity and antifouling nature of the PVDF-co-HFP flat sheet polymeric membranes for humic acid removal

In this chapter, modification of PVDF-co-HFP flat sheet membranes with methoxy poly(ethylene glycol) (mPEG) of three different molecular weights (550 Da, 2000 Da, and 5000 Da) is discussed along with its effects on the hydrophilicity and antifouling characteristics of the membranes. mPEG of different molecular weights was added with Poly(vinylidene fluoride-co-hexafluoropropylene) (PVDF-HFP) in N-methyl-2-pyrrolidone (NMP) to prepare the membranes by using non solvent induced phase separation (NIPS) technique. The improvements in the membrane attributes were studied under two categories viz. morphological and permeation. Field emission scanning electron microscopy (FESEM) and atomic force microscopy (AFM) were used to study the morphological properties of the prepared membranes. Presence and stability of the additive (mPEG) in the prepared membranes were confirmed by using the Fourier transform infrared spectroscopy (FTIR). Permeation studies of the prepared membranes were done in the form of pure water flux (PWF) and hydraulic permeability. Equilibrium water content (EWC) and water contact angle of the prepared membranes were calculated to analyse the increase in hydrophilicity of the prepared membranes. Antifouling studies on the prepared membranes were done by using bovine serum albumin (BSA) and humic acid (HA).

Content of this chapter is published as below:

R. Singh and M. K. Purkait, Evaluation of mPEG effect on the hydrophilicity and antifouling nature of the PVDF-co-HFP flat sheet polymeric membranes for humic acid removal, Journal of Water Process Engineering 14 (2016) 9–18.

4.1. Experimental

4.1.1. Materials

PVDF-co-HFP (MW: 400000 Da) and mPEG (550 Da, 2000 Da and 5000 Da) were used as based polymer and additive to prepare polymeric ultrafiltration membranes by using NMP as solvent and DI water as non-solvent in phase inversion process. Bovine serum albumin (BSA) (Molecular weight 68,000 Da) and humic acid (HA) were used as model protein and membrane foulant. The complete details of all the chemicals is reported in Chapter 2 (Table 2.1).

4.1.2. Fabrication of the polymeric membrane

The asymmetric membranes were prepared in the flat sheet configuration using the phase inversion technique by immersion precipitation as described in section 2.2 of Chapter 2. Composition of different membrane casting solutions is presented in Table 4.1.

Table 4.1. Composition of membrane casting solutions containing different molecular weight of mPEG

Membrane	PVDF-co-HFP (wt%)	mPEG (mol. wt.) (5 wt%)	NMP (wt%)
P1	15	550	80
P2	15	2000	80
P3	15	5000	80

4.2. Characterization of the fabricated membranes

In order to evaluate the effect of mPEG on membrane morphology and permeation properties, the membranes were characterized by considering important characterization parameters like membranes average pore size, pore area, pore size distribution,

hydrophilicity, porosity, fouling resistance, equilibrium water content, pure water flux and % protein and foulant rejection as explained in Chapter 2.

4.3 Permeation experiments

The permeation experiments were used to calculate the compaction factor (CF) and pure water flux (PWF) of the membranes as discussed in Chapter 2.

4.4 Ultrafiltration experiments

Membranes practical aspects viz. fouling, separation, and permeate flux were analysed by using BSA and HA as explained in Chapters 2 and 3. Furthermore, the effect of pH on the mPEG reformed membranes was analysed by using the best performing membrane (P3), based on the PWF of the membranes.

4.5 Results and discussions

4.5.1 Functional group analysis of the fabricated membrane

Figure 4.1 shows the FTIR analysis of the prepared membranes. Bands which confirm the presence of PVDF-co-HFP in the prepared membranes are present at 1390 cm^{-1}, 1453 cm^{-1}, 882 cm^{-1}, and 678 cm^{-1}. The band at 1390 cm^{-1} is about CF_2 deformations present in the PVDF-co-HFP structure and the peaks are prominent in the membranes. Band at 882 cm^{-1} is of C-F vibrations present in the base polymer of the membrane. PVDF-co-HFP is made up of the structure which constitutes of m-vinyledene fluoride units, -(-CH~-CF_2-)-m, added head to tail. However, there are irregularities present in the structure due to the head-to-head and tail-to-tail defective addition [75]. The band characteristics of these defects can be seen at obscure bands 1453 cm^{-1} and 678 cm^{-1}. This confirms that PVDF-co-HFP used for the study is defect free and is present in its purest form. These obscure bands at 1453

cm^{-1} and 678 cm^{-1} are of CH_2 bending mode and of the CF_2 wagging of -(-CF_2- CF_2-)- units of the PVDF-co-HFP structure, respectively.

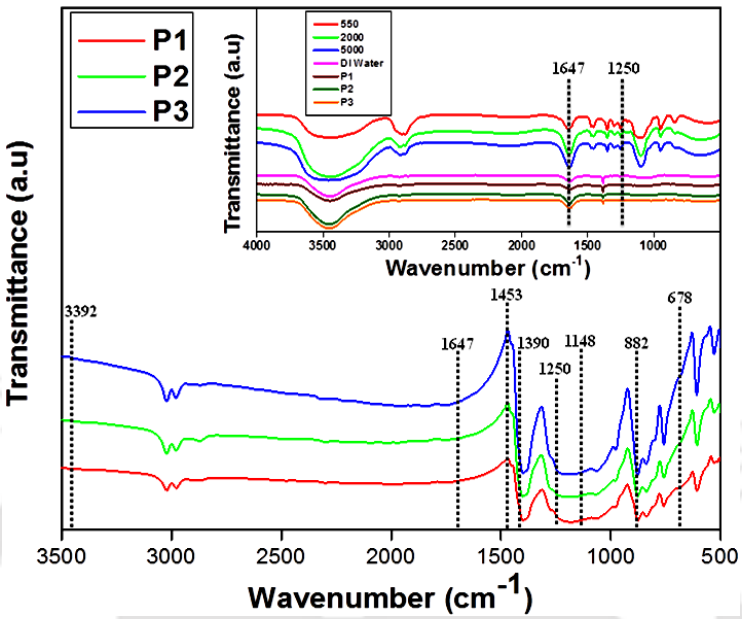

Figure 4.1. FTIR spectroscopy of the membranes and in the inset the stability analysis of the membranes

The Fig. 4.1 confirms about the bands and these bands confirm about PVDF-co-HFP that it is indeed present in the membranes. Peaks at 1250 cm^{-1} and 1148 cm^{-1} confirms the presence of mPEG in the prepared membranes. C-H stretching in mPEG structure is shown by the band at 1250 cm^{-1} and ether bonds present in mPEG are confirmed by the band 1148 cm^{-1}. OH stretch of mPEG can also be seen at 1647 cm^{-1} and 3000 cm^{-1}. Thus, the FTIR analysis confirms that the constituent of the membrane casting solution were present in the casted membranes too.

The results of mPEG stability in the membranes were depicted in the inset of Fig. 4.1. The obtained results of the membranes P1, P2, and P3 were compared with DI water, mPEG 550, mPEG 2000 and mPEG 5000 FTIR curves. The outcome of the comparison shows that there is no prominent peak available for the additives in the results. This

confirms that there is no leaching or removal of mPEG from the membranes and the additives are firmly embedded into the membranes.

4.5.2 Morphological studies of the fabricated membranes

Additives impose an important impact on the membrane morphology and performance as explained in Chapter 1. Shi et al., reported that, sponge like portions were present in the majority when the PVDF-co-HFP polymer dope contained no additive [77]. These sponges like portions gave way to finger like pores, on addition of PVP as an additive. It was also reported that macrovoid formation in membranes was heavily affected by the additive used. Macrovoid (large elongated pore) structures are generally used as support layers for composite membranes [78]. However, presence of macrovoids in a membrane compromises the mechanical integrity of the membrane and can cause collapse of the membrane during high pressure applications [79]. In general, macrovoid formation is undesirable, and must be prevented. Many theories have been proposed to explain the mechanism of macrovoid formation. These include theories based on surface tension induced free convection at the interface between the casting solution and the coagulation bath [79], spinodal decomposition [80] and instantaneous liquid-liquid demixing followed by macrovoid growth by diffusion [77]. It was experimentally observed that macrovoid formation can be suppressed by using a solvent-nonsolvent pair that do not mix well with each other, or by allowing the solvent to evaporate from solution film before immersion in the bath [78,81]. Shi et al., however, reported that size of macrovoid may increase or decrease with additive concentration, depending on two factors [77]. Firstly, with increase in the molecular weight of the additive, the rate of demixing tends to increase, resulting in rapid phase separation and thus increased macrovoid formation. On the other hand, there is also an increase in the interaction between solvent and additive, resulting in delayed dope

precipitation and a tendency to reduce macrovoid formation. Sinha et al., noted that there was not much variation in membrane morphology of PSF membrane with the change in molecular weights of PEGME in their membranes, reason being cited not much difference between the different molecular weights of the additive [23]. In this study, the fabricated membranes are quite similar, if general structure of the membranes is considered. Membranes had a top dense skin layer and a porous sub-layer, which is having distinguished finger like structures (pores or channels). It can be seen from the top surface images in Fig. 4.2a, that there is an increase in pore density and pore size with an increase in the molecular weight of mPEG. The membrane P0 shows the least porous nature and P3 the highest, which is the reason for higher flux of membrane P3. Further, it can be seen that there is significant formation of macrovoids owing to the high miscibility of water and NMP. When additive molecular weight was increased from 2000 Da to 5000 Da, the number of macrovoids decreased, due to increased viscosity of the polymer dope solution. Figure 4.2b shows the FESEM images of the cross section of the fabricated membranes with and without (P0) mPEG of different molecular weights. Cross sectional images in Fig. 4.2b shows the formation of finger like structures in the membranes P1, P2, and P3. Whilst, the finger like structures are absent in the membrane P0, this is because of absence of mPEG in the membrane. This in itself confirms that the mPEG not only helps in increasing the hydrophilicity and antifouling character of the membranes but also plays the role of a good pore former. The formed membranes are asymmetric in nature, with thin skin layer and a porous sub-layer.

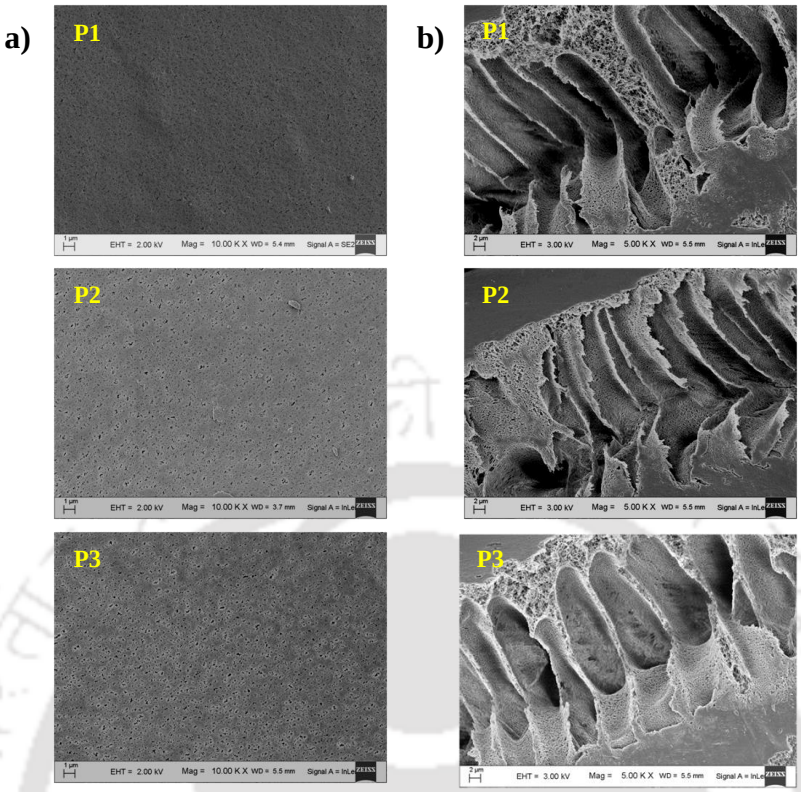

Figure 4.2. FESEM images of the membranes: a) Top surface b) Cross section

Figure 4.3 shows the results of the AFM analysis and it can be predicted from the figure that the roughness of the membranes enhance with an increase in the additives molecular weight from 550 Da to 5000 Da. The average roughness values for the prepared membranes are reported in the Table 4.2. Also, the top surface images were used to analyse the pore size and pore size distribution of the fabricated membranes by using ImageJ software as was done in Chapter 3.

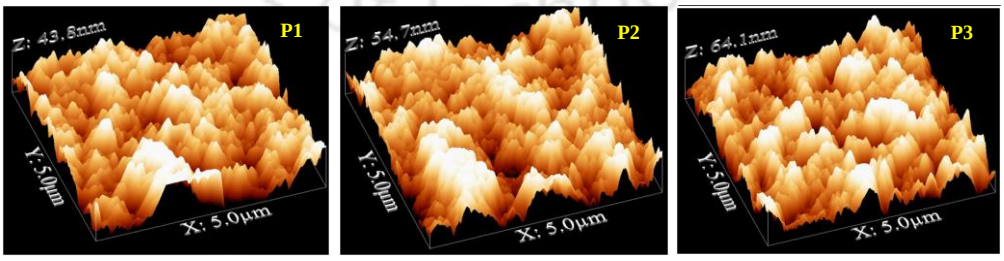

Figure 4.3. 3D AFM images of the membranes

Table 4.2. Membrane characterization parameters

Membrane	Porosity	Permeability (L/m^2h kPa)	Compaction factor	PWF (L/m^2h)	EWC	CA (°)	Average Roughness
P1	0.14	0.98	2.72	468.59	36.17	71.32 ± 1	09.22 nm
P2	0.31	1.46	2.63	748.45	51.01	65.41 ± 1	10.68 nm
P3	0.53	2.41	2.47	927.27	62.62	59.45 ± 2	12.20 nm

Figure 4.4 shows, the pore size distribution and cumulative pore number of the fabricated membranes. From the figure it is clear that the pore size of the fabricated membranes, increased from 10.39 nm (P1) to 21.49 nm (P3) via 15.52 nm (P2). This confirms the statement that with increase in the molecular weight of the additive both pore size as well as pore density increases.

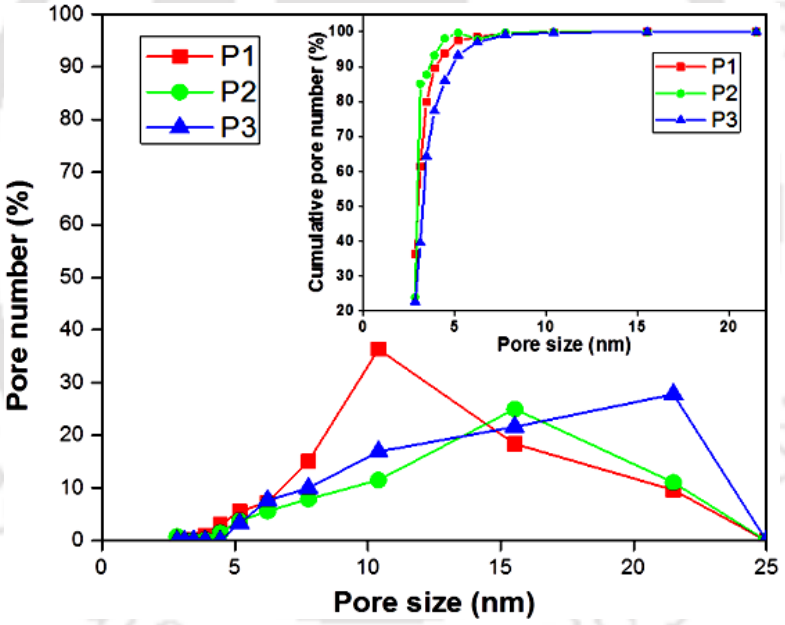

Figure 4.4. Pore size distribution of the membranes and in the inset the cumulative pore number vs pore size analysis

4.5.3 Permeation studies of the fabricated membranes

Membrane evaluation for the effect of mPEG additive on their permeation performance was carried out by doing critical permeation experiments. Initially, CF, PWF and P_m of the membranes were evaluated and after that UF experiments were carried out by taking BSA and HA as the model protein and foulant, respectively to study the rejection as well as the permeate flux behaviour of the fabricated membranes.

4.5.3.1 Compaction factor (CF) studies

CF depicted the structure of the membranes mainly relating to the porous sub layer as discussed in previous Chapters. The value of CF depends upon the presence of the structures like macrovoids in the membranes. Higher the number of macrovoids present in the membrane higher will be the CF and vice versa. The CF study is shown in Fig. 4.5, with the effect of compaction on the fabricated membranes with time in the form of PWF. The Fig. 4.5 clearly shows that the PWF declines sharply with time because of compaction of the fabricated membranes initially and after almost 60 min attains a steady state.

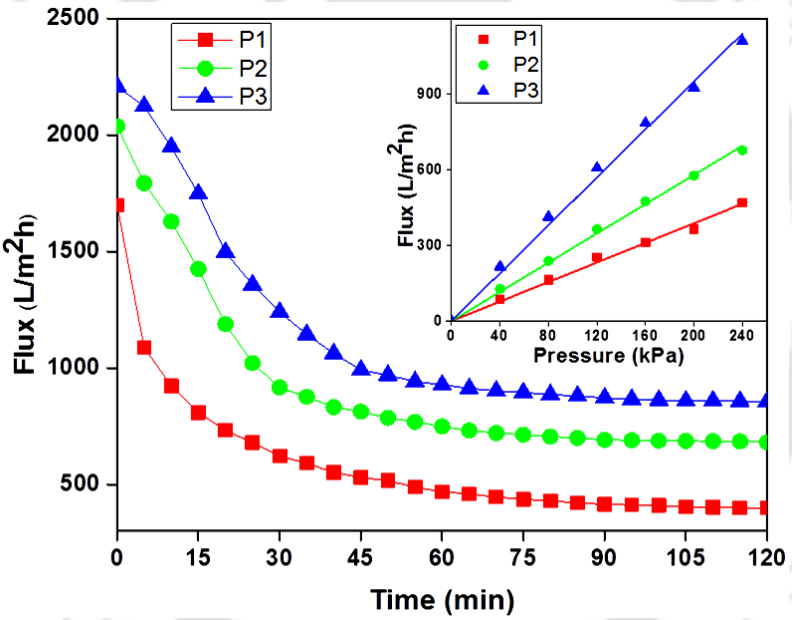

Figure 4.5. PWF profile of the membranes during compaction and in the inset the effect of transmembrane pressure on the membranes

The reason behind this is the reduction in the pore size because of the fact that the walls of the membrane pores come closer, become denser and attain uniformity. This results in the reduction of pore size of the membranes because of which the PWF declines with time. From the figure it is clear that the steady state PWF increased from 468.59 L/m^{2}h (P1) to 927.27 L/m^{2}h (P3) with increase in molecular weight of mPEG. The reason behind this is the increment in the number of pores on the surface of the fabricated membranes with the

increment in the molecular weight of the additive mPEG. The calculated CF values are summarized in Table 4.2 for all the fabricated membranes. It can be seen from the tabulated data that the CF decreases from 2.72 to 2.47 with the increment in the molecular weight of the mPEG from 550 Da to 5000 Da. The reason behind this fact is the decrease in macrovoid formation due to increase in viscosity of the dope solutions with an increase in the molecular weight of the additive explained in the preceding section (section 4.5.2).

4.5.3.2 PWF and Pm studies of the fabricated membranes

The effect of mPEG additive on the PWF of the fabricated membranes was analyzed at various transmembrane pressures. The results of the experiments are shown in the inset of Fig. 4.5. The range of the transmembrane pressures was from 0 - 240 kPa. The result of these experiments shows that as the transmembrane pressure increases, the PWF of the fabricated membranes also increases linearly. The results also confirm that the PWF increases with an increase in molecular weight of the additive which is in line with the CF study. For instance, if the PWF values are considered, they are increased from 469 L/m^2h to 1112 L/m^2h at 240 kPa, when the molecular weight of the additive was increased from 550 Da to 5000 Da. The reason behind such behaviour is the increment in the effective driving force, which is transmembrane pressure here, required for the water permeation and the additive molecular weight. The water permeability of the fabricated membranes was calculated from the slope of the inset of Fig. 4.5, using the relation (4). From the inset of Fig. 4.5, it is clear that the permeability of the fabricated membranes also increases with increase in the molecular weight of the additive mPEG. From the Table 4.2, it can be seen that the permeability increases from 0.98 L/m^2 h kPa (P1) to 2.41 L/m^2 h kPa (P3). The P_m of a membrane is directly related to the pores of a membrane and it confirms the fact that mPEG of different molecular weights affects the pore formation phenomena when added

to the membranes. Feng et al. also discussed in their study [63] that increase in the molecular weight of the additives increases their stability to be present in the fabricated membranes owing to their high molecular weight. This makes their removal from the membranes quite impossible. The FTIR result of the present study for the stability of the additive in the membranes also confirms this, as the additives are firmly embedded in the membranes and doesn't leach out. These additives being hydrophilic in nature further imparts hydrophilicity to the fabricated membranes and thus makes the membranes more hydrophilic in nature.

4.5.3.3 EWC study of the fabricated membranes

EWC holds a close relationship with PWF and was calculated by using the Eqn. 2.10. The values are tabulated in Table 4.2 and the tabulated values shows that with an increase in the molecular weight of the mPEG the EWC also increases as 36.17 (P1), 51.01 (P2) and 62.62 (P3). The value of EWC depends upon the number of pores and cavities present in the membranes as they are the holding place for the water. Thus, the reported EWC values confirm that, increase in number of pores in the membranes is associated with the increased molecular weight of mPEG. Both EWC and PWF are true to their close relation and coincide with each other as it is seen that both increases with an increase in the molecular weight of the additive mPEG in the membranes.

4.5.3.4 Porosity and hydrophilicity study of the fabricated membranes

Porosity and hydrophilicity are vital parameters in accordance to their importance in the membrane permeation and separation processes. These two parameters are also in close relationship with PWF and EWC, which depends on the morphology of the membranes. Generally, hydrophilicity is measured in terms of CA. As described in section 2.3.5 of Chapter 2, if the CA of a membrane comes out to be more than 90° then the membrane is

considered hydrophobic in nature and if the CA comes out to be below 90° then the membrane is considered hydrophilic [1]. A membrane is more hydrophilic if the CA is very less i.e., lesser the CA value more hydrophilic will be the membrane and vice versa. Porosity being the measure for the permeation of membranes was calculated by using the Eqn. 2.14. The values for CA, the measure of the hydrophilicity of the fabricated membranes and porosity are tabulated in Table 4.2. The values of both CA and porosity reveal that CA decreases and porosity increases with the increased molecular weight of mPEG. The CA values for membranes containing different molecular weight mPEG are 71.32 for 550 Da (P1), 65.41 for 2000 Da (P2), and 59.45 for 5000 Da (P3). Similarly, the porosity values are 0.14 for 550 Da (P1), 0.31 for 2000 Da (P2), and 0.53 for 5000 Da (P3). Both CA and porosity values are in line with the PWF, EWC and ImageJ software results for pore size distribution. The study done by Young and Chen describes perfectly the cause of variation in the porosity values [82]. According to their study it's the viscosity of the casting solutions which increases with increase in molecular weight of the additive and thus plays a role in the porosity of the membranes. Higher the viscosity of the casting solution higher will be the ratio of nonsolvent inflow to solvent outflow, which results into higher porosity in the fabricated membranes. The additive when added to the casting solution had two effects on the casting solution. First, it reduces the miscibility of the casting solution with the nonsolvent; which results in instantaneous demixing. Second, it increases the viscosity of the casting solution which results into delayed demixing [9,83]. Thus, the cause for higher porosity with higher molecular weight of additive can be explained on the basis of viscosity. The high viscosity decreases the miscibility of the casting solution with the nonsolvent and thus results into a highly porous membrane. This decrease in the miscibility of the casting solution with the nonsolvent also enhances the entrapment of the additive in

the membrane matrix and thus helps in the increment of the hydrophilicity of the fabricated membranes.

4.5.3.5 Ultrafiltration studies

The protein and foulant rejection profiles along with fouling of the membranes was evaluated after studying the permeation characteristics of the fabricated membranes. These properties also depend upon the membrane structure and the properties of the feed solution. BSA and HA solutions were used as the feed, to evaluate these properties of the fabricated membranes as explained in section 4.4. Figure 4.6 shows the time dependent flux studies of the fabricated membranes with BSA.

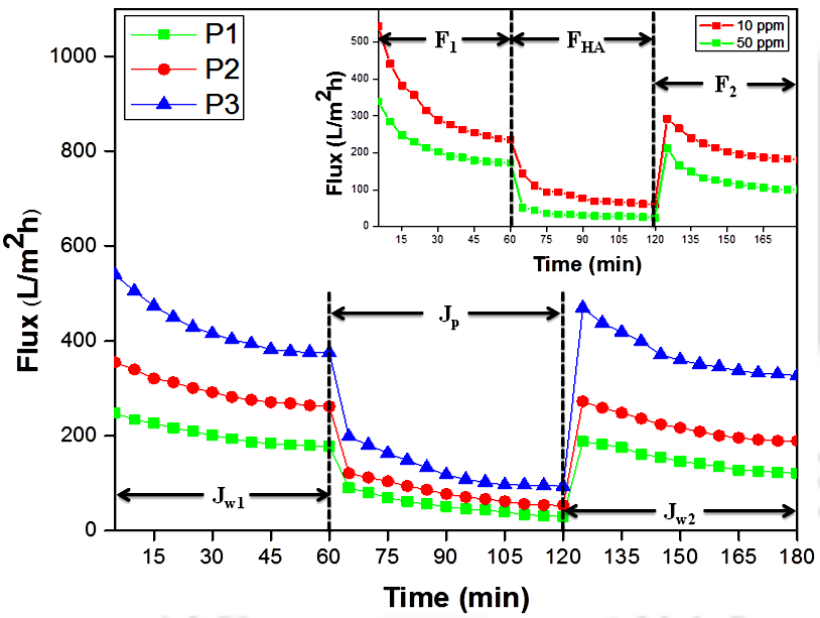

Figure 4.6. Time dependent ultrafiltration experiment of the membranes with BSA and in the inset with HA

On comparison of PWF (J_{w1}) to BSA solution UF (J_p) than there is very much difference between the two as initially the later decreases acutely. The reason for this is the adsorption or deposition of BSA molecules onto the membrane surface. At later stages both attain a steady state flux remarked as J_{w1} and J_p, which is reported in Table 4.3. J_{w2} is the PWF calculated with the membrane which was given hydraulic washing after the BSA solution

UF run. There is not much difference between J_{w1} and J_{w2}, which points towards the better antifouling properties of the fabricated membranes. This difference was also recognized by the FRR and CE results discussed in the succeeding sections. Thus, these results totally confirm that the residual presence of the additive mPEG in the fabricated membranes is the reason for the better antifouling profile of the membranes. Further, the antifouling property enhances when the molecular weight increases from 550 Da to 5000 Da for the membranes.

Table 4.3. Membrane ultrafiltration study data

Membrane	J_{w1} (L/m^{2}h)	J_p (L/m^{2}h)	J_{w2} (L/m^{2}h)	F_r $(\frac{J_{w2}-J_p}{J_{w1}})$	F_{ir} $(\frac{J_{w1}-J_{w2}}{J_{w1}})$	F_t $(1-\frac{J_p}{J_{w1}})$	$Flux_{RR}$ $(\frac{J_{w2}}{J_{w1}}\times 100)$
P1	203.26	52.85	148.52	0.470	0.269	0.739	73.07
P2	295.31	79.96	219.47	0.472	0.256	0.729	74.31
P3	426.52	127.87	373.09	0.575	0.125	0.700	87.47

The BSA solution UF gives similar trend as for PWF, if the effect of molecular weight of the additive mPEG on the fabricated membranes was considered. The membrane having higher molecular weight additive gives more flux as compared to the membrane having lower molecular weight additive. The BSA flux values are 52.85 L/m^{2}h for 550 Da, 79.96 L/m^{2}h for 2000 Da, and 127.87 L/m^{2}h for 5000 Da. This tendency of higher flux for higher molecular weight additive containing membrane is due to the high porosity of the membranes, which was explained in the preceding sections.

The protein (BSA) rejection profile of the membranes was also not very much different as explained in the preceding section. Figure 4.7 shows that the BSA rejection increases from 88 % (P1) to 95 % (P3) with increase in molecular weight of mPEG from 550 Da to 5000 Da, respectively. The reason behind this is the protein adsorption onto the membrane surface and into the pores, which results in narrowing of the pores. The hydrophobic and electrostatic interactions between the proteins and membrane surface play

a vital role in this. More are these two properties in between the two, more will be the phenomena of protein adsorption and pore narrowing. The membrane structure also plays a vital role in this as if the pores or the membrane surface is not uniform, then more will be the protein adsorption and entrapment of protein molecules in the membrane pores. In this case as the molecular weight of the additive mPEG increases in the fabricated membranes, the membranes become denser and spongy in nature. This imparts more resistant to the permeation of the protein molecules.

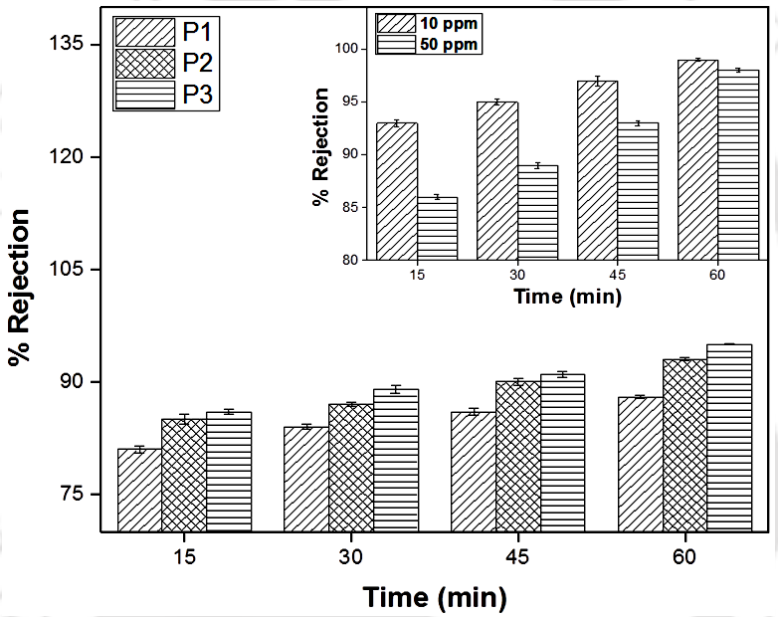

Figure 4.7. BSA and HA (in the inset) rejection profile of the membranes at pH 7

The HA separation study has shown in the inset of Fig. 4.6, which reveals the effect of mPEG present in the prepared membranes on the removal of HA from the feed solution. In this study, two different concentrations of HA solutions were used, 10 ppm and 50 ppm, as feed to the membrane system. Membrane P3 being the best membrane with respect to PWF profile was chosen. The study was carried out as it was explained in section 4.4, the DI water and two solutions of HA with different concentrations were permeated in the first two phases of this study, namely, F_1 and F_{HA}. On completion of these two phases, the membrane was cleaned by giving hydraulic washings and the last phase of the study F_2 was

carried out. The results shown in the inset of Fig. 4.6, clears that there is not much change in the flux profile after phase F_{HA} of the study. Results of HA rejection are reported in the inset of Fig. 4.7, where it is clear that the membrane P3 is successful in the removal of HA upto 100% in case of 10 ppm and 98% in case of 50 ppm HA solution. The rejection profile of HA as shown in the inset of Fig. 4.7, which reveals that the rejection increases with process time and within 1 h gives the above reported rejection values. The increase in rejection with time is due to the agglomeration of the HA particles on the membrane surface. This acts like a barrier for the HA particles and further reduces the passage of HA particles through the membrane. Thus, both BSA and HA separation studies confirm that the prepared membranes are antifouling in nature and are suitable for the successful removal of pollutants from the feed without much loss in the flux profile. This separation study also proves the practical application of the fabricated membranes.

The UF study of BSA with the fabricated membranes at neutral pH also reveals different fouling aspects of the fabricated membranes. Total fouling (R_t) which is the sum of reversible (R_r) and irreversible (R_{ir}) fouling of the membranes are calculated by using Eqns. 2.18, 2.19, and 2.20. The results of the calculations are presented in Fig. 4.8. From the figure, it is quite clear that the R_t is decreased from 0.73 to 0.70, when the molecular weight of the additive mPEG is increased from 550 Da to 5000 Da. The R_{ir} also decreases with increased molecular weight of the additives pertaining to the less persistent adsorption of protein molecules on the membrane. This decrease in the membrane resistances is due to the presence of the mPEG in the prepared membranes and as seen in the figure the membrane resistances decreases with the increased molecular weight of mPEG, showing positive effect of increasing molecular weight on membrane resistances. R_{ir} being low, therefore, the initial flux can be recovered with simple hydraulic washing of the fabricated

membranes. R_t being lower shows that there is a minor loss of total flux due to the adsorption of protein molecules on the membrane. The reason for this is the increased hydrophilicity and antifouling nature of the fabricated membranes.

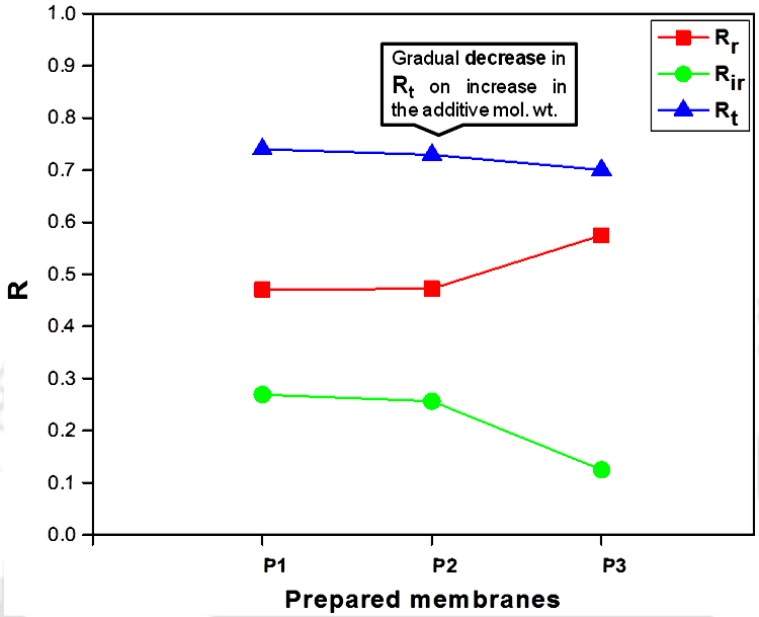

Figure 4.8. Fouling resistances of the prepared membranes

Figure 4.9 contains the results for FRR and CE of the membranes calculated by using Eqns. 2.16 and 2.17, respectively. The fabricated membranes have shown promising FRR, which increases from 73.07% (P1) to 87.5% (P3), when the mPEG mol. wt. was increased from 550 Da to 5000 Da. This reveals that the fabricated membranes contain good antifouling nature because of which these membranes are not losing much of their initial flux value. The CE also reveals the same result, as it can be seen from the figure, the CE values increased from 63.60% in case of P1 to 82.11% in case of P3 membrane. This also adds to the fact that the fabricated membranes are having a good antifouling profile. The membranes can be cleaned very easily and can retain their flux values for longer periods.

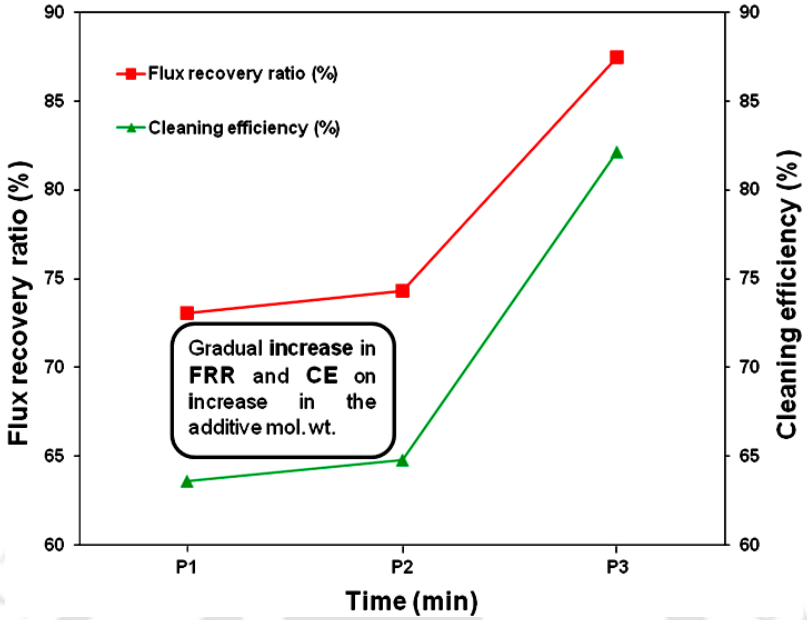

Figure 4.9. Flux recovery ratio and cleaning efficiency of the prepared membranes

4.5.3.6 Effect of feed solutions pH on the protein and foulant separation

The function of a protein is determined by its shape. Both pH and temperature play a role in changing the structure of protein molecules. The structure of the protein molecule BSA also depends upon pH and temperature of the solution. But in this case we emphasized in the study of pH effects on the BSA flux of the fabricated membranes, the results of which are shown in Fig. 4.10.

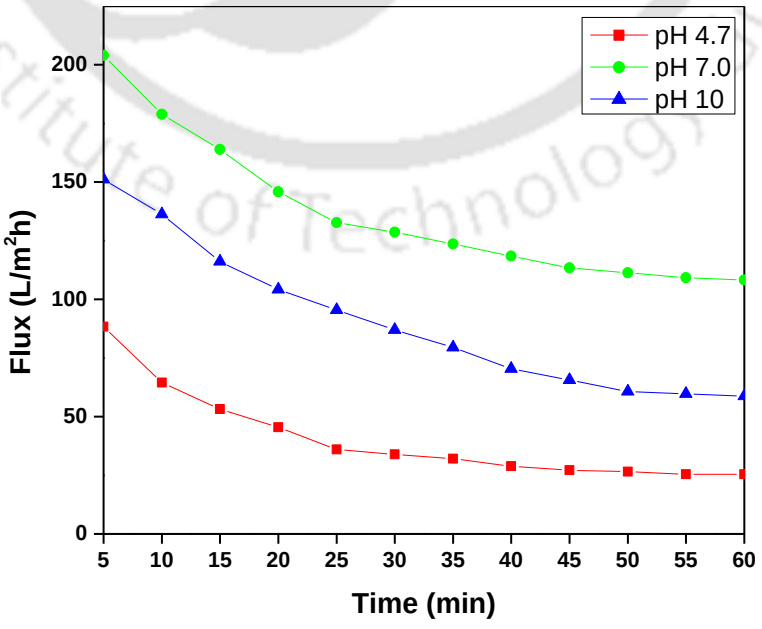

Figure 4.10. PWF of the membranes at different pH values of BSA feed solution

The two types of interactions which are changed by the effect of pH in a protein molecule are salt bridges (ionic bonds between positively and negatively charged side chains of amino acids) and hydrogen bonding. Thus, the rejection of the BSA protein molecule depends on the pH of the solution. It can be seen from the Fig. 4.10 that the flux of BSA is the least and therefore, the rejection highest, at its isoelectric point (IP) (pH value 4.7 at room temperature). There is no charge present on BSA molecules at its IP, that's why they remain in the most compact size and get adsorbed uniformly on the membrane surface. This adsorbed layer of BSA molecules was the reason for the decreased flux and higher rejection. At neutral pH (pH 7) the BSA molecules carries a total negative charge. Therefore, the intra particle distance among the BSA molecules enhances due to electrostatic repulsion between them. This results in a highly permeable layer on the membrane surface and thus results in a higher flux and higher rejection. The fabricated membrane gives higher rejection and lower flux with a BSA solution of pH 10 as compared with pH 7 BSA solution. This can be explained on the basis of coulomb's law, because the negative charge on the BSA molecules is higher at pH 10 as compared to pH 7. The residual mPEG in the fabricated membranes consists of $–CH_3$ groups, which carries a positive charge on them due to the positive inductive effect. This charge difference results in a total attractive force between the BSA molecules and the membrane surface. This leads to a dense BSA layer on the membrane surface due to greater adsorption of the BSA molecules. The result of which is a higher rejection and lower flux at pH 10. In Table 4.4, a comparative study based on the effect of various additives on the membranes antifouling properties is shown. It may be concluded from Table 4.4, that the present membrane is a better option as compared to the other membrane systems.

Table 4.4. Comparison of foulant rejection with some reported PVDF based membranes

Membrane	Additive	Foulant Tested				References
		I	Rejection (%)	II	Rejection (%)	
PVDF	TiO_2	BSA	88.2	EPS	84.4	[84]
PVDF	OMWCNTs	BSA	86.9	-	-	[85]
PVDF	PFSA/PEG	BSA	90.1	-	-	[86]
PVDF	Tween 80/ DMAc/ Water	BSA	93.7	Dextran	86.2	[87]
PVDF-HFP	PEG 6000	BSA	~84	-	-	[88]
PVDF-co-HFP	**mPEG**	**BSA**	**95**	**HA**	**99**	**Present work**

*The best rejection percentage with the additive used is reported

EPS: Extracellular polymeric substances

OMWCNTs: Oxidized Multiwalled carbon nanotubes

PFSA: Perfluorosulfonic acid

4.6 Summary

Flat sheet polymeric membranes were prepared by taking PVDF-co-HFP as the base polymer and mPEG of three different molecular weights as the additive. All the membranes as seen from the FESEM images contains consistent pores and spread uniformly throughout the membrane surface. AFM images have shown, as the additives molecular weight increases in the membrane the membrane sur-face roughness also increases from 9.22 nm (P1) via 10.68 nm (P2) to 12.20 nm (P3). This roughness is due to the presence of the additive mPEG on the surface. This makes the membrane and its surface hydrophilic, which in turn reduces fouling. This is the reason that the membrane flux increases with the increase of mPEG molecular weight in the prepared membranes. The prepared membranes reported flux values of 468.59 L/m^2h (P1), 748.45 L/m^2h (P2), and 927.27 L/m^2h (P3). The

prepared membranes porosity, EWC, and P_m all increases with increasing molecular weight of mPEG in the prepared membranes. The CA and CF decreases from 71.32° to 59.45° and 2.72 to 2.47, respectively, with increased molecular weight of mPEG. The results of FTIR analysis confirmed that the additive mPEG is firmly embedded in the membranes. This makes the justifications stronger, given in mPEG's regard for better hydrophilicity and antifouling nature of the membranes. This study has shown that mPEG has a profound effect on the PVDF-co-HFP membranes in the perspectives of both morphological as well as permeation properties of the membranes. Membrane P3 had the best flux performance and thus selected for the separation of HA from the feed solutions. Rejection values of 99% and 98% were reported for 10 and50 ppm HA solutions, respectively. This study thus shows that the molecular weights of an additive also play an important role in the morphology and permeation properties of membranes.

Chapter 5
Flyash based carbon nanotubes modified hydrophilic and antifouling ultrafiltration polysulfone membranes

In this chapter, synthesis and use of flyash (waste from coal industry) based carbon nanotubes (CNTs) for the modification of polymeric ultrafiltration membranes is discussed. Phase inversion method was used to synthesize asymmetric polysulfone (PSF) membranes using 1-methyl-2-pyrrolidone (NMP) as solvent. Polyethylene glycol (PEG) and synthesized flyash CNTs with different proportions like 0.1%, 0.3%, 0.5%, 0.7%, and 0.9% were used as pore former and additive, respectively. Further, the membranes were characterized by different characterization techniques, such as FTIR, AFM, FESEM, and TGA. Liquid-liquid displacement porosimetry (LLDP) was used to demonstrate the pore size distribution. Antifouling effect of the modified membranes was perceived with the help of bovine serum albumin (BSA) aqueous solution.

5.1. Experimental

5.1.1. Materials

The industrial waste coal flyash (F type) material used in this study was collected from NTPC, Visakhapatnam, India. Polysulfone (PSF) was used as the membrane base material and polyethylene glycol (PEG) as the pore former in the membrane synthesis by phase inversion. Chapter 2 explains the phase inversion method of membrane preparation in detail. The synthesized CNTs were used as additives in the membranes. The complete details of all the chemicals used in this study are reported in Chapter 2 (Table 2.1).

5.2. Synthesis and characterization of CNTs

5.2.1. Modification of raw materials

The complete procedure of CNT synthesis is shown in Fig. 5.1. Solution of NaOH in deionized water was prepared with different concentrations as (.5 M, 1 M, 2 M, and 4 M). 15 g of raw material (flyash) per 100 ml of above prepared solution was added to 3 neck round bottom flask and the reaction temperature was maintained at 80 °C with total reflux using cold water condenser.

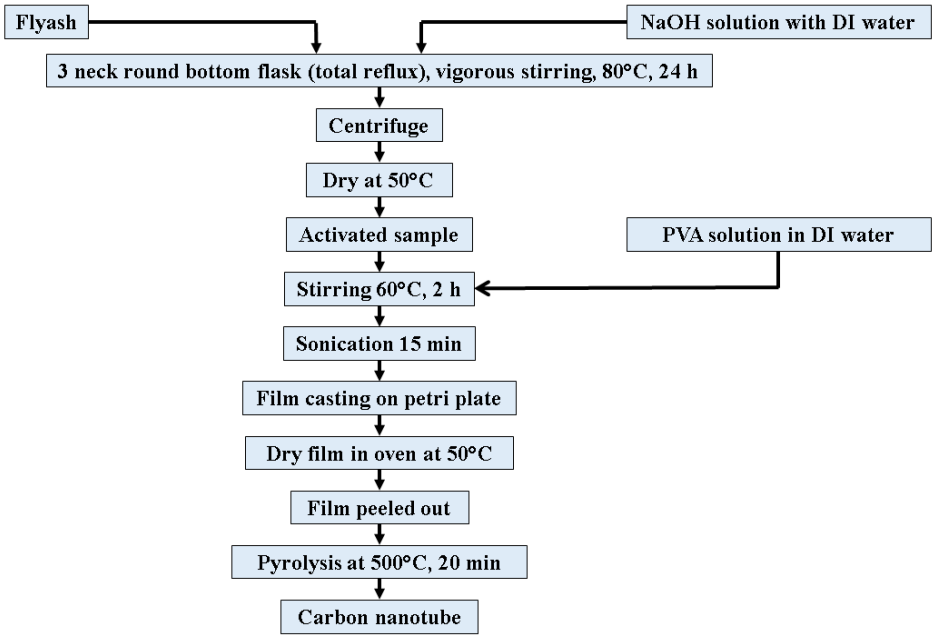

Figure 5.1 Flow sheet for formation of carbon nanotubes

Experiment was carried out under vigorous stirring using magnetic stirrer. After 24 h, the reaction was stopped and the reaction mixture was cooled to room temperature. Subsequently, the reaction mixture was centrifuged at 3000 rpm for 20 min followed by decantation. The process of centrifuge was done several times with deionized water to remove any trace of NaOH which get adhere on the surface of raw material. The moist paste of raw material and NaOH was collected in petri dishes and kept in oven at 50 °C till

complete drying. The acquired substance was then grinded into fine powder. The final product is characterized to determine the various structural and chemico-physio properties. The product prepared is termed as activated flyash.

5.2.2. Fabrication of bio-composite film

A mixture of 2 wt% polyvinyl alcohol was prepared in deionized (DI) water using conical flask followed by stirring for better mixing with the help of magnetic stirrer. The prepared activated samples was added in different wt % (5%, 10%, 15% and 20%) to the solution of (polyvinyl alcohol) PVA [89].The temperature was maintained at 60 °C using oil bath. After 2 h the solution was cooled at room temperature and then sonicated for 15 minutes, the resultant solution was poured in a petri dish and bubbles were removed by shaking. Petri dish was placed in an oven maintained at 50 °C and when film becomes completely dry it was peeled out.

5.2.3. Pyrolysis of bio-composite film

The bio-composite film was kept in the furnace using crucible for pyrolysis till 20 minutes and temperature of furnace was maintained at 500 °C followed by cooling at room temperature. The material after pyrolysis got graphitization structure in tubular alignment along with some unconverted substrate. Finally, the carbon nanotubes formed were further characterized.

5.2.4. Characterization of synthesized CNTs

The elemental analysis of the synthesized CNTs was carried out by using X-ray diffraction as explained in section 2.4.2 of Chapter 2. The morphological analysis of the CNTs was carried out by using FESEM, again as explained in Chapter 2.

5.3. Synthesis and characterization of CNTs modified polymeric membranes

5.3.1. Membrane synthesis

As explained in section 5.1.1, the asymmetric membranes were fabricated by using the technique of phase inversion with immersion precipitation. Membrane casting solutions containing base polymer (PSF, 12 wt%), pore former (PEG, 8 wt%) and different amounts of CNTs (0.1 wt%, 0.3 wt %, 0.5 wt %, 0.7 wt %, and 0.9 wt %) as additive were prepared by using 1-methyl-2-pyrrolidone (NMP) as solvent. The composition of various membrane casting solutions is given in Table 5.1. The membranes for ease of understanding were named as CM_0, CM_1, CM_2, CM_3, CM_5, CM_7, and CM_9 as shown in Table 5.1.

Table 5.1 Composition of different membrane casting solutions

Membrane	PSF (wt. %)	PEG (wt. %)	Flyash CNTs (wt. %)	NMP (wt %)
CM_0	12	8	0.0	80.0
CM_1	12	8	0.1	79.9
CM_3	12	8	0.3	79.7
CM_5	12	8	0.5	79.5
CM_7	12	8	0.7	79.3
CM_9	12	8	0.9	79.1

5.3.2. Characterization of the CNTs modified membranes

Characteristics of membrane which decides its performance are porosity, number of pores, pore size, and pore size distribution. Both the morphological as well as permeation studies are required to characterize the membranes. There are also some other important membrane

parameters like EWC, PWF, CF, water contact angle, hydraulic permeability, permeate flux as well as BSA rejection percentage which also dictate the performance or response of membrane under different conditions. These membrane characterizations were carried out as explained in Chapter 2. The morphological characterization of the membranes was done by using FESEM and AFM. Additionally, thermo gravimetric (TGA) analysis of the membranes was carried out to observe the membrane stability with temperature of surrounding.

5.3.3. Liquid-liquid displacement porosimetry (LLDP) method

The overall pore area, average size, and gross number of pores in fabricated membranes were calculated by using LLDP method as explained in Chapter 2.

5.3.4. Permeation experiments

The permeation experiments were carried out in similar fashion as explained in previous Chapters.

5.3.5. Pure water flux (PWF), compaction factor (CF) and hydraulic permeability (P_m)

The PWF, CF, and P_m of the membranes were calculated by using Eqns. 2.10, 2.11, and 2.12 as given in Chapter 2.

5.3.6. Equivalent water content (EWC), porosity, and hydrophilicity

The membrane EWC and porosity were calculated by using Eqns. 2.13 and 2.14. The hydrophilicity of the membranes was estimated by the method explained in section 2.3.5 of Chapter 2.

5.3.7. Ultrafiltration experiment

The influence of the amount of CNTs on membrane capability to separate proteins was carried out in a membrane cell mentioned in section 2.3.4 of Chapter 2 by using BSA as a model protein. The ultrafiltration experiment procedure was same as followed in other chapters of this work.

5.4. Results and discussion

5.4.1. XRD analysis of the synthesized CNTs

The powder XRD pattern and mineral composition is represented in Figure 5.2. XRD pattern of original flyash represent mainly the presence of crystalline (quartz, mullite, hematite etc.) and rest of the part of flyash is composed of amorphous material. Major peaks for quartz are found at 20.90° and 26.59°. The less intense peaks are of mullite at 16.45°, 29.33°, 39.375°, and 40.69°. Furthermore, the short peak at 48.497° shows hematite phase in the flyash.

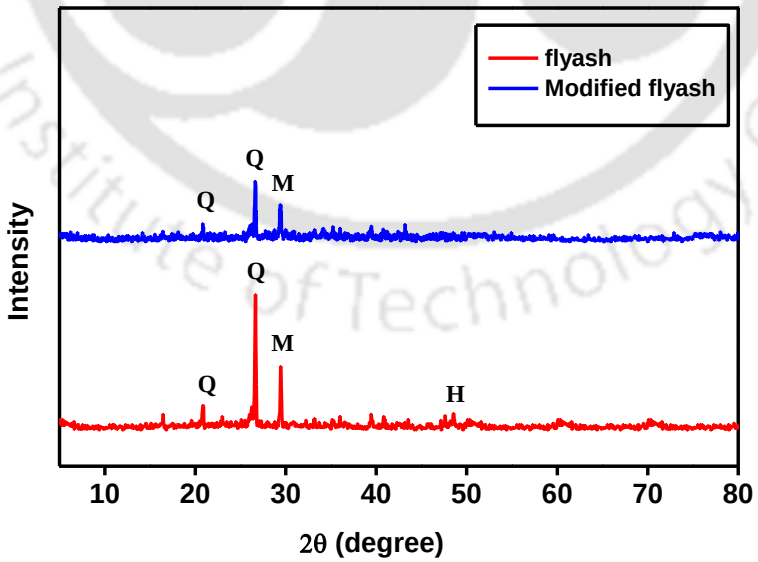

Figure 5.2 XRD pattern of raw and modified flyash

The dissolution of solid alumino silicates by alkali hydrolysis produces aluminate and silicates species [90,91]. Release of alumina and silica into solution after surface dissolution of solid particle is assumed as most defended mechanism for alkali activation. A complex mixture of silica, alumina, and alumino silicates formed and after some time it lead to formation of gel like structure. Because phases get dissolved in solution and after condensation they again appears with some reduction in existing ones or some new get originates. This is the reason that some existing peaks gets smaller or some are completely disappeared. After alkali treatment the glassy component is transformed into the material having cementacious properties. The main product is alkali alumino silicates gel with low ordered crystalline structure.

5.4.2. FESEM analysis of the synthesized CNTs

Figure 5.3 (A) show the raw particles of flyash in which the edges of particle are relatively smooth whereas in Fig.5.3 (B) particle become rough and a layer of amorphous material build around it having increased particle size of 3.691 µm.

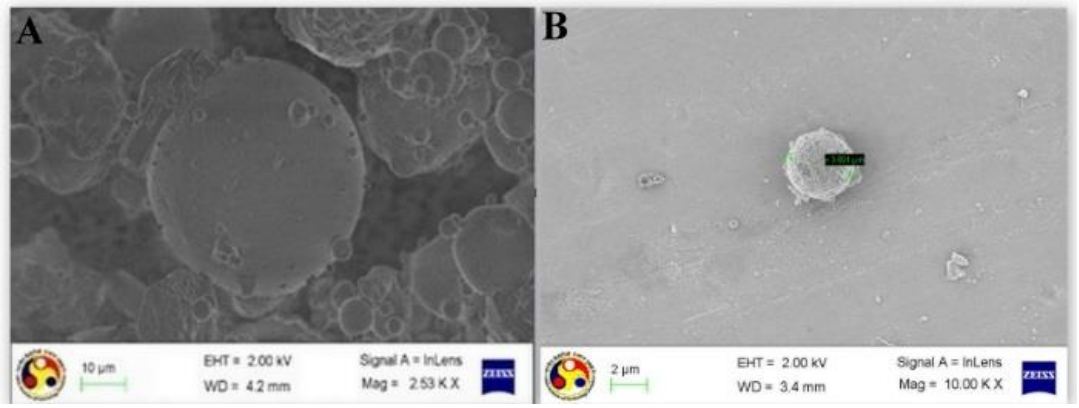

Figure 5.3 (A) FESEM image of flyash particles (B) Modified flyash particle

As per the Fig. 5.4 (A) surface of flyash based carbon nanotube is not completely without the flyash particles and this adherence of flyash particles on carbon nanotubes indicate imperfection in graphitization. Furthermore, dispersed nanotubes are shown in

Figure 5.4 (B), the diameter of the CNT is 30.20 nm and length is 683.8 nm so the aspect ratio of the CNTs is around 22.62.

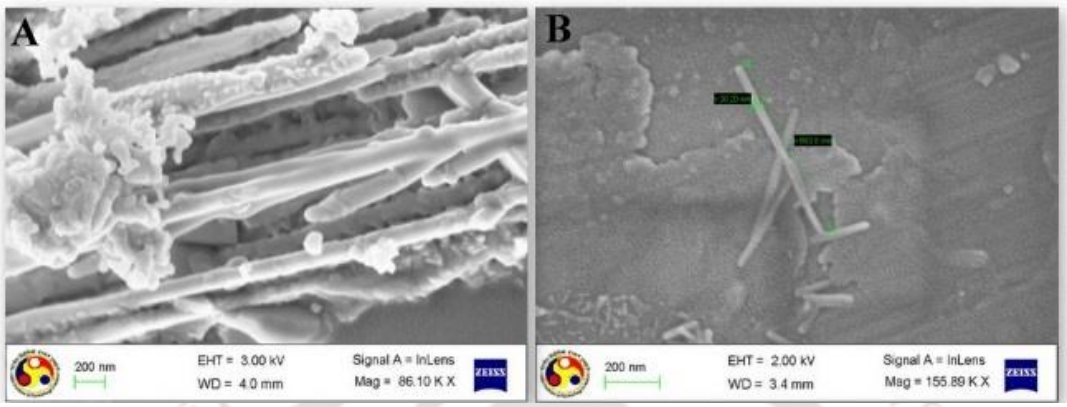

Figure 5.4 (A) FESEM image of flyash based carbon nanotubes bundle (B) Flyash based carbon nanotube

5.4.3. FTIR analysis of the CNTs modified membranes

Fourier transform infrared spectroscopy spectrum of membrane CM_1 (0.1 wt% flyash CNTs) and CM_0 (without CNTs) is shown in Fig. 5.5. The figure confirms the presence of solvent and base material in the synthesized membranes. A broad hump, found between wave number 3200-3600 cm^{-1} is distinctly characteristic band for the hydroxyl group present in the flyash CNTs. The bands corresponding to stretching vibrations of C=O and – C – O at 1660 cm^{-1} and 1136 cm^{-1}, respectively confirms the successful presence of the flyash CNTs in the membrane matrix. Peak at 2925 cm^{-1} accounts for stretching vibration for -CH_2 present in PSF. Furthermore, the adsorption bonds at 1320 cm^{-1} strongly confirms the presence of PSF.

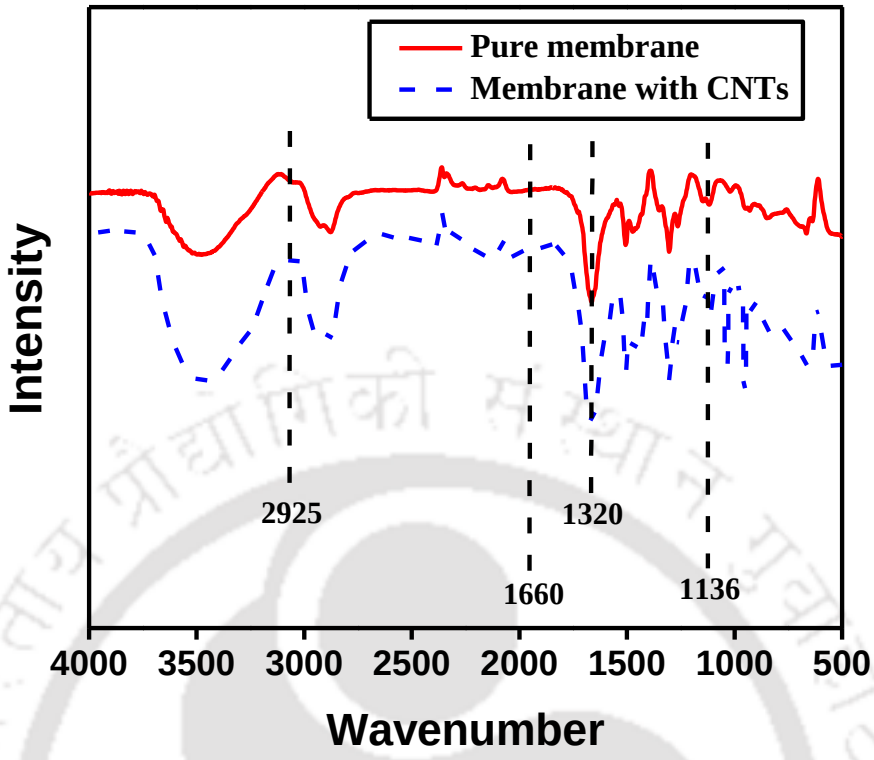

Figure 5.5 FTIR spectrum of the membranes

5.4.4. TGA analysis of the CNTs modified membranes

The thermal stability of membrane was demonstrated by TGA analysis, which is shown in Fig. 5.6. The figure depicts the TGA results of pure membrane (CM_0) and composite membrane (CM_1) with CNTs as additives. The minor weight loss between 100-200 °C is due to the removal of physisorbed water molecules from the membrane surface. Between 500-600 °C major mass loss occurs because of polymeric structure combustion. Due to incorporation of CNTs in membrane the thermal stability of membrane is improved as by observing the Fig. 5.6 it can be seen that the TGA curve is shifted and the degradation temperature significantly increases for membrane modified with CNTs.

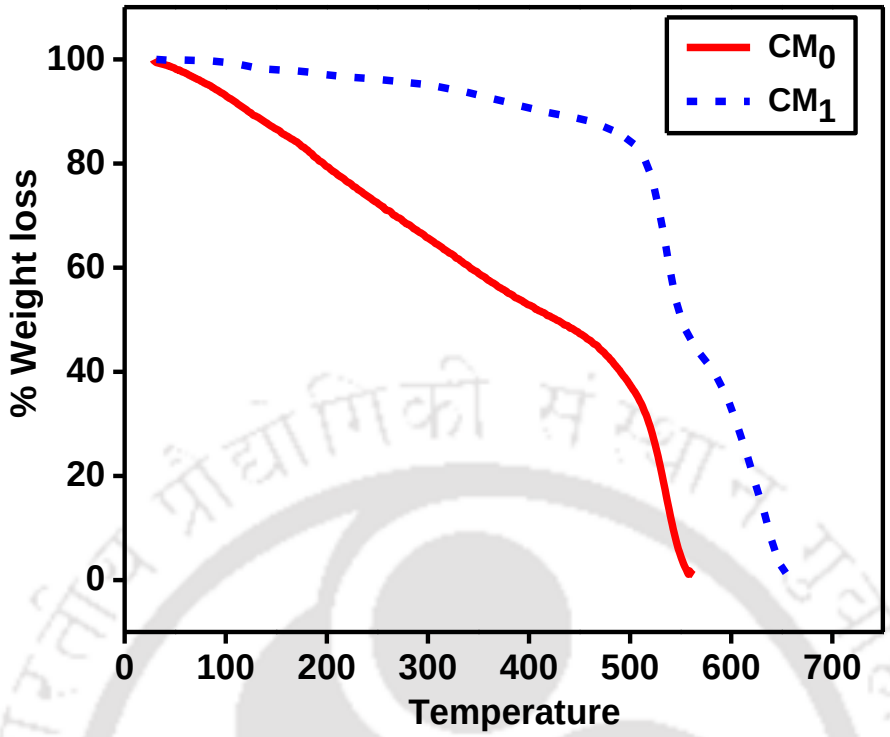

Figure 5.6 Thermal gravimetric analysis of CM_0 and CM_1 membrane

5.4.5. FESEM analysis of the CNTs modified membranes

In this study, FESEM images and experimental LLDP method are the basis of morphological outcomes. FESEM images are used to study the pores assembly and thickness of the membranes. This further helps in the quantitative analysis of the membranes.

Figure 5.7 shows the top surface FESEM micrographs of the membranes. The figure shows that uniform pores are formed and distributed in the membrane, which confirms that PEG successfully performs its role of a pore former. Furthermore, this inference is confirmed by the PWF results of the membranes reported in the subsequent sections. Additionally, the flyash CNTs plays a significant role in membranes porosity and uniform pore size distribution. The flyash CNTs generates a mechanical stress between the polymer and nanocomposite during the phase inversion process. Furthermore, the top surface of the

membranes is smooth and free of any lump or mass. This states that the flyash CNTs is well dispersed in the membrane matrix. Moreover, the absence of any cracks on the membrane surface indicates that the addition of flyash CNTs in the membranes does not affect the strength of the membrane.

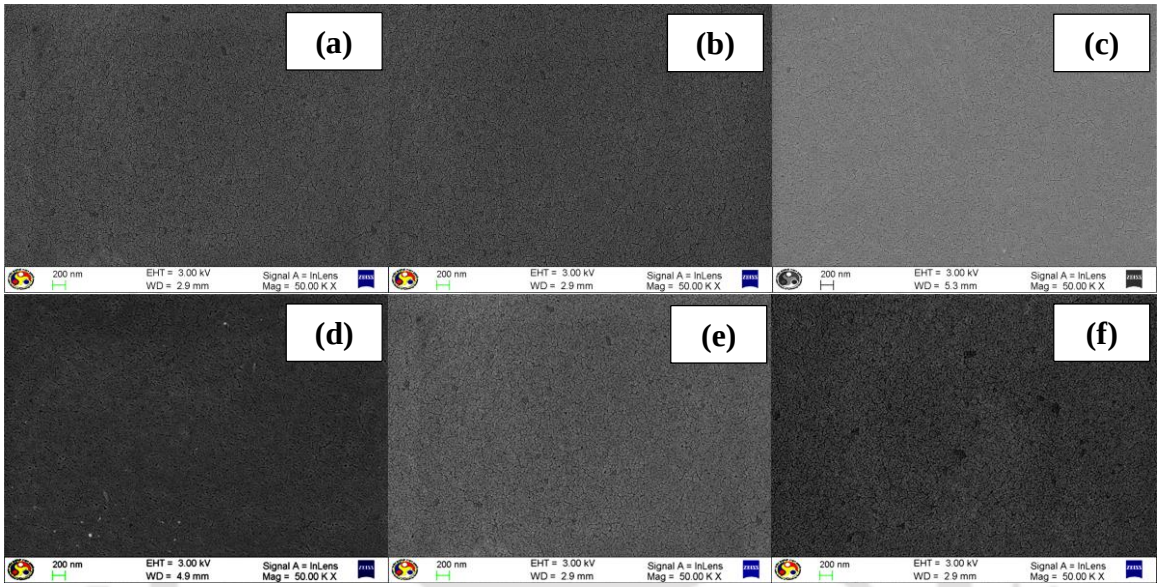

Figure 5.7 Top surface FESEM images of the membranes: (a) CM_0 (b) CM_1 (c) CM_3 (d) CM_5 (e) CM_7 and (f) CM_9

Figure 5.8 shows the cross sectional FESEM images of membranes with different wt% of CNTs. The figure depicts that the membranes have asymmetric morphology with two layers one is thin and other one is dense, these two layers are responsible for the retention and permeation of solutes, respectively. The formation of the asymmetric membranes takes place during the phase inversion process. The polymeric solution in the non-solvent bath precipitates at the interface, which results in the formation of the thin skin layer and porous sub layer with finger like channels [1].

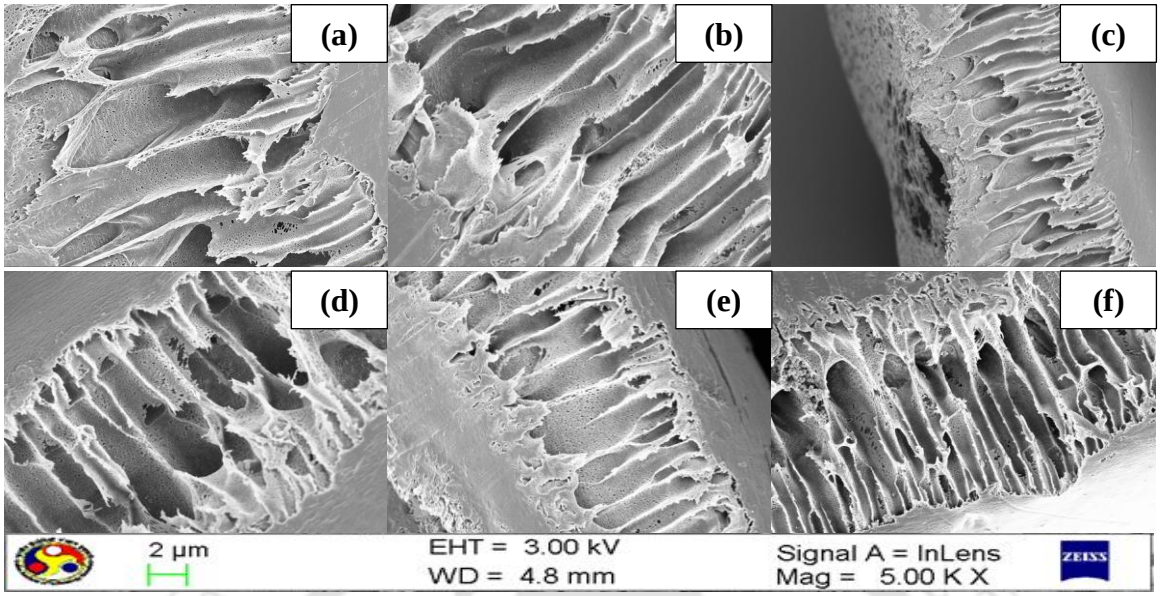

Figure 5.8 Cross sectional FESEM images of membranes (a) CM_0 (b) CM_1 (c) CM_3 (d) CM_5 (e) CM_7 and (f) CM_9

5.4.6. AFM analysis of the CNTs modified membranes

The topological roughness of prepared membranes in three dimensional systems is generated by atomic force microscope (AFM) study. AFM analysis gives a rough estimation of pore distribution pattern and also signifies the probability of pores formation in the membrane. Importantly, it elaborates the membrane roughness which plays an important role in membrane fouling.

Figure 5.9 presents the 3D AFM micrographs of the selected CNT modified membranes, namely CM_0, CM_5, and CM_9 for analysing the effect of flyash CNTs on the membrane surface roughness. The figure shows that the membrane surface roughness significantly decreases with the amount of flyash CNTs is increased in the membranes.

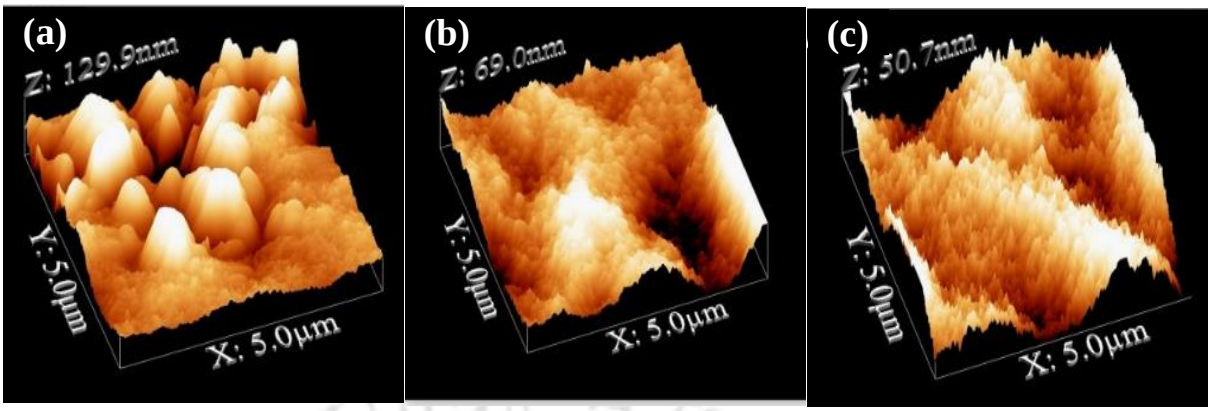

Figure 5.9 Topographical AFM images of (a) CM_0 membrane (b) CM_5 membrane and (c) CM_9 membrane

5.4.7. LLDP analysis of the CNTs modified membranes

Liquid–liquid displacement porosimetry (LLDP) analysis provides the order of average pore size, total pore area, and number of pores. In this evaluation size of pore, permeability of pore, number of pores, and finally the area of pore being calculated using Eqns. 2.1, 2.2, 2.4, and 2.5 and the outcomes are presented in Table 5.2.

Table 5.2 Results obtained from LLDP experiment

Membrane	L_n (m h^{-1} MPa^{-1})× 10^6	A_t (m^2) × 10^{15}	N_t (m^{-2}) × 10^{-18}	r_m (nm)
CM_0	8.31	11.8	9.19	2.82
CM_1	12.2	15.59	21.82	2.78
CM_3	13.9	18.61	25.1	2.73
CM_5	16.1	22.11	37.98	2.72
CM_7	12.8	16.12	23.58	2.75
CM_9	11.5	14.5	18.61	2.78

Figure 5.10 shows that for CM_0 membrane the major sum of pores are of 2.23 nm (30.60 %), 2.15 nm (17.99 %) and 3.07 nm (11.10 %). For CM_1 membrane pores of size 1.95 nm, 1.89 nm, and 1.83 nm cover 27.11 %, 15.87%, and 12.54% of total pores in membrane. Similarly, CM_3 membrane contains 25.18%, 13.68%, and 19.77 % pores with pore size 1.7 nm, 1.72 nm, and 1.61 nm, respectively. CM_5 membrane occupies 28.58 %, 19.57%, and 15.45% pores with pore size 1.73 nm, 1.65 nm, and 1.54 nm, respectively. CM_7 membrane contains 23.34 %, 17.81%, and 8.98% pores with pore size 1.87 nm, 1.81 nm, and 1.76 nm, respectively.

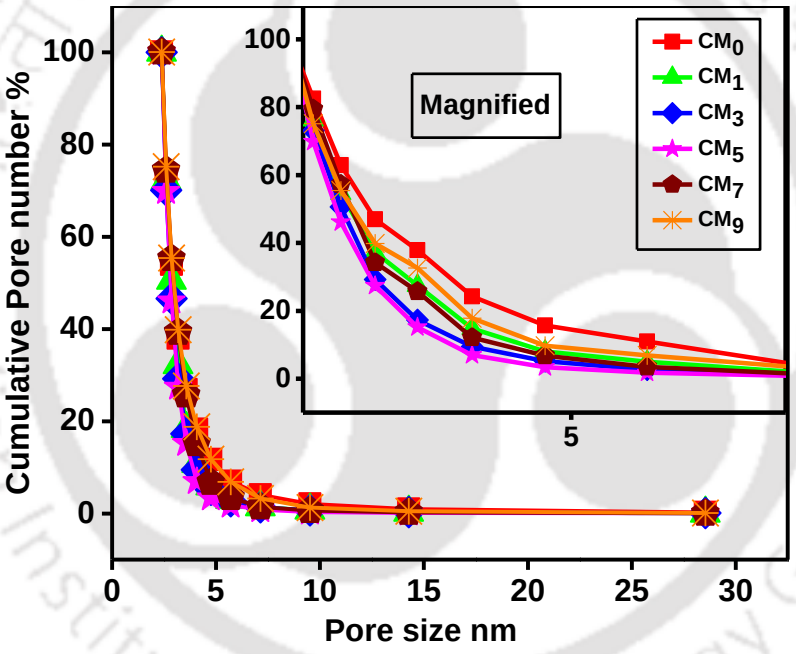

Figure 5.10 Cumulative pore number variation with respect to membrane pores size

Finally CM_9 membrane contains 24.27%, 18.82 %, and 9.42 % pores with pore size 2.03 nm, 1.92 nm, and 1.88 nm, respectively.

The average pore size calculated by LLDP method for CM_0, CM_1, CM_3, CM_5, CM_7, and CM_9 are found to be 2.82 nm, 2.78 nm, 2.73 nm, 2.72 nm, 2.75 nm, and 2.79 nm respectively. It can be seen from Fig. 5.11 that as pore size increases the percentage of

cumulative pore number reduces due to which the cumulative permeability also reduces with increase in pore size, which ultimately depends upon the number of pores.

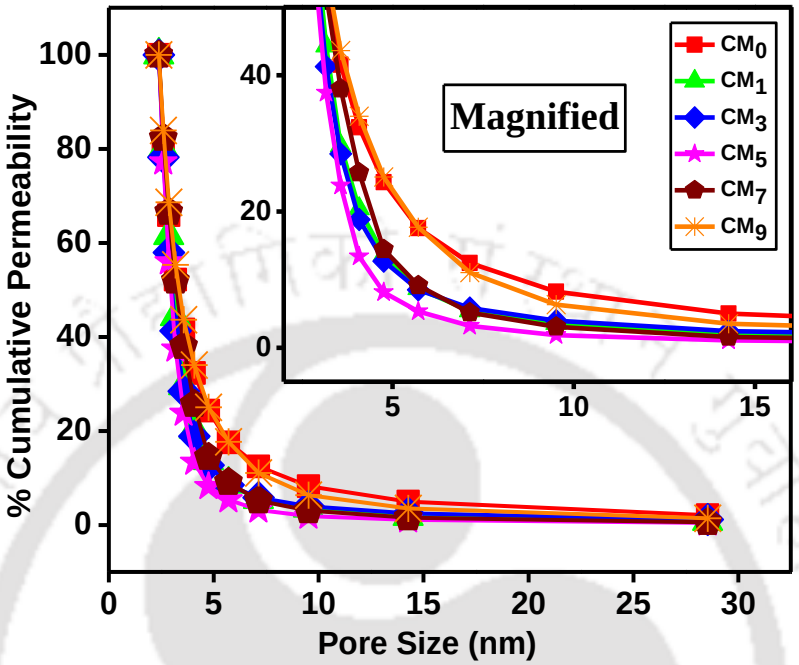

Figure 5.11 Variation of Cumulative permeability with pores size

The Eqn. 2.9 was used to calculate mean pore size (r_m) order of the mean pore size is found as $CM_0 > CM_9 > CM_1 > CM_7 > CM_3 > CM_5$. This order may be due to the reason that to accommodate more number of pores the pores get closer to each other and cause reduction in pore size. As the wt% of CNTs get increased beyond 0.5 % the impurities present in CNTs, mainly the unconverted flyash, blocks the pores due to which number of pores in membrane reduces. The total hydraulic permeability coefficient of different membrane system is found as 8.31 m h^{-1} MPa^{-1}, 12.2 m h^{-1} MPa^{-1}, 13.9 m h^{-1} MPa^{-1}, 16.1 m h^{-1} MPa^{-1}, 12.8 m h^{-1} MPa^{-1}, and 11.5 m h^{-1} MPa^{-1} for CM_0, CM_1, CM_3, CM_5, CM_7, and CM_9 membrane, respectively.

5.4.8. Permeation studies of the CNTs modified membranes

Permeation behaviour of membranes with different amount of additives was examined to observe the influence of different amount of additives on the membrane performance. Some parameters like CF, PWF, and P_m were used to quantify the performance of membranes. Finally, the permeate as well as rejection flux performance with BSA protein through prepared membranes is examined. The results of these membrane parameters are presented in Table 5.3.

Table 5.3 Characterization parameter of membrane

Membrane	EWC %	Porosity	PWF (L m^{-2} h^{-1})	P_m (L m^{-2} h^{-1} kPa)	SWCA (°)	C.F
CM_0	59.40	0.85	473.90	0.72	73.4±1	2.34
CM_1	37.69	0.79	410.03	0.68	67.8±1	2.51
CM_3	35.48	0.52	177.05	0.60	62.3±2	4.2
CM_5	28.15	0.61	111.84	0.57	54.5±1	6.75
CM_7	41.54	0.68	240.90	0.63	50.6±2	3.48
CM_9	53.19	0.75	325.58	0.66	46.2±2	2.99

Figure 5.12 shows how the PWF varies with the amount of additive present in the membranes. It depicts the PWF of the nascent membrane (CM_0) is the highest as compared to the CNTs modified membranes. This is because the pore size of the membranes reduces with the addition of the CNTs in the membranes as discussed in Section 5.4.7. Furthermore, the P_m of the prepared membranes also varies with the amount of the flyash CNTs in the membranes as shown in Table 5.3.

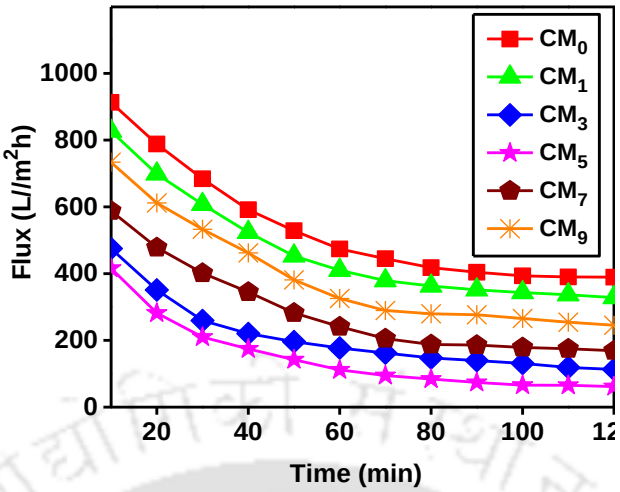

Figure 5.12 Membrane flux profile during compaction at constant pressure

5.4.9. Ultrafiltration studies of the CNTs modified membranes

Rejection and flux study of membrane basically rely on morphological structure along with the feed solution characteristics. In the current study, 1000 mgL^{-1} aqueous solution of BSA is employed as feed solution to examine the flux and rejection behaviour of prepared membranes. The time varying flux pattern of the ultrafiltration study of the present membranes with DI water and BSA aqueous solution is presented in Fig. 5.13.

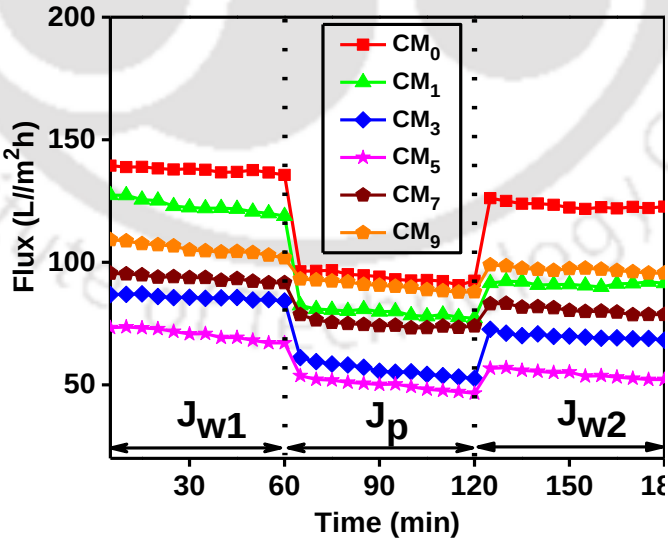

Figure 5.13 BSA antifouling flux profile of the membranes

Prior to BSA ultrafiltration the PWF (J_{w1}) changes marginally but it reduces significantly at the first operation of BSA ultrafiltration. This behaviour of the membranes is due to the

adsorption of BSA protein molecules on the surface of the membranes. However, after some time equilibrium is achieved and a pattern close to steady state is achieved.

Figure 5.14 shows the BSA rejection (%) results of the membranes. It can be seen from the figure that the membrane CM_5 shows highest BSA rejection (84.11%) and CM_0 the least (61.73%). This can be explained on the basis of membrane pore size. Membrane CM_5 having the least pore size among all of the prepared membranes justify highest BSA rejection and membrane CM_0 with highest pore size expected to be poor in BSA rejection.

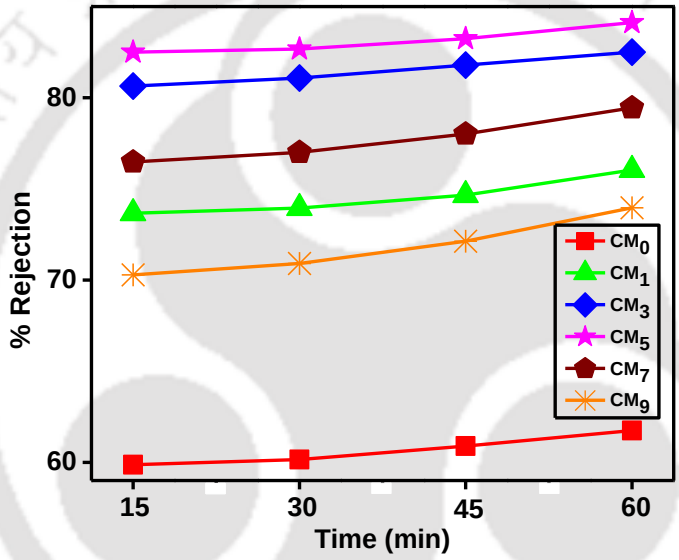

Figure 5.14 Plot of BSA rejection of different membrane with time

Reversible and irreversible fouling are two types of fouling, which are explained in detail in the previous Chapters. The effect of flyash CNTs as additives on membrane fouling is similar to AMPS effect on PSF ultrafiltration membranes as was explained in Chapter 3. The results of total fouling (F_t), reversible fouling (F_r), and irreversible fouling (F_{ir}) with the different membranes are presented in Figure 5.15. The figure shows that the F_t is reduced significantly on addition of flyash CNTs as additives to the PSF membranes. This rightly interprets the less flux loss of the membranes, which is ultimately due to the less adsorption and deposition of protein molecules on the membrane surface. Also, the F_{RR} comes out to be 89.45%, 75.18%, 81.49%, 77.01%, 86.14%, and 91.99% for membranes

CM_0, CM_1, CM_3, CM_5, CM_7, and CM_9, respectively. From the Fig. 5.15, it is also clear that CM_5 membrane is least fouled and CM_0 is highly fouled membrane.

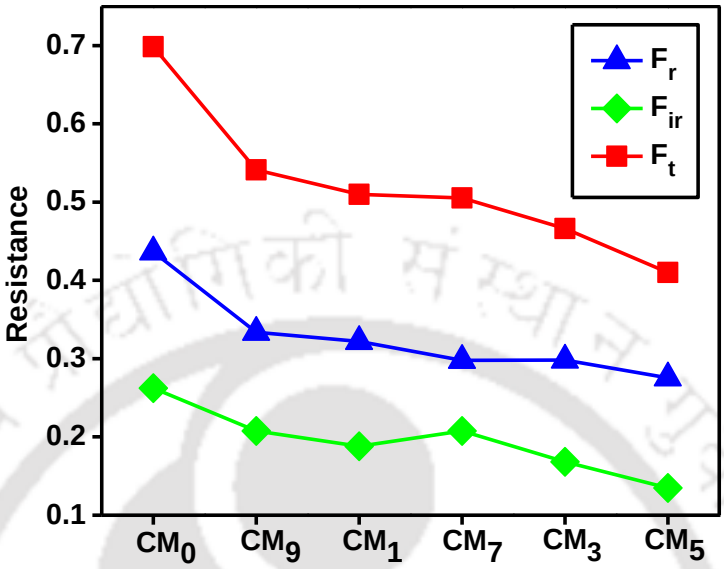

Figure 5.15 Plot of R_t, R_r, and R_{ir} for different membranes

5.5 Summary

Flyash CNTs modified membranes were prepared efficaciously. The membranes have shown significant antifouling nature and BSA rejection. Also, the membranes have shown positive effect on different membrane parameters, like PWF, P_m, EWC, porosity, and SWCA. The membranes have shown BSA rejection and antifouling profiles of the membranes confirms that the membranes are suitable for the biological separations. Additionally, the membrane shows better antifouling nature upon addition of the flyash CNTs as additives to the membranes because the total membrane fouling decreases from 0.69 to 0.41 and the SWCA decreases from 73.4° to 46.2°. These results are exciting and affirmative about the antifouling characteristic feature of the membranes. Furthermore, this study proposes a method for reducing a lot of waste generated by the coal gasifiers in the form of flyash, the disposal of which is a problem. Therefore, this study is also important for the safety and cleanliness of the environment.

Chapter 6
Cu_2O photocatalyst modified polysulfone mixed matrix ultrafiltration membrane for pharmaceutical removal

This chapter discusses about the synthesis, characterization of an effective and efficient mixed matrix polysulfone (PSF) ultrafiltration membrane modified with Cu_2O photocatalyst, synthesized using electrodeposition method, for pharmaceutical removal. Cu_2O photocatalyst, polyethylene glycol, and N-methyl-2-pyrrolidone were used as additive, pore former, and solvent, respectively in the phase inversion method. Characterization techniques, such as XRD, FTIR, FESEM, FESEM-EDX, and AFM were used to characterize the photocatalyst and blended membranes so as to analyse their structural and functional attributes. Further, the membranes were analysed by using permeation techniques to analyse their flux profiles. Similarly, antifouling nature and hydrophilicity of the membranes were studied by permeating aqueous BSA solutions and measuring the static water contact angle (SWCA), respectively. Lastly, the pharmaceutical removal studies were carried out using ibuprofen (IBP).

6.1. Experimental

6.1.1. Materials

Polysulfone (PSF), polyethylene glycol (PEG), 1-methyl-2-pyrrolidone (NMP), potassium bromide (KBr), bovine serum albumin (BSA), and Ibuprofen (IBP) are the chemicals which were used for this chapter. Deionized water was used throughout the experiments. Detail of all the chemicals is given in Table 2.1 of Chapter 2.

Content of this chapter is published as below:

R. Singh, V.S.K. Yadav, and M. K. Purkait, Cu_2O photocatalyst modified antifouling polysulfone mixed matrix membrane for ultrafiltration of protein and visible light driven photocatalytic pharmaceutical removal, Separation and Purification Technology 212 (2019) 191–204.

6.1.2. Synthesis and characterization of Cu_2O photocatalyst

Electrochemical synthesis route was followed for the synthesis of Cu_2O photocatalyst as reported by Yadav and Purkait [92]. $Cu(NO_3)_2 \cdot 3H_2O$ solution of concentration 0.1 M was taken in an electrolytic cell enclosing a cathode (graphite), anode (copper), and current source. The mechanism of Cu_2O synthesis in this assembly was electrodeposition. On the application of a constant current of 0.2 A copper starts deposits over the cathode surface. The electrodeposition cycle was continued for 30 minutes. Later, the deposited photocatalyst over the cathode was scrapped and cleaned by using acetone. Lastly, the photocatalyst containing acetone solution was heated for 1 h at 100°C so as to get clean and dry Cu_2O photocatalyst.

The electrochemically synthesized Cu_2O photocatalyst was characterized by using different standard characterization techniques, such as FTIR, X-ray diffraction (XRD), particle size analysis using Delsa nano, FESEM, and FESEM-EDX to find its material properties as explained in Chapter 2.

6.1.3. Preparation of IBP solution

The 10 mg L^{-1} IBP solution was prepared freshly by using DI water as the solvent for each experiment. The mixture was magnetically stirred and sonicated for the effective dissolution of IBP in the aqueous phase until the completion of the mixing process. The pH of the IBP solutions was attuned appropriately by using 0.1 M HCl and 0.1 M NaOH solutions.

6.1.3. Membrane preparation

Non solvent induced phase separation, commonly known as phase inversion technique was used for the preparation of flat sheet PSF polymeric membranes as explained previously in

Chapter 2. As shown in Table 6.1, 12 wt% PSF and 6 wt% of PEG (pore former) were used along with varying amounts of Cu_2O (0-2 wt%) for the preparation of Cu_2O PSF mixed matrix membranes using NMP as solvent.

Table 6.1. Membrane constituents

Membranes	PSF (wt.%)	PEG (wt.%)	Cu_2O photocatalyst (wt.%)	NMP (wt.%)
RY0	12	6	0.0	82
RY1	12	6	0.5	81.5
RY2	12	6	1.0	81
RY3	12	6	1.5	80.5
RY4	12	6	2.0	80

6.2. Characterization of the Cu_2O photocatalyst membranes

6.2.1 Membrane morphological studies

The morphology of the membranes top surface and cross section was studied by using FESEM (FESEM, Zeiss LSM 510 Meta). The membranes pore size and pore size distribution was analysed from FESEM top surface images by using ImageJ software as explained in Chapter 2. Also, the details of the procedures followed for the morphological analysis is given in Chapter 2.

6.2.2 Membrane constituent studies

Field emission scanning electron microscope with energy dispersive X-ray spectroscopy (FESEM-EDX) and Fourier transform infrared spectroscopy (FTIR) were used for the confirmation of the presence, distribution, and stability of Cu_2O photocatalyst in the membranes as explained in Chapter 2.

6.2.3 Membrane permeation studies

Membrane permeation studies were carried out as explained in Chapter 2 of this work.

6.2.3.1 Membrane compaction

The membrane compaction study was carried out in a similar fashion as explained in Chapter 2 for 2 h at 240 kPa transmembrane pressure. The compaction factor (CF) of the membranes was calculated by using Eqn. 2.11.

6.2.3.2 Membrane flux profile and hydraulic permeability analysis

The pure water flux (PWF) of a membrane is an important factor to decipher a membranes proficiency. It was calculated by sung Eqn. 2.10. Furthermore, hydraulic permeability is again an important parameter to assess a membrane for its permeation properties and is calculated by using Eqn. 2.12.

6.2.3.3 Membrane equilibrium water content

The membrane equilibrium water content (EWC) commonly states about the membrane porosity and hydrophilicity or hydrophobicity and is calculated by using Eqn. 2.13.

6.2.3.4 Membrane porosity

Membrane porosity is a vital trait of a membrane, which defines its permeation and selectivity capabilities and is calculated by using Eqn. 2.14.

6.2.3.5 Membrane hydrophilicity

The membrane hydrophilicity was calculated by measuring the static water contact angle over the membrane surface as explained in section 2.3.5 of Chapter 2.

6.2.4 Membrane antifouling studies

The membrane fouling studies were carried out with BSA as a model protein as explained in section 2.3.6 of Chapter 2. The BSA rejection flux recovery ratio (F_{RR}), and cleaning

efficiency (C.E) were calculated by using Eqns. 2.15, 2.16, and 2.17. Furthermore, The analysis of the membrane antifouling nature is crucial because of its positive effect on a membranes performance and life. The antifouling analysis was carried out by evaluating the individual membrane foulings, namely reversible (R_r), irreversible (R_{ir}), and total (R_T) fouling and calculated by using Eqns. 2.19, 2.20, and 2.18, respectively.

6.2.5 Photocatalytic removal of IBP by membranes

The photocatalytic removal of IBP membranes was evaluated by using IBP aqueous solutions of 10 mg L^{-1} concentrations under both dark as well as visible light conditions. Membrane samples of 0.1 g quantity were weighed and cut into smaller pieces. These pieces were then transferred to different 100 mL capacity conical flasks containing 50 mL of 10 mg L^{-1} IBP aqueous solution. Prior to the analysis, the samples were kept for stirring under dark conditions for 1 h for proper onset of adsorption and desorption equilibrium of IBP with the membranes for both dark and illuminated (visible light) experiments.

6.2.5.1 Membrane IBP removal under dark conditions

The conical flasks containing the IBP aqueous solution and membranes were placed in an incubator cum shaker at 120 rpm and 25°C for 1 h and sample solutions (~3 mL) were taken for analysis at 15 min interval.

6.2.5.2 Membrane IBP removal under light conditions

The IBP photocatalytic removal under the effect of visible light was carried out in a time programmable commercial photochemical reactor (Lelesil Innovative Systems, Mumbai). The visible light source for these experiments was a 250 W lamp with emissions in the range of 390 to 800 nm. The lamp was surrounded by a water cooled quartz jacket so as to maintain a constant temperature. This ensures that the removal takes place only under the

influence of light and not heat. The sample solutions (~3 mL) were taken at an interval of 15 min.

Both the experiments, dark as well as visible light, were carried out for 1 h duration and to assess the removal of IBP in the aqueous solution, UV-Vis analysis was carried out at 222 nm wavelength using a UV-visible spectrophotometer (Perkin-Elmer Precisel, Lambda-35). The removal of IBP was calculated in terms of % rejection by using the following relation:

$$\%\ Rejection = \left(1 - \frac{C_I}{C_F}\right) \times 100 \qquad 6.1$$

Where, C_I and C_F represents the IBP initial and final concentrations in the aqueous solutions.

6.3 Results and discussion

6.3.1 Cu_2O photocatalyst characterization

The Fig. 6.1 (a) shows FTIR analysis of the synthesized Cu_2O photocatalyst. The bands for O-H stretching vibrations and bending mode can be seen at 3400 and 1630 cm^{-1}, respectively. The occurrence of these peaks may be due to the moisture present on the Cu_2O photocatalyst surface [93]. Furthermore, the bands in the range of 500 and 800 cm^{-1} firmly represent the Cu-O, Cu-O-Cu, and O-Cu-O framework vibrations [94]. The XRD analysis for the Cu_2O photocatalyst is shown in Fig. 6.1 (b). Prominent peaks corresponding to the Cu_2O photocatalyst planes (111), (200), (211), (220), and (311) are available at 36°, 41°, 52°, 63°, and 74°, respectively. The results of the morphological and qualitative (elemental) analysis of the photocatalyst carried out by using FESEM and FESEM-EDX were shown in Fig. 6.1 (c) and (d), respectively. The resultant FESEM micrographs of the photocatalyst shows that the synthesized photocatalyst particles are of uniform round sintered shape.

Furthermore, the FESEM-EDX analysis confirms that the photocatalyst is of high quality and is free from any kind of impurities.

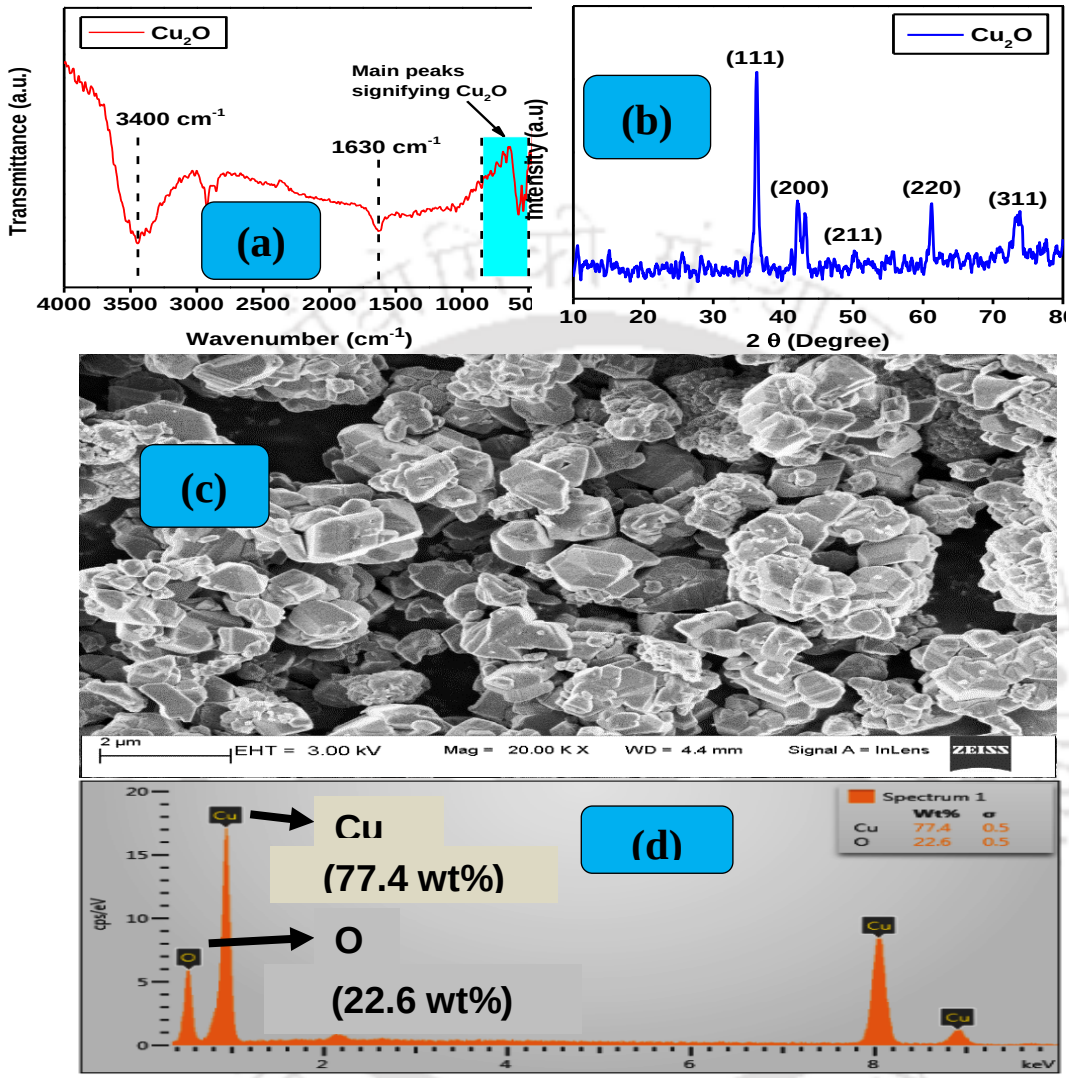

Figure 6.1. Cu_2O photocatalyst (a) FESEM, (b) FESEM-EDX, (c) FTIR, and (d) XRD analysis

Additionally, Fig. 6.2 (a) represents the particle size distribution of the Cu_2O photocatalyst. The analysis shows that the particle size of the photocatalyst lies in between 110-750 nm with distribution median size (D_{v50}) of 204 nm.

The Cu_2O photocatalyst formation mechanism was explained by Yadav and Purkait [92] in their study describing CO_2 reduction by using Co_3O_4 and Cu_2O as electrocatalysts.

The Cu from the electrolyte solution starts depositing over the cathode surface after accommodating an electron generated at anode.

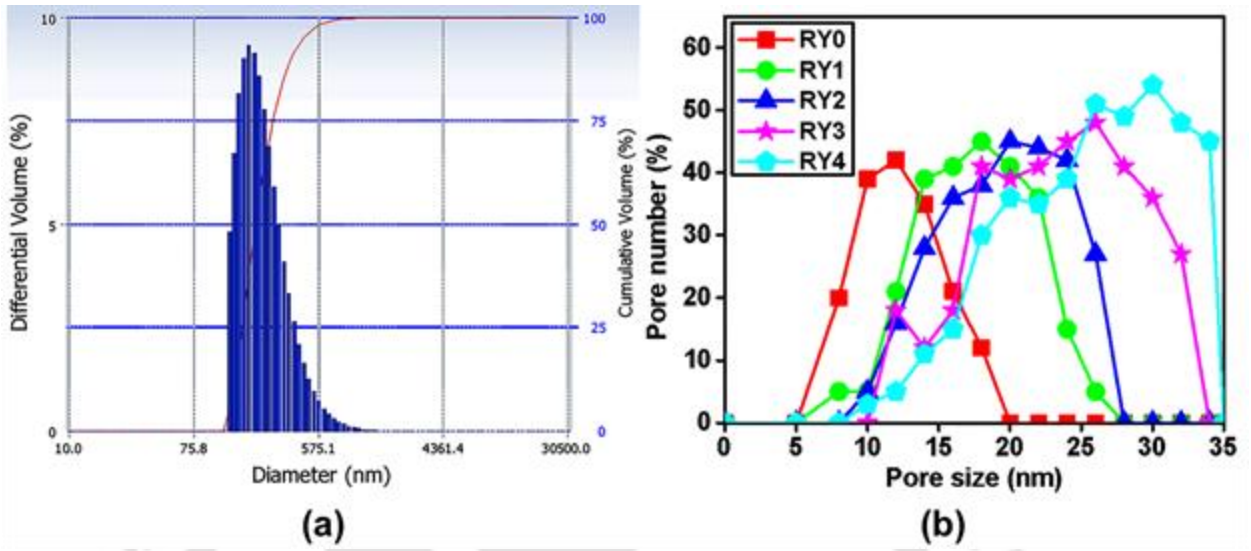

Figure 6.2. Particle and pore size distribution of synthesized Cu_2O photocatalyst (a) and membranes (b)

The driving force for this reaction was the continuous formation of Cu^{2+} ions at the anode. Also, the deposition of every Cu^{2+} ion over the cathode surface results in the formation of new $Cu(NO_3)_2 \cdot 3H_2O$ (copper nitrate trihydrate molecule) in the electrolyte solution. Finally, upon heating the deposited Cu in the presence of oxygen produces Cu_2O.

6.3.2 Membrane morphological studies

FESEM and AFM analysis was carried out to study the effect of Cu_2O photocatalyst on the PSF membranes. Figure 6.3 (a) shows the top surface images (air side) of the synthesized membranes in the study. The figure shows that uniform pores are formed and distributed in the membrane. Furthermore, pore former PEG successfully executes its job and results in membranes with high porosity and interconnected pores. The plausible reason for this is the spinodal demixing, which results in the formation of a membrane with well interconnected pores. This happens due to the fast enough diffusion process, which makes

the polymer solution highly unstable and allow it to cross the spinodal curve [58]. The presence of well interconnected pores was further confirmed by the results of PWF profiles of the membranes presented in the subsequent sections. Additionally, the Cu_2O photocatalyst plays significant role in the membrane porosity and uniform pore size distribution. The reason behind this is the mechanical stress generated between the polymer and photocatalyst due to the shrinkage of the polymer during the casting process [95]. Furthermore, the top surface of the PSF MMM was smooth and no lump or mass of the Cu_2O photocatalyst was seen. Unlike in many other cases where the used additives, such as silica [96] and alumina [97] have shown lumps or masses over the membrane surface. Therefore, it can be stated that the Cu_2O photocatalyst was well dispersed in the membrane matrix. Moreover, the absence of any cracks on the membrane surface indicates that the addition of Cu_2O photocatalyst in the membranes does not affect the strength of the membranes. On the other hand, Fig. 6.3 (b) represents the cross sectional micrographs of the membranes. The membranes exhibited the distinctive asymmetric structure, where the three regions of the membranes, viz. selective layer towards the air side, loofah like layer at the bottom, and a thick and porous sub-layer with channels in the middle of membranes can be seen clearly. The upper selective layer provides selectivity and the porous sub-layer acts as a support for the membrane. Furthermore, the continuous finger like channels across the membranes cross section confirms that the membrane pores are present continuously in the membranes. The formation of these finger like structures is again the result of instantaneous demixing [48]. Also, the addition of Cu_2O photocatalyst results in fairly wider finger like structures. This was due to the hydrophilic nature of the Cu_2O photocatalyst, which results in enhanced mass transfer amid solvent and non-solvent in the course of phase inversion process ensuing the development of wider finger like channels

[98]. Figure 6.2 (b) shows the membrane pore size distribution. The average pore size for the membranes RY0, RY1, RY2, RY3, and RY4 are 12.41, 18.50, 20.06, 26.52, and 30.11 nm, respectively.

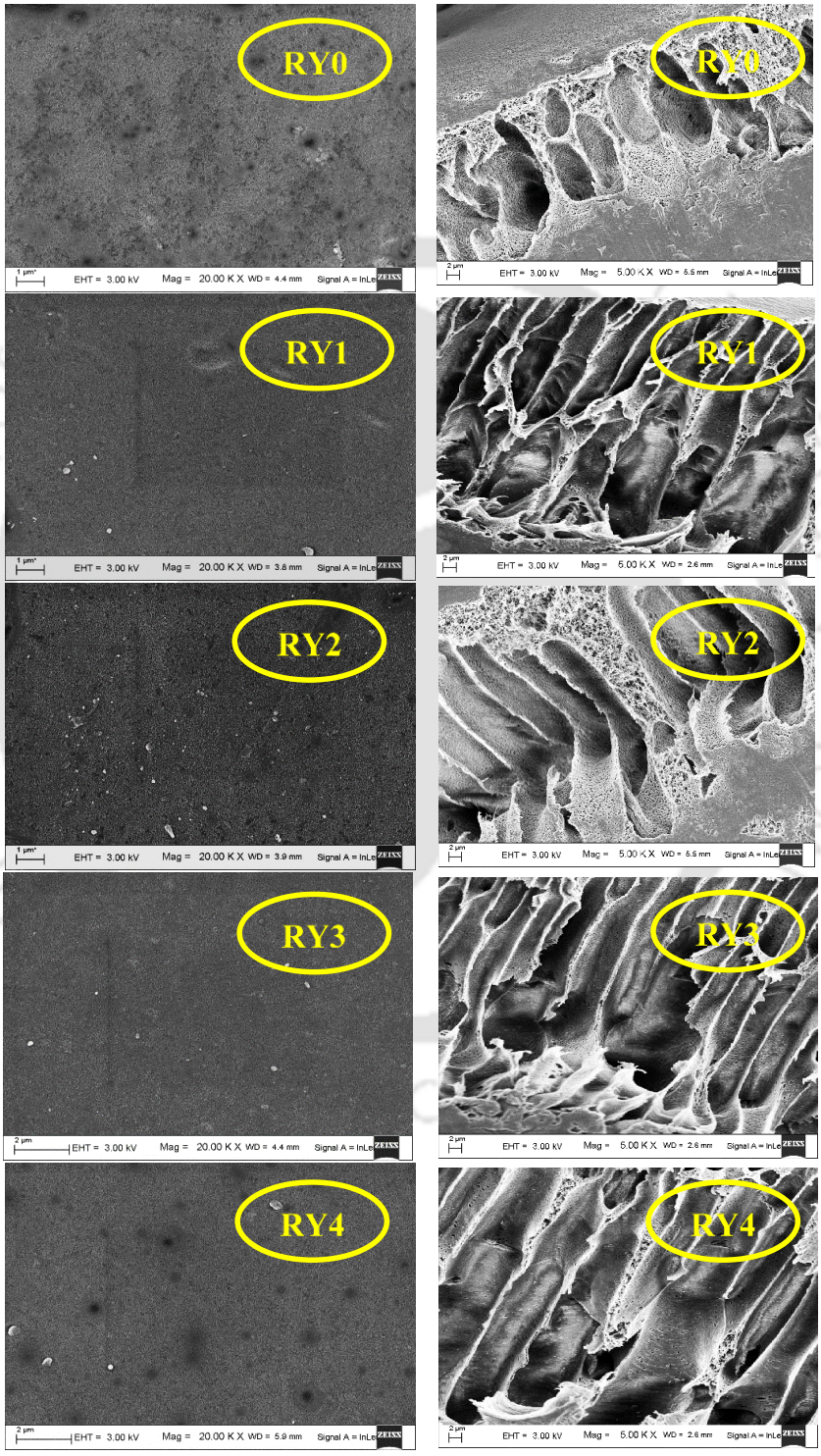

Figure 6.3. FESEM images of the membranes (a) Top Surface and (b) Cross section

Figure 6.4 shows the 3D surface AFM images of the membranes. The obtained membrane surface roughness values were presented in Table 6.2. It can be seen from the figure that the membrane (RY0) without additive shows highest average roughness of 5.50 nm compared to membrane (RY4) with highest amount of the additive Cu_2O photocatalyst shows average roughness of 2.99 nm. It is well versed that the membranes with smooth surfaces are of better antifouling nature. Since, the reason for membrane surface roughness is the presence of valleys on their surfaces. These valleys helps in the accumulation of contaminants over the membrane surface and hence boosts the membrane fouling tendency. The AFM results are in agreement with the antifouling studies of the membranes with BSA, which shows that the membranes are antifouling in nature.

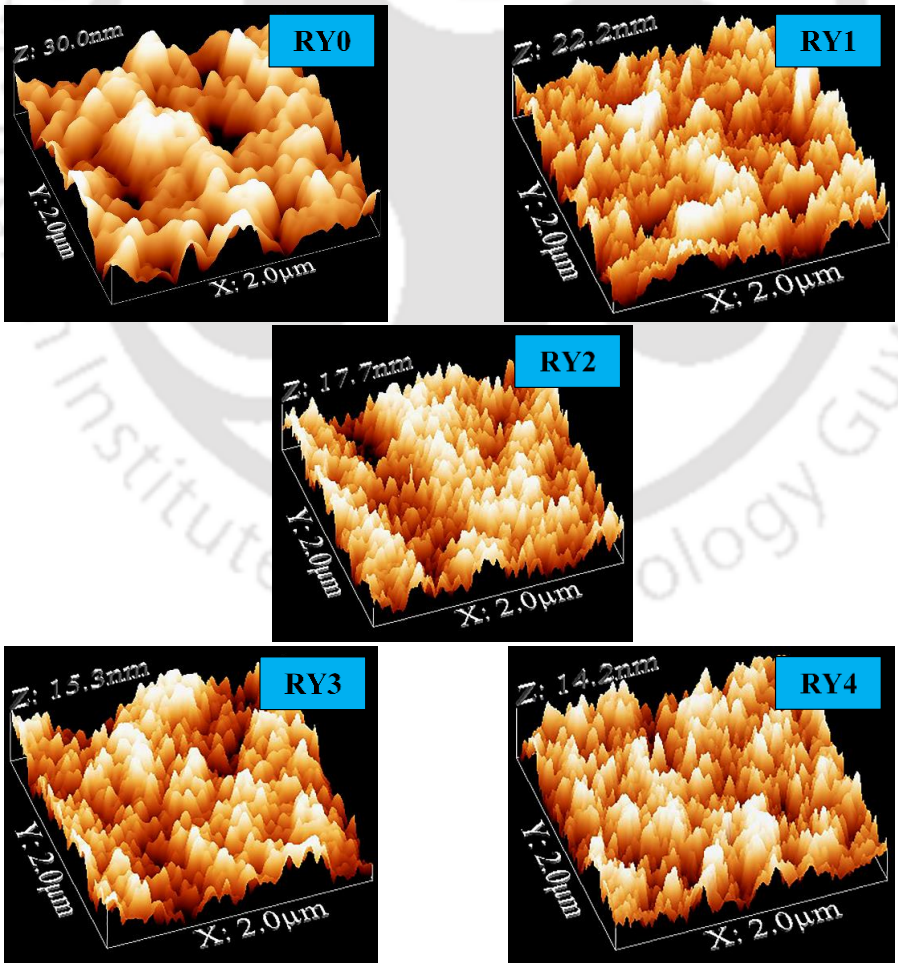

Figure 6.4. 3D AFM analysis of the membranes

Table 6.2. Few of the characterization parameters of the membranes

Membranes	Compaction factor (CF)	Average roughness (nm)	P_m (L m^{-2} h^{-1} kPa)	EWC (%)	Porosity
RY0	6.48	5.5	0.36	63.68	0.25
RY1	6.30	3.47	0.65	67.92	0.27
RY2	6.12	3.96	0.99	75.27	0.31
RY3	5.23	2.78	1.41	78.53	0.36
RY4	4.02	2.99	1.86	80.98	0.44

6.3.3 Membranes elemental analysis

6.3.3.1 FESEM-EDX analysis of the membranes

The presence and quality of dispersion of Cu_2O photocatalyst was analyzed by using FESEM-EDX analysis. It can be seen from Fig. 6.5 that peaks for the Cu_2O photocatalyst constituents, that is, Cu and O were present. In addition, the peaks for sulfur present in PSF were also seen. This confirms the uniform presence of the Cu_2O photocatalyst in the membranes. Here, it is important to note that the peak intensity for carbon is so high due to the use of carbon tape for placing the samples over the stubs.

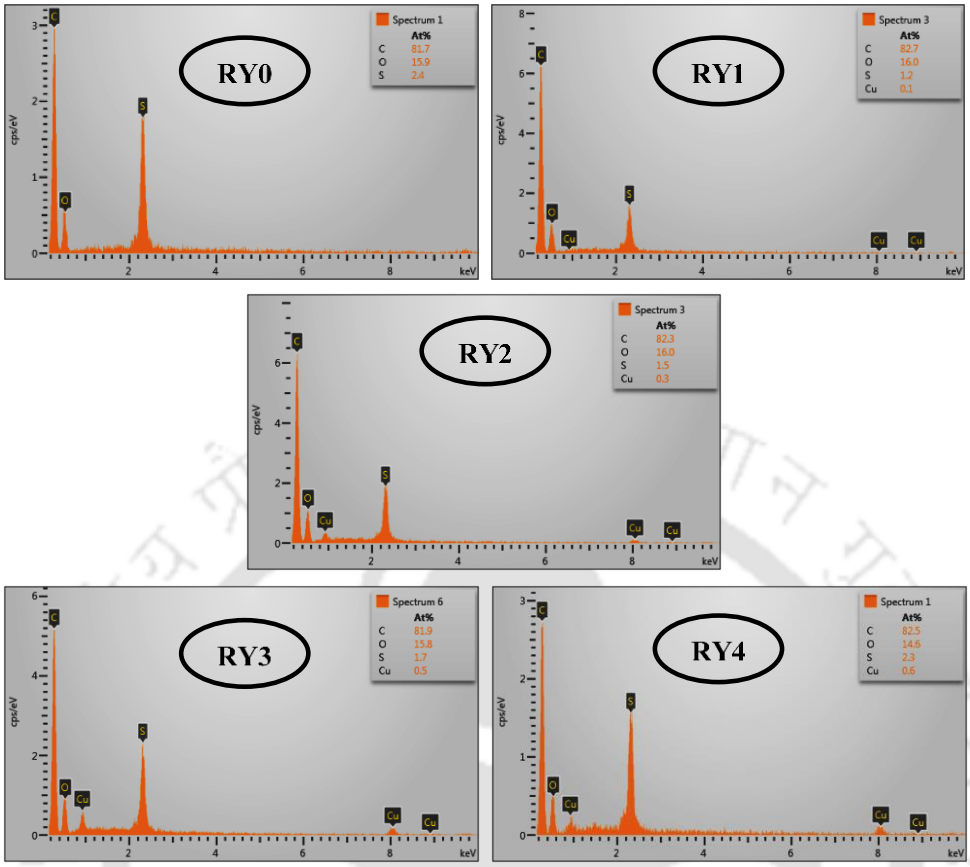

Figure 6.5. FESEM-EDX confirming the presence of Cu_2O photocatalyst in the membranes

6.3.3.2 FTIR based analysis of the membranes

The membrane FTIR analysis is shown in Fig. 6.6 (a). The bands present at 1320 and1160 cm^{-1} represents the sulfone and aromatic secondary amines present in PSF. Furthermore, bands at 1240 and 1408 cm^{-1} for C-O-C and aromatic ring vibrations confirms that PSF is present in the membranes. On the other hand, a dismal peak at 2923 cm^{-1} represents C-H asymmetric section for PEG (pore former). This confirms that the pore former goes out of the casting solution and is present in a very less amount. This was further confirmed by the morphological analysis of the membranes discussed in the preceding sections. The presence of Cu_2O photocatalyst in the membranes was justified by the main peaks at 634 cm^{-1} (P=O bending) and 1014 cm^{-1} (P=O stretching) [99].

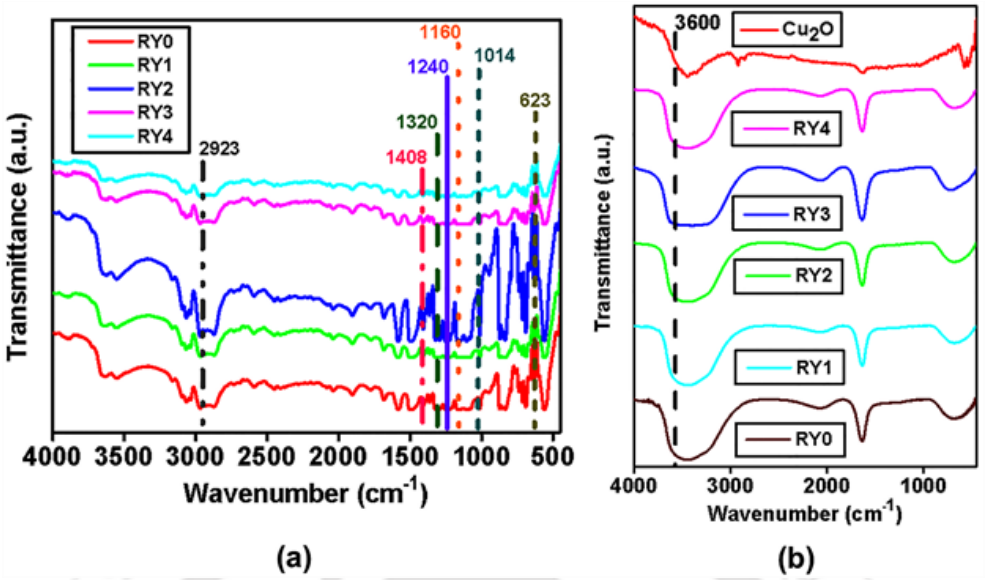

Figure 6.6. FTIR analysis of the membranes and stability analysis of Cu_2O photocatalyst in the membranes

The stability analysis of Cu_2O photocatalyst was also carried out by using FTIR. The results for this study are presented in the inset of Fig. 6.6 (b). The confirmation of stable presence of Cu_2O photocatalyst in the membranes was depicted by comparing the membrane results with DI water. The results shows that there is no peak representing Cu_2O photocatalyst in the figures and thereby confirms that it is firmly embedded in the membrane matrix and is stable there even for longer period of times. This supports the fact that the membranes are positively modified with the Cu_2O photocatalyst and it plays an important role in membranes porosity, hydrophilicity, antifouling performance, and IBP removal.

6.3.4 Influence of the additive on membrane permeation properties

The influence of additives on the membrane permeation performance was analysed by the virtue of CF, PWF, hydraulic permeability (P_m), EWC, porosity, hydrophilic and antifouling studies, which are explained in the subsequent sections.

6.3.4.1 Membrane compaction analysis

Membrane compaction factor indicates about the extent of macrovoids present in a membrane, that is, higher the CF higher will be the number of macrovoids, which upshots the compaction of the membranes. The Fig. 6.7 represent the membrane compaction. The figure as well as tabulated CF values (Table 6.2) shows that the CF of the membranes decreases from 6.48 (RY0) to 4.02 (RY4) with increasing amount of the Cu_2O photocatalyst in the membranes. Furthermore, the Fig. 6.7 shows that initially the flux of the membranes decline sharply with time and after 1 h run attains stability. This is due to the effect of membrane compaction, wherein the membrane pores become denser, nearer, and uniform resulting in the decrease of the membrane pore size and hence membrane flux. Likewise, increased membrane flux can be seen in the figure with increased amount of the additive in the membranes. As explained earlier, this is due to the effect of Cu_2O photocatalyst on the membrane morphology, that is, enhanced porosity. The steady state membrane flux increased from 34.23 L m^{-2} h^{-1} (RY0) to 179.54 L m^{-2} h^{-1} (RY4).

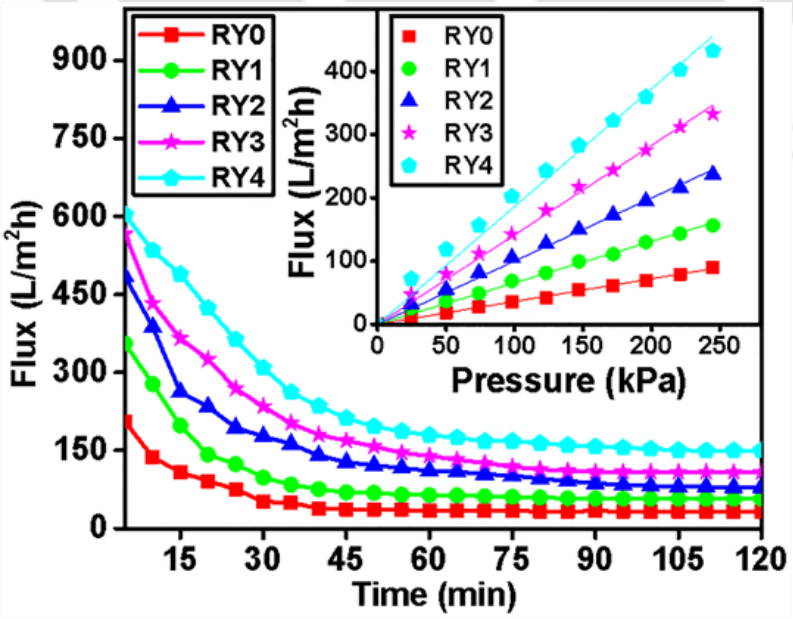

Figure 6.7. Pure water flux profile of the membranes with respect to time and pressure (inset)

6.3.4.2 Membrane flux profile and hydraulic permeability analysis

The membrane PWF was calculated at different transmembrane pressures (0-240 kPa) to analyze the flux outlines of the membranes. Figure 6.7 (inset) shows the results of this analysis. The figure shows that a higher PWF is obtained in case of higher additive amounts in the membranes. For instance, the RY4 membrane with 2% of additive shown increased membrane PWF 432.70 L m^{-2} h^{-1} in comparision to RY0 membrane, which shows 90.16 L m^{-2} h^{-1}, at 240 kPa. Furthermore, a linear increase in the PWF of the membranes can be seen with increase in the operative driving force (transmembrane pressure). Similarly, the membranes hydraulic permeability (P_m) was estimated by using the slope of the graph (Fig. 6.7 (inset)). The results shows that the P_m for RY0 is 0.36 L m^{-2} h^{-1} kPa, which increases up to 1.86 L m^{-2} h^{-1} kPa for RY4 with an increase in the amount of the additive in the membrane. The P_m results for all the membranes are presented in Table 6.2. These results confirmed that the pore former (PEG) as well as the photocatalyst (Cu_2O) helps in the formation of uniform pores as well as hydrophilicity of the membranes.

6.3.4.3 Membrane EWC and porosity study

The results of the previous sections are further confirmed by the membrane EWC and porosity estimation. The EWC is within a close proximity with PWF of a membrane, since both of them depends upon the membrane porosity. The EWC of the membranes is reported in Table 6.2. The calculated values infers that the membrane porosity was increased with increased Cu_2O photocatalyst in the membranes, since the values were increased from 63.68 % (RY0) to 80.98 % (RY4). This was further confirmed by the analysis of the membranes porosity. The membrane porosity is presented in Table 6.2. The membrane porosity shows similar trend as was in case of PWF of rise with higher amount of the

photocatalyst present in the membranes. The membrane porosity increased from 0.25 (RY0) to 0.44 (RY4).

6.3.4.4 Membrane hydrophilicity study

The membrane hydrophilicity depends upon the presence of hydrophilic entities in the membranes. Therefore, it is advised to use hydrophilic additives which thereby impart hydrophilicity to the membranes. The measure of a membranes hydrophilicity is its static water contact angle (SWCA). The results for the same are reported in Fig. 6.8 (a.i). Unsurprisingly, the SWCA is decreased as the amount of the Cu_2O photocatalyst is increased in the membranes from 71.5° to 45.3°. Furthermore, the SWCA not only depends upon the surface hydrophilicity of a membrane but also on factors, like surface roughness, membrane pore size, porosity, and pore size distribution. For instance, if two membranes with similar hydrophilicity are compared then the membrane with smooth surface will give lower SWCA as compared to the one having higher surface roughness [100]. Therefore, in this study both the membrane conditions viz., membrane surface hydrophilicity and roughness, were in favor of better hydrophilicity of the membranes. These results are in favor of antifouling studies of the membranes with BSA. Since, the hydrophilicity is responsible for antifouling nature of the membranes [48].

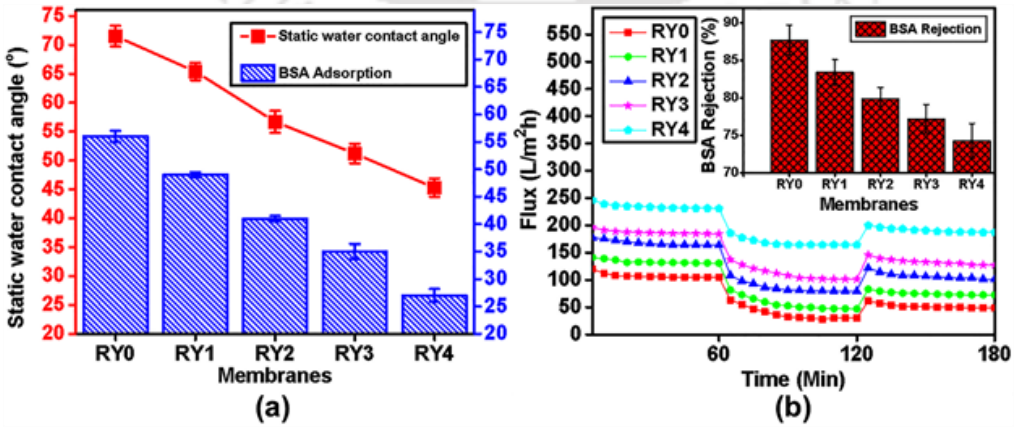

Figure 6.8. (a.i) SWCA and (a.ii) BSA adsorption; (b) antifouling profile and BSA rejection (inset) results of the membranes

6.3.4.5 Membrane antifouling studies

Fouling of membranes is the biggest challenge for the successful development and implementation of membranes on commercial as well as industrial levels. Therefore, it is necessary to mitigate the problem of fouling in the synthesized membranes. Therefore, to analyze this BSA adsorption as well as permeation studies were carried out with the prepared membranes.

In the BSA adsorption study, the lesser the BSA adsorbed better the antifouling nature of the membrane and vice versa. The results of the BSA adsorption study are shown in Fig. 6.8 (a.ii). It can be seen from the figure that the nascent membrane (RY0) has shown the highest (27 µg cm^{-2}) BSA adsorption compared to other membranes and the membrane containing 2 wt% of the Cu_2O photocatalyst (RY4) as additive shown the least BSA adsorption (56 µg cm^{-2}). Altogether, the membranes shown decrease in BSA adsorption with higher amounts of the additive. The reason behind this is the hydrophilicity and hydration capacity of the membranes [15]. As explained in the previous section, the hydrophilicity of the membranes was increased with an increase in the additive amount. Therefore, the membranes are with better antifouling nature and have better capabilities of hydration. This helps the membranes to form a water layer over their surfaces and restricts the protein adsorption. Thereby, stating that the prepared membranes are better antifouling in nature.

In this study, BSA solution (1000 mg L^{-1}) was permeated through the membranes to examine their antifouling performance. The membrane flux rejection profiles were analyzed for censoriously assessing the antifouling capabilities of the membranes. The results of this study are shown in Fig. 6.8 (b). The pure water flux profile is shown at the beginning (F_{W1}), thereafter the BSA permeation profile (F_{BSA}), and lastly again the pure

water flux profile after cleaning the membranes. This last run with pure water determines the degree of irreversible fouling taken place in the membranes.

The Fig. 6.8 (b) depicts that the F_{W1} profile changes moderately but in the initial stages of the F_{BSA} profile a steep decrease can be seen. This is due to the fact that the BSA molecules adhered to the membrane surface, which results in the reduction of the membrane pore size. The extent of protein deposition over a membrane surface depends upon the membranes hydrophobicity as well as electronic interactions amidst the membrane surface and protein molecule [64,101]. The decline in the BSA flux stabilizes after reaching an equilibrium amidst the membrane surface and protein molecules or saturation of the membrane surface with the protein molecules and a steady state flux F_{BSA} was achieved.

The reversible and irreversible membrane fouling contributes to the total membrane fouling. Where, the reversible fouling can be taken care of by simple washings, whereas the irreversible fouling needs either chemical or enzymatic cleaning. In case, the total membrane fouling is high that means there would be higher membrane flux loss. Therefore, it is suitable for a membrane or membrane process to have low total membrane fouling. In this study, it can be seen from the reported values for reversible, irreversible, and total membrane fouling that they are in decreasing order with increase in the amount of the additive. This shows that the additive is having a positive effect on the membrane fouling. Therefore, the calculated flux recovery ratio (F_{RR}) also depicts the same results as shown in Fig. 6.9 (a). F_{RR} evaluate the membranes antifouling performance. Higher F_{RR} value depicts membranes with better antifouling performance. The F_{RR} values are higher for the membranes with higher amount of the additive. F_{RR} values increased from 48.11 (RY0) to 81.53 (RY4). This states that the deposited BSA molecules can be removed from the membrane surface by simple hydraulic washing. The cleaning efficiency of the membranes

confirms it as shown in Fig. 6.9 (b). The membrane RY4 shows highest cleaning efficiency of 34.43% as compared to other membranes. Thereby, confirming the positive effects of the additive Cu_2O photocatalyst on the antifouling nature of the membranes. Furthermore, the membranes show low reversible, irreversible, and total membrane fouling as depicted in Fig. 6.9 (inset). This confirms that the pristine membrane will be more prone to fouling as compared to the Cu_2O photocatalyst containing mixed matrix PSF membranes.

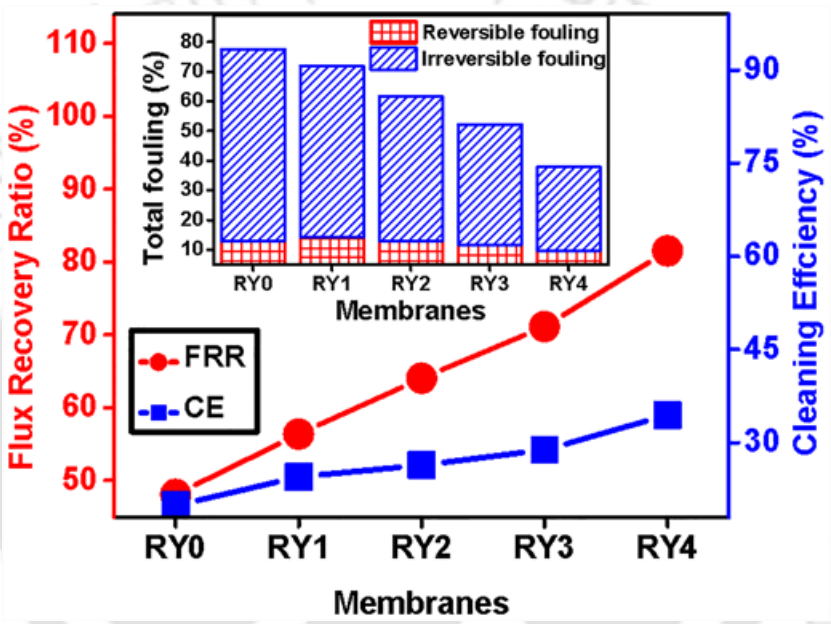

Figure 6.9. Flux recovery ratio (a) and cleaning efficiency (b) of the membranes along with the reversible, irreversible, and total fouling of the membranes in the inset

The BSA rejection profile of the membranes is shown in Fig. 6.8 (b) (inset). The figure clearly depicts that the BSA rejection decreases from 87.7% (RY0) to 74.3% (RY4) with increased amount of the additive in the membranes. Unsurprisingly, this is due to the membrane porosity and pore size along with the presence of positive surface charge on the Cu_2O photocatalyst as compared to the negative charge present on the BSA molecules at pH 7 [94]. These circumstances augments the permeation of the BSA molecules across the membranes.

6.3.5 Photocatalytic removal studies of IBP with membranes

Photocatalytic removal of IBP is presented in this section. The result shows that the use of the Cu_2O photocatalyst modified PSF membranes in light yield in higher removal of IBP as compared to the dark conditions. This confirms that the prepared membranes are excellent performers under simulated sunlight and could be a great product in terms of a photocatalyst.

6.3.5.1 Membrane IBP removal under dark conditions

The results of the membranes for IBP removal under dark conditions is presented in Fig. 6.10 (a, b, and c) at basic, neutral, and acidic pH.

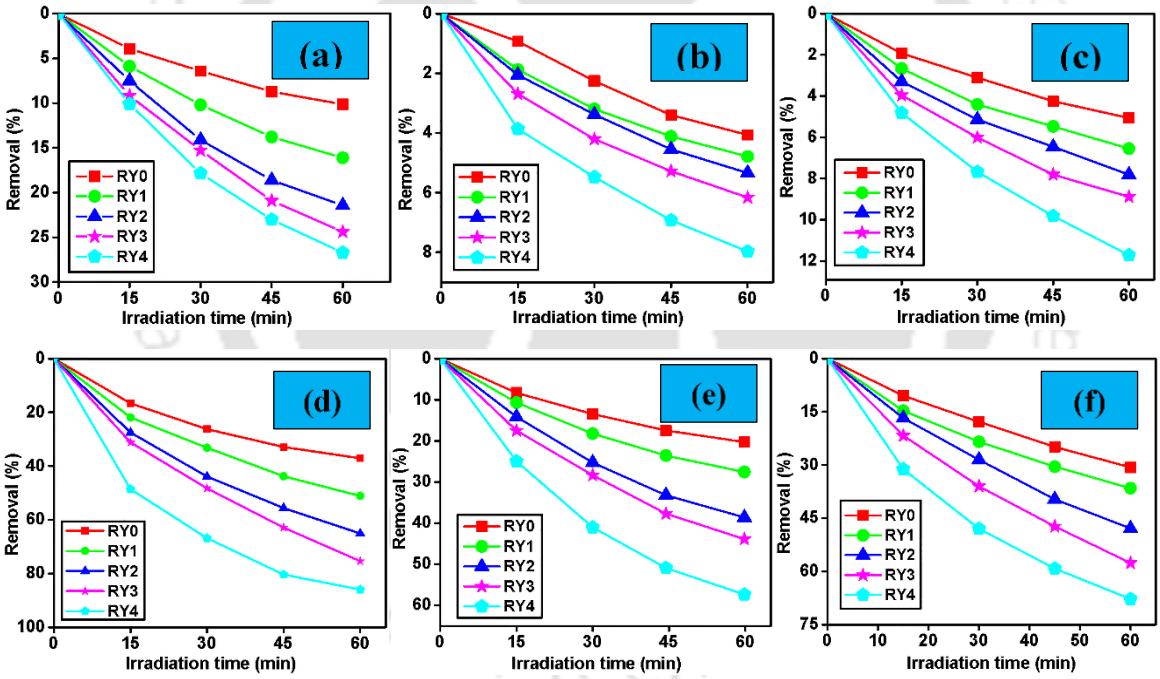

Figure 6.10. Photocatalytic removal of IBP under different conditions, Dark: (a) acidic, (b) basic, (c) neutral; and Simulated solar light: (d) acidic, (e) basic, (f) neutral

It can be seen from the figures that the IBP removal is the least from 4.0% (RY0) to 7.9% (RY4) in case of basic pH. It is somewhat higher in case of neutral conditions from 5.0% (RY0) to 11.7% (RY4). Lastly, highest in case of acidic conditions from 10.1% (RY0) to 26.7% (RY4). This difference in removal was due to the surface charge and electrical

properties of IBP. Since, IBP is a weak acid with pKa values in between 4.52 to 4.9 [102]. Therefore, under weak acidic conditions (2.7 to 4.9) IBP exists as an electrically neutral species and in a molecular form. Whereas, the Cu_2O photocatalyst was present as a positive charge containing species. Thereby, facilitating the adsorption of IBP over the catalyst surface and in the membranes. On the other hand, in the neutral and alkaline conditions (pH > 4.9) both the catalyst as well as IBP were electronegative and thus repel each other [103]. Henceforth, decreased removal of IBP under these conditions is seen. Thus, the results of this study confirms that weak acidic conditions (especially at pH 4.5) aids fast and complete removal of IBP. Therefore, for acidic conditions pH 4.5 was selected.

6.3.5.2 Membrane IBP removal under light conditions

Figure 6.10 (d, e, and f) presents the results for the membrane based IBP removal studies carried out under visible light conditions at basic, neutral, and acidic conditions. The figures shows that the photocatalytic removal of IBP is way more compared to dark conditions. The photocatalytic IBP removal under acidic conditions is the highest, increasing from 37.1% (RY0) to 86.0% (RY4). Then it is in case of neutral conditions, increased from 30.1% (RY0) to 67.8% (RY4). Lastly, the basic conditions shown the least photocatalytic removal of IBP from 20.3% (RY0) to 57.4% (RY4). The reasons for these differences in photocatalytic removal of IBP under different pH conditions was same as explained in the previous section.

6.3.5.3 Cu_2O photocatalyst concentration effect on IBP removal

The Cu_2O photocatalyst concentration shows positive effect on the removal of IBP under both dark as well as light conditions. The removal increases in both the cases as shown in Fig. 6.10. The pseudo-first-order rate kinetics via Langmuir-Hinshelwood expression can be used to explain IBP removal kinetics as given below [104]:

$$\ln\left(\frac{C_t}{C_O}\right) = -kt$$

12

Where, C_o represents the IBP concentration (mg L^{-1}) at adsorption-desorption equilibrium, C_t the concentration (mg L^{-1}) of IBP at time t (min), and k the rate constant (min^{-1}).

Figure 6.11 represent the values of $\ln(C_o/C_t)$ for different membranes as a function of time. Furthermore, the rate constant (k) was estimated from the linear fit data and is shown in Fig. 6.12. The k values shows that the removal rate under acidic conditions was increased from 1.77×10^{-3} min^{-1} (RY0) to 5.18×10^{-3} min^{-1} (RY4) in case of dark conditions and from 7.63×10^{-3} min^{-1} (RY0) to 32.63×10^{-3} min^{-1} (RY4) in case of light conditions. This confirms that the present system contains prominent photocatalytic properties for the removal of IBP under visible light. This makes it both efficient and cost effective.

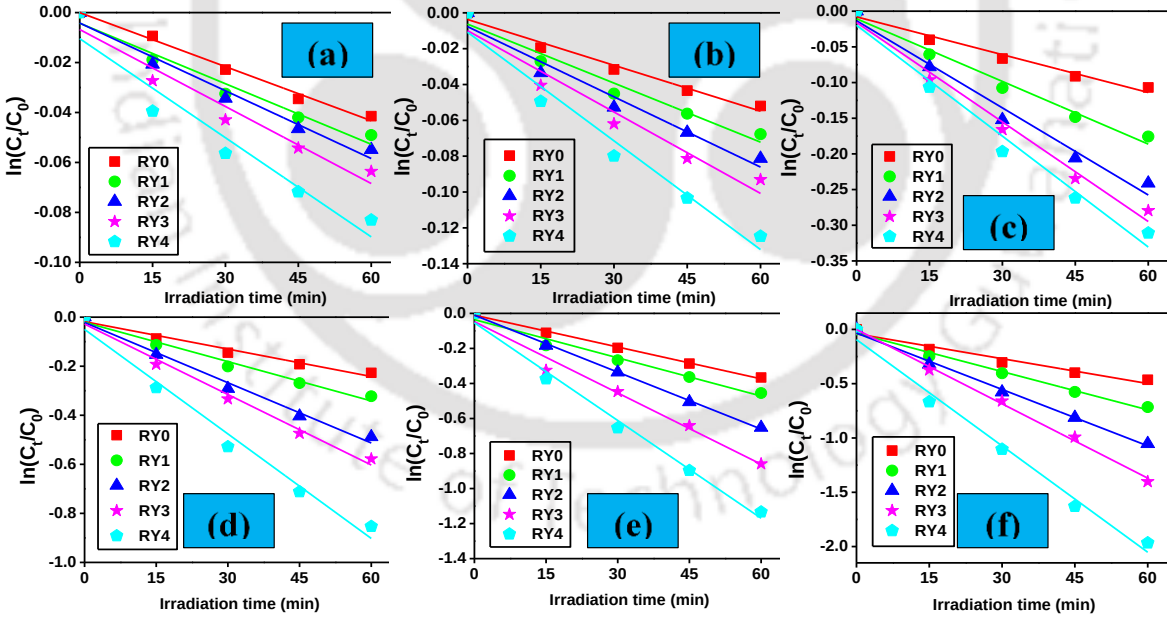

Figure 6.11. Plots of $\ln(C_t/C_0)$ vs time for different conditions, Dark: (a) basic, (b) neutral, (c) acidic; simulated solar light: (d) basic, (e) neutral, (f) acidic, and their corresponding linear fittings

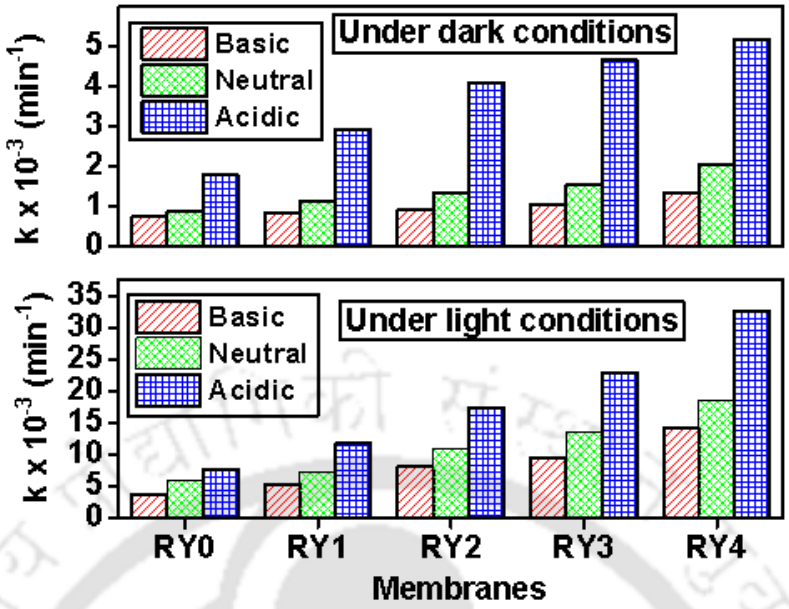

Figure 6.12. The IBP removal rates of different membranes under different pH conditions

6.3.5.4 Cyclic stability of the Cu_2O photocatalyst modified membranes

The cyclic stability of the membranes for photocatalysis under visible light was carried out by using the same membrane for four consecutive cycles under acidic condition by giving hydraulic washing after each cycle. The membrane RY4 with the best results, as shown in Fig. 6.10, was selected for this stability study. Fascinatingly, the membrane RY4 exhibited exceptionally stable photocatalytic removal of IBP under visible light irradiation, as shown in Fig. 6.13. It can be seen from the figure that the membranes show stable photocatalytic activity up to the fourth cycle. Therefore, it can be stated that the said membranes carry extremely stable photocatalysis potential for wastewater treatment and pharmaceutical applications. Furthermore, the presence of the photocatalyst in membrane form makes it easier to use and regenerate for cost-effective applications.

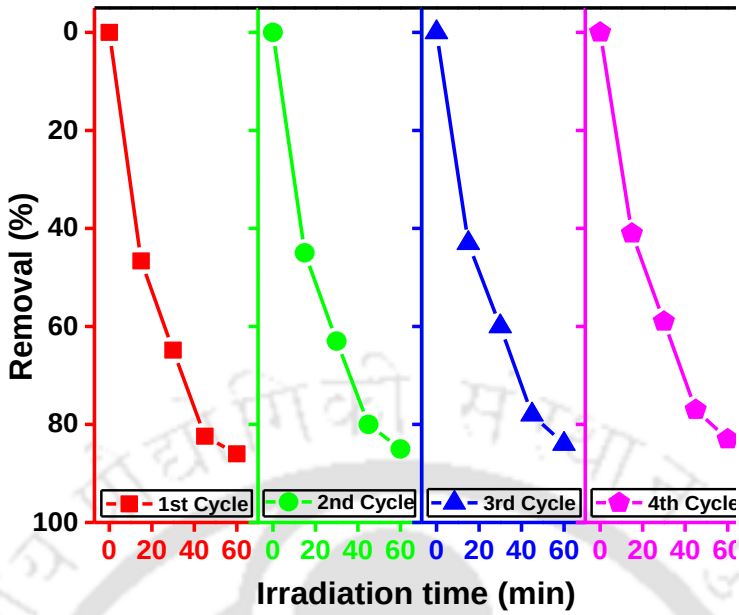

Figure 6.13. The cyclic stability analysis of the RY4 membrane under visible light and acidic conditions for four cycles

6.3.5.5 Structural stability of the Cu_2O photocatalyst modified membranes

In order to confirm the structure, phase, and crystallinity XRD analysis, using D8 Advance, Bruker instrument in the range of 20–80° 2θ with a scan rate of 3°/min, of the fresh and used (RY4_4th Cycle) membranes was carried out as shown in Fig. 6.14. The prominent diffraction peaks for RY4 detected at 35.7° and 38.9° correspond to the characteristic Cu_2O planes (1 1 –1) and (1 1 1), respectively. After 4th photocatalytic cycle, RY4 shows identical XRD pattern with slightly reduced intensity, may be due to the reduction in crystallinity. This confirms that the Cu_2O photocatalyst is sturdily present in the membranes even after four cycles, without any notable formation of other oxidation states.

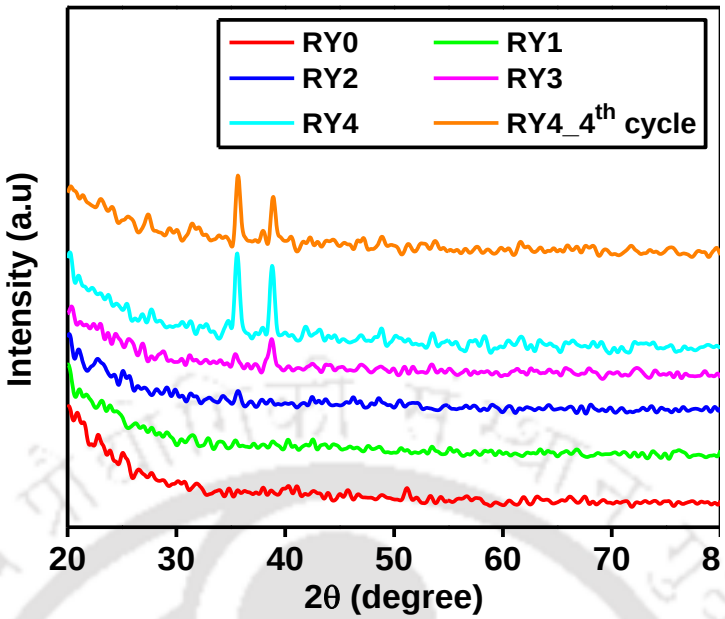

Figure 6.14. XRD patterns of the membranes including fresh as well as used RY4 membrane.

6.3.5.6 Optical analysis of the Cu_2O photocatalyst modified membranes

The optical absorbance assessment of the membranes was carried out by using the UV–vis diffuse reflectance spectroscopy (DRS). The instrument used for the analysis was a commercial spectrophotometer (PerkinElmer, UV win Lab). The UV–vis absorbance spectra of the fresh membranes are shown in Fig. 6.15, in the range of 250–800 nm. It can be seen from the figure that the membranes with increasing amount of Cu_2O photocatalyst show systematic increase in the visible absorption. However, the membrane RY0 containing no additive shows negligible absorbance in this region. This confirms that the membranes containing Cu_2O photocatalyst exhibits strong absorption in the visible region with a broad envelope covering 400–750 nm and thus it can be concluded that the membranes are best for photocatalytic activity under visible light. Additionally, inset of Fig. 6.15 shows a comparison of the absorbance spectra of fresh and used (up to four cycles) RY4 membrane. The figure shows that there is negligible change in the absorbance spectra of the RY4 membrane even after four cycles of use. This further states that the membranes

are highly stable with their activity intact firmly and thus can be reused for very high number of cycles.

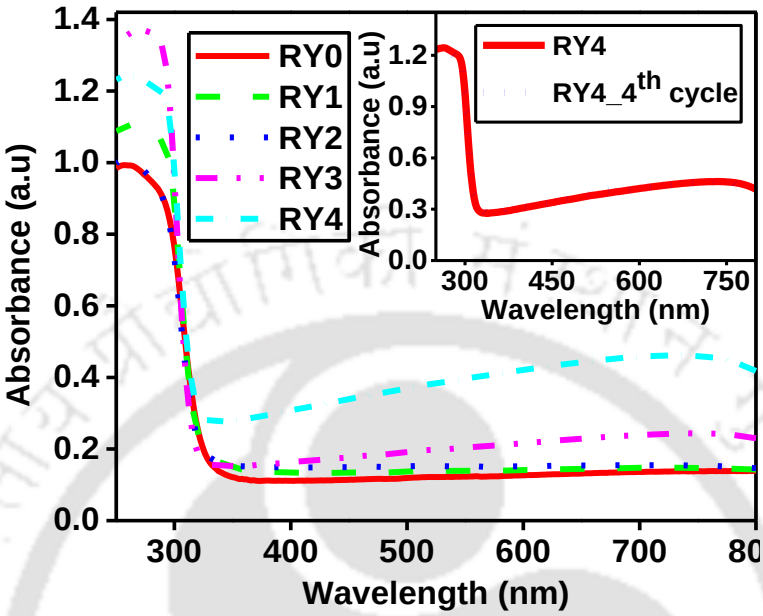

Figure 6.15. The UV-Vis absorbance spectra of different membranes. Inset: UV-Vis absorbance spectra of fresh and used RY4 membranes.

6.4 Summary

Cu_2O photocatalyst modified mixed matrix PSF ultrafiltration membranes were synthesized successfully. The membranes shown effective and efficient removal of IBP under simulated light conditions. The additive has significant effect on membrane properties, such as flux, EWC, SWCA, porosity, pore size distribution, surface roughness, Pm, hydrophilicity, and antifouling performance. The membrane EWC was increased from 63.68% to 80.98%, porosity from 0.25 to 0.44, and the surface roughness depicting antifouling nature and BSA rejection decreased from 5.5 to 2.99 and 87.7% to 74.3%, respectively. These results confirm that the prepared membranes are hydrophilic and antifouling in nature. The best IBP removal was achieved under acidic conditions with membrane RY4 containing highest amount of the additive Cu_2O photocatalyst in both dark and light conditions. 4.0% (RY0) to 7.9% (RY4) (at basic pH), 5.0% (RY0) to 11.7% (RY4)

(at neutral pH), and 10.1% (RY0) to 26.7% (RY4) (at acidic pH) under dark conditions. On the other hand, it was 20.3% (RY0) to 57.4% (RY4) (at basic pH), 30.1% (RY0) to 67.8% (RY4) (at neutral pH), and 37.1% (RY0) to 86.0% (RY4) (at acidic pH) under light conditions. These results approve that the prepared membranes are prominent for the pharmaceutical removal applications and holds promising prospects for commercial applications. The DRS analysis of the fresh and used membranes depicts consistent photocatalytic activity. Furthermore, the cyclic and structural stability analysis shows the membrane are stable for longer period of time with their photocatalytic activity intact. This confirms that the membranes are suitable for commercial use for longer period of times without losing any photocatalytic activity.

Chapter 7
pH and thermo-responsive mixed matrix polysulfone ultrafiltration membrane for photocatalytic dye removal

In this chapter, the synthesis and characterization of a stimuli responsive *poly(*N-vinylcaprolactam-TiO_2-acrylic acid) *(VCL-TiO_2-AA) polymer nanocomposite in various ratios and modification of polysulfone (PSF) membranes with the synthesized VCL-TiO_2-AA is discussed. The modified membranes were analysed for their hydrophilic, photocatalytic, and pH and thermos-responsive behaviour. Also, the synthesized* stimuli responsive *nanocomposite is characterized by using FESEM and FESEM-EDX techniques. The* stimuli responsive *nanocomposite was directly blended to the membrane casting solution and this casting solution was used to synthesize membranes by phase inversion method. The membranes were characterized for its morphology by using FESEM. FTIR and FESEM-EDX analysis were carried out to analyse the elemental analysis of the membranes. Furthermore, the effect of the synthesized stimuli responsive VCL-TiO_2-AA polymer nanocomposite was analysed on the membrane performance in terms of fouling, temperature and pH responsiveness, and photocatalytic removal of MB dye under dark and UV light conditions at different pH values. Furthermore, the ultrafiltration performance and antifouling nature of the modified membranes were investigated and analysed.*

7.1. Experimental

7.1.1. Materials

Polysulfone (PSF), polyethylene glycol (PEG), 1-methyl-2-pyrrolidone (NMP), potassium bromide (KBr), humic acid (HA), N, O-Bis-(trimethylsilyl) acetamide, poly(acrylic acid) (AA), and poly(N-vinylcaprolactam) (VCL) are the chemicals which were used for this

chapter. Deionized (DI) water was used throughout the experiments. Detail of all the chemicals is given in Table 2.1 of Chapter 2.

7.1.2 Synthesis of modified TiO_2 nanoparticles

Agglomeration is a major problem with TiO_2 nanoparticles, which occurs during their dispersion in a solvent. Therefore, to rectify this problem the TiO_2 nanoparticles were modified with N, O-Bis-(trimethylsilyl) acetamide (a silane) agent. This reduces the hydrophilic nature of the TiO_2 nanoparticles by adding Si groups on the surface of the particles. The TiO_2 nanoparticles were added to a 3-neck round bottom flask and dispersed in ethanol with the help of sonication. Thereafter, the flask was kept in an oil bath for 24 h at 70°C under reflux after adding BSA at a concentration of 5 wt% of the total TiO_2 nanoparticles content. On completion of the process, the modified TiO_2 (m-TiO_2) nanoparticles were separated from the reaction mixture by using centrifugation. Subsequently, the m-TiO_2 nanoparticles were washed a number of times with ethanol. Finally, the m-TiO_2 nanoparticles were dried at 60°C for 24 h before storing them for further use.

7.1.3 Synthesis of stimuli responsive VCL-TiO_2-AA polymer nanocomposite

The stimuli responsive poly(N-vinylcaprolactam-TiO_2-acrylic acid) (VCL-TiO_2-AA) polymer nanocomposite was synthesized by free radical co-polymerization of VCL and AA with m-TiO_2 nanoparticles. The m-TiO_2 nanoparticles were taken in a 3-neck round bottom flask and sonicated for their uniform dispersion in ethanol. Thereafter, different ratios of VCL and AA were added to the uniformly dispersed m-TiO_2 nanoparticles as shown in Table 7.1. The 3-neck round bottom flask containing the mentioned materials was then

purged with N_2 gas for 30 min so as to remove O_2, which may act as a radical scavenger, and to create inert atmosphere in the 3-neck round bottom flask. Later, the 3-neck round bottom flask was kept in an oil bath for 24 h at 70°C under reflux conditions after addition of initiator Azoisobutyronitrile (AIBN) and cross linker N,N'-methylenebisacrylamide (MBAA). Afterwards, the obtained stimuli responsive VCL-TiO_2-AA polymer nanocomposite was centrifuged and washed several times with fresh ethanol so as to remove unwanted and unreacted reagents. The stimuli responsive VCL-TiO_2-AA polymer nanocomposite was dried at room temperature for 1 week in a desiccator. Finally, it was stored in air tight bottles till further use.

Table 7.1 Composition of the stimuli responsive VCL-TiO_2-AA polymer nanocomposite reaction mixture

S. No.	Ratio	TiO_2 (Wt%)	VCL (Wt%)	AA (Wt%)	MBAA (Wt%)	AIBN (Wt%)
1.	1:2(RM1)	33	30	30	7	0.3
2.	2:1(RM2)	67	15	15	3	0.3
3.	1:1(RM3)	50	22.5	22.5	5	0.3

7.1.4 Characterization of the stimuli responsive VCL-TiO_2-AA polymer nanocomposite

The synthesized stimuli responsive VCL-TiO_2-AA polymer nanocomposite were characterized by using different standard characterization techniques, such as FESEM, FESEM-EDX, and FTIR for the assessment of the morphology and confirmation of the chemical groups present in the nanocomposite as explained in Chapter 2.

7.1.5 Fabrication of modified PSF membranes

The modified PSF membranes were synthesized by using phase inversion technique as explained in Chapter 2. The composition of the membrane casting solution is given in Table 7.2.

Table 7.2 Composition of the membrane casting solutions

Nanocomposite	Membrane	PSF (Wt %)	Nanocomposite (Wt %)	PEG 6000 (Wt %)	NMP (Wt %)
Nil	RM0	12	0	5	83
RM1	RM11	12	1	5	82
	RM12	12	3	5	80
	RM13	12	5	5	78
	RM14	12	7	5	76
RM2	RM21	12	1	5	82
	RM22	12	3	5	80
	RM23	12	5	5	78
	RM24	12	7	5	76
RM3	RM31	12	1	5	82
	RM32	12	3	5	80
	RM33	12	5	5	78
	RM34	12	7	5	76

7.2 Characterization of modified PSF membranes

All of the synthesized membranes were analysed for their PWF profile. Later, membranes with only maximum and minimum amount of the different types of synthesised stimuli responsive VCL-TiO_2-AA nanocomposite as additive were taken up for further characterization and permeation based studies of the membranes.

7.2.1 Morphological studies of the modified PSF membranes

The membranes were analysed for their top and cross-section by using FESEM discussed in Chapter 2.

7.2.2 Elemental analysis of the modified PSF membranes

The compositional studies of the membranes were carried out by using various standard characterization techniques, such as FESEM-EDX and FTIR as explained in Chapter 2.

7.2.3 Permeation studies of the modified PSF membranes

7.2.3.1 Membrane compaction studies of the modified PSF membranes

The compaction profile of the membranes was analysed in this study in a similar fashion as discussed in previous Chapters of this work and was calculated by using Eqn. 2.11.

7.2.3.2 Pure water flux and hydraulic permeability of the modified PSF membranes

The flux of a membrane is an important measure for its permeation capability. The better the flux better the membrane for an application. Since, it will be capable of giving required amount of permeate in a given time. Therefore, it is important to analyse the flux profile of a membrane. The pure water flux (PWF) of the membranes was calculated by using Eqn. 2.10.

The hydraulic permeability is also an important membrane property which again helps in evaluating the membranes permeation capabilities. In this study, the membrane hydraulic permeability was calculated by using Eqn. 2.12.

7.2.3.3 Equilibrium water content, porosity, and hydrophilicity of the modified PSF membranes

Equilibrium water content (EWC) is another important membrane parameter to assess the membranes porosity and hydrophilicity. It was measured by following the procedure given in Chapter 2 and was calculated by using Eqn. 2.13.

The most important trait of a membrane is its porosity, which is an important factor for deciding a membranes permeability and selectivity. The membrane porosity was calculated by using Eqn. 2.14.

The hydrophilicity of a membrane is also an important parameter as the fouling of a membrane depends upon it. The static water contact angle (SWCA) measured over the membrane surface gives the extent of hydrophilicity of a membrane. The SWCA was measured by following the procedure given in Chapter 2.

7.2.4 Antifouling studies of the modified PSF membranes

Membrane fouling is a serious problem associated with membranes, which declines their overall performance and therefore required to be kept at minimum. Thereby, the prepared membranes were tested for their antifouling nature by using HA as the model foulant as explained in Chapter 2. In this study, the membranes were first compacted at 300 kPa pressure for 60 min and then permeated with DI water for 60 min. This run with the DI water will gives pure water flux of the membrane denoted by F_{W1}. Thereafter, the membranes were permeated with 1000 mg L^{-1} aqueous solution of HA for 60 min. This run with HA gives membrane flux denoted by F_{HA}. Afterwards, the membranes were hydraulically washed at 40°C and 25°C. The membranes were then again permeated with DI water for 60 min to give us second pure water flux of the membranes denoted by F_{W2}. This measures of the membrane antifouling, such as HA rejection, flux recovery ratio (F_{RR}),

cleaning efficiency (CE), and membrane resistances were all calculated by using Eqns. 2.15-2.20.

7.2.5 pH- and thermo-responsive permeability studies of the modified PSF membranes

The pH- and thermo-responsiveness of the membranes was tested by using the membrane cell setup previously described in Chapter 2. The membranes were initially compacted for 60 min at 340 kPa. Thereafter, they were soaked in an aqueous solution of desired pH or temperature for 15 min. The pH of the feed was set between 2 to 11 by using 0.1 N HCl and 0.1 N NaOH solution. The membranes were permeated for 15 min with the desired feed at 150 kPa. Eqn. 2.10 was used to measure the flux of the membranes. The temperature was kept constant at 25°C for pH responsive experiments and pH was kept at 7 for thermoresponsive experiments. The membrane permeability was again tested after cleaning the membranes with DI water. The results shows that the membrane permeability remains constant and shows no change after the pH- and thermo-responsive experiments.

7.2.6 Photocatalytic dye removal using modified PSF membranes

The photocatalytic dye removal using modified PSF membranes was studied with 10 mg L^1 aqueous solutions of MB dye under both dark as well UV light conditions. The 0.1 g of membrane samples were weighed and cut into smaller pieces. Thereafter, these membrane pieces were taken into 100 mL capacity conical flasks along with 50 mL of 10 mg L^{-1} MB dye solution. Subsequently, these conical flasks were kept for stirring before the analysis (under both dark and UV light conditions) for so that an apposite adsorption and desorption equilibrium sets between the membrane and dye molecules. Later for the analysis of dye

removal under dark conditions, the conical flasks were kept in an incubator cum shaker at 120 rpm for 1 h and samples were taken after every 15 min for analysis.

On the other hand in case of dye removal analysis under UV light conditions, the conical flasks containing the membrane samples and dye aqueous solutions were kept in a time programmable commercial photochemical reactor (Lelesil Innovative Systems, Mumbai). The source of UV light in this experiment was a 100 W lamp with peak emissions at 380 nm. The reactor temperature was kept constant by circulating cool water in the quartz jacket surrounding the reactor. This validates that the dye removal is taking place under the influence of UV light and not heat. Similar to the dark condition experiment, here also the samples for analysis were taken after every 15 min.

The UV-Visible spectrophotometer (Perkin-Elmer Precisel, Lambda-35) was used to analyze the samples of both the experiments. The dye removal was estimated by suing the following relation:

$$\%\ Removal = \left(1 - \frac{DC_I}{DC_F}\right) \times 100 \qquad 7.1$$

Where, DC_I and DC_F stands for MB dye initial and final concentrations in the aqueous solutions.

7.3 Results and discussions

7.3.1 Characterization of stimuli responsive VCL-TiO_2-AA polymer nanocomposite

The morphological analysis of the stimuli responsive VCL-TiO_2-AA polymer nanocomposites carried out by using FESEM is shown in Fig. 7.1. The figure shows that the synthesized nanocomposites are of uniform shape and size.

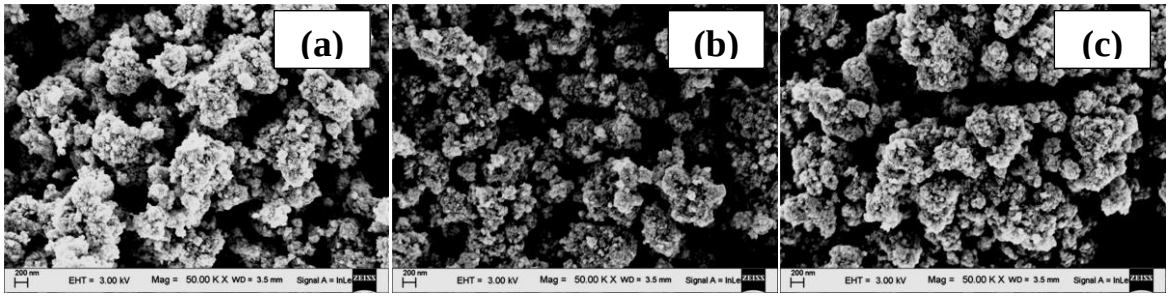

Figure 7.1 FESEM micrographs of the different stimuli responsive VCL-TiO_2-AA polymer nanocomposites: (a) RM1, (b) RM2, and (c) RM3

7.3.2 Morphological studies of the modified PSF membranes

The top surface images of the membranes were shown in Figure 7.2 (a). The cross sectional micrographs of the membranes are shown in Fig. 7.2 (b). The micrographs shows that the membranes have asymmetric structures containing a dense, selective top layer and porous sublayer. The addition of stimuli responsive VCL-TiO_2-AA polymer nanocomposites ensued substantial change in the morphology of the membranes. The figures shows that the porosity of the membranes was enhanced on addition of the nanocomposite. Since, the addition of the nanocomposite results in the decrease of the thermodynamic steadiness of the system. Due to this rapid demixing between the solvent and non-solvent formation of highly porous membranes ensues [48]. Altogether, the macrovoids present in the pristine membrane were also disappeared from the membranes containing the nanocomposite due to the addition of the nanocomposite. Furthermore, the pore size calculated by using FESEM images and ImageJ software is reported in Fig. 7.3. The average pore size for the membranes RM0, RM11, RM14, RM21, RM24, RM31, and RM34 are 7.57, 10.85, 14.78, 16.22, 17.60, 18.34, and 20.73 nm, respectively.

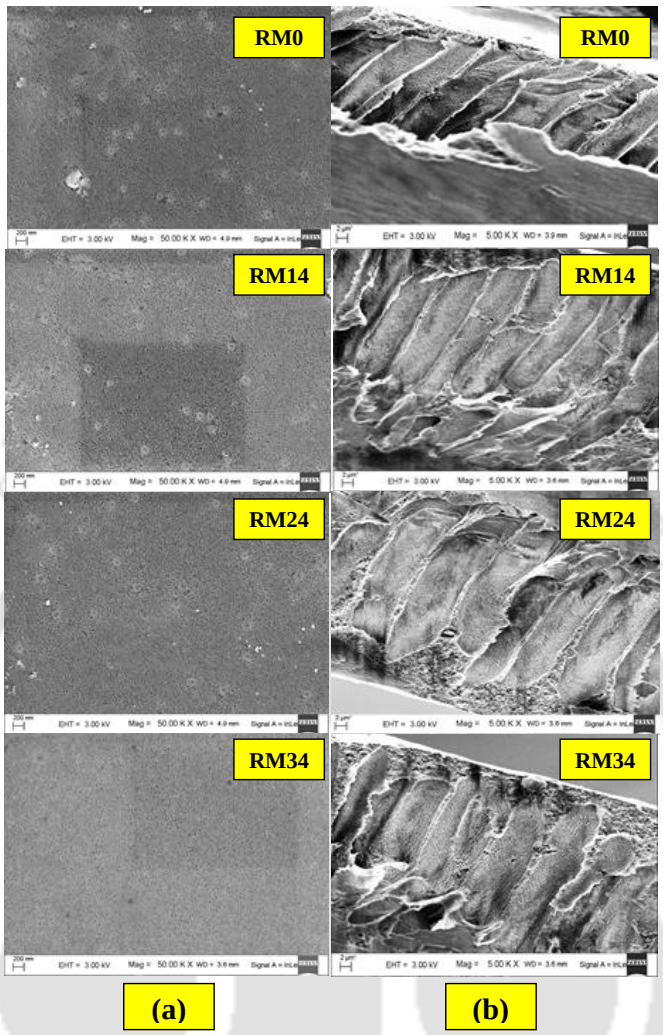

Figure 7.2. FESEM top surface (a) and cross-section (b) images of the membranes

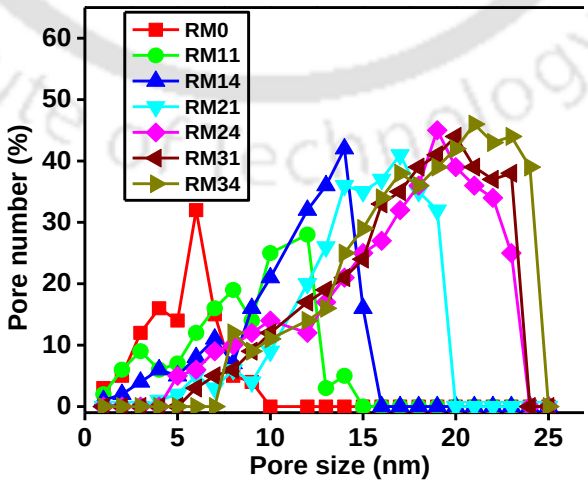

Figure 7.3 Pore size distribution of the membranes

7.3.3 Elemental analysis of the modified PSF membranes

7.3.3.1 FESEM-EDX analysis of the modified PSF membranes

The presence and uniformity of the stimuli responsive VCL-TiO_2-AA polymer nanocomposite in the membranes was confirmed by FESEM-EDX analysis as shown in Fig. 7.4. The peaks for titanium (Ti), Sulphur (S), oxygen (O), carbon (C), and nitrogen (N) represents the stimuli responsive VCL-TiO_2-AA polymer nanocomposites added membranes. The FESEM-EDX results of the pristine membrane R0 lacks the presence of Ti and N peaks which states that the additive stimuli responsive VCL-TiO_2-AA polymer nanocomposite is absent.

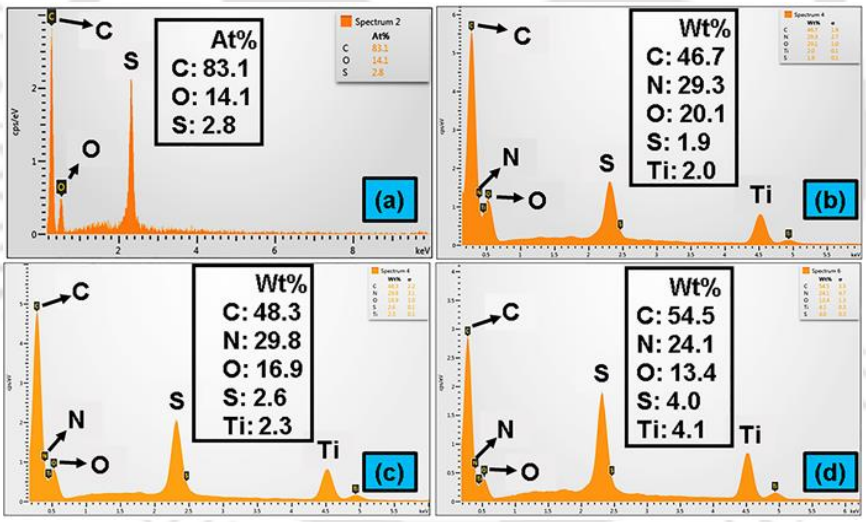

Figure 7.4. FESEM-EDX analysis of the selected membranes: (a) RM0, (b) RM14, (c) RM24, (d) RM34

7.3.3.2 FTIR analysis of the PSF modified membranes

The PSF modified membranes were further analysed by using FTIR spectroscopy for their compositional analysis. Figure 7.5 shows ATR-FTIR spectra of plain and blended PSF membranes. The new peaks around 1476 cm^{-1} and 1658 cm^{-1} represents amide group. Also,

the new peak at 1739cm^{-1} confirms the presence of − COOH group. The peak at 2950 cm^{-1} broadens due to the addition of C − H stretching, present in the polymer nanocomposite. These peaks authenticate the presence of stimuli responsive VCL-TiO_2-AA polymer nanocomposite in the membranes. Furthermore, the peaks at 1155 cm^{-1} and 1295 cm^{-1} corresponds to the − C − O − C − and S = O groups present in the polysulfone polymer, thereby confirming the presence of the same. However, these peaks are shifted a little bit in the modified membranes, which is due to the confrontation and interaction of the molecules upon phase inversion process. Also, the position of the band corresponding amide group depends on the degree of hydrogen bonding and physical state of the compound, which further signifies the peak shifts [105]. Thus, the figure confirms that stimuli responsive polymer nanocomposite is securely present in the membrane matrix.

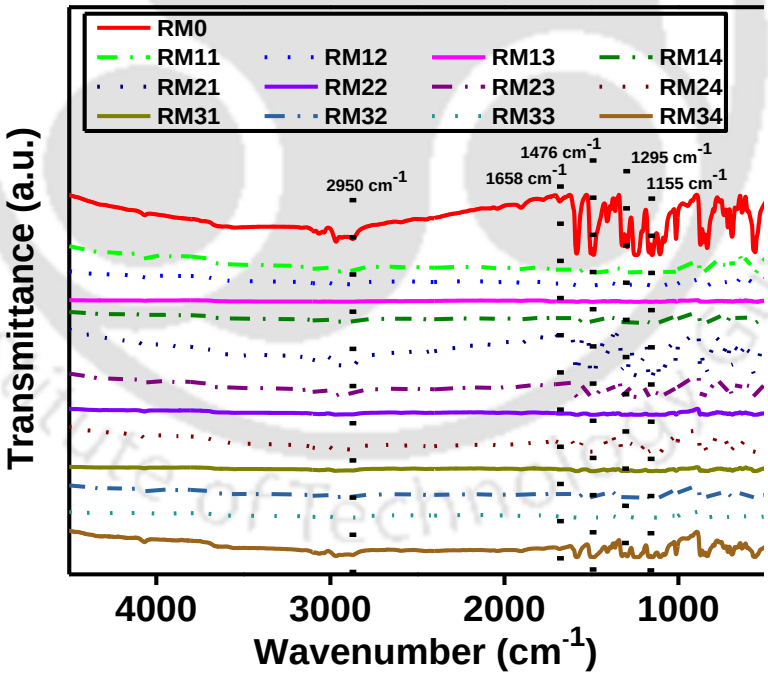

Figure 7.5 FTIR analysis of the membranes

7.3.4 Effect of stimuli responsive VCL-TiO_2-AA polymer nanocomposite on membrane permeation properties

In this section, the effect of stimuli responsive VCL-TiO_2-AA stimuli responsive polymer nanocomposite on the membranes was analyzed in terms of CF, PWF, EWC, hydraulic permeability (P_m), porosity, hydrophilicity, and antifouling studies. These membrane parameters will provide in depth knowledge of the prepared membranes and hence about the effect of the additive on the membranes.

7.3.4.1 Compaction analysis of the PSF modified membranes

The membranes were compacted to analyze the presence of macrovoids in the membranes. This is inferred by the value of CF, that is, higher the membrane CF value more will be the macrovoids present in the membranes. The membrane compaction analysis is shown in Fig. 7.6 and presented in Table 7.3. The results shows that the CF decreases for the stimuli responsive VCL-TiO_2-AA polymer nanocomposite added membranes RM11 (2.66) to RM34 (1.34) and is higher for the pristine membrane R0 (2.75).

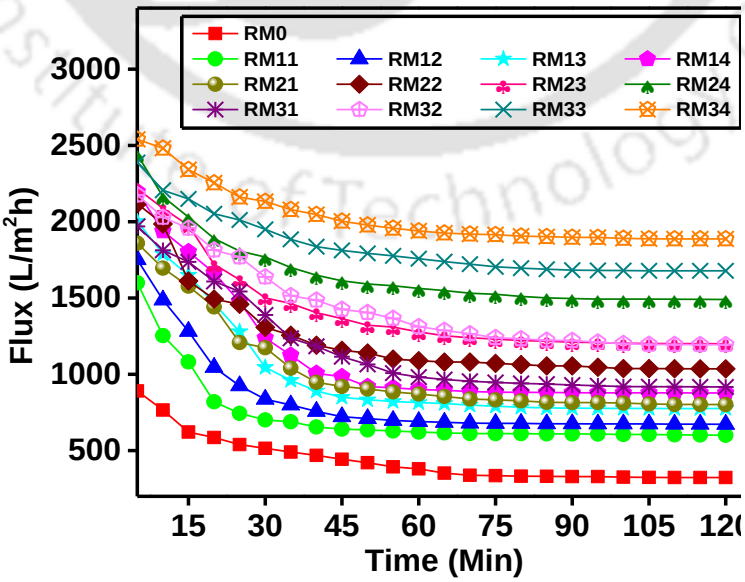

Figure 7.6 Pure water flux profile of the membranes with respect to time

Table 7.3 Few of the characterization parameters of the membranes

Membranes	Compaction factor (CF)	Permeability (P_m) (L m^{-2} h^{-1} kPa)	EWC (%)	Porosity	SWCA (°)
RM0	2.75	0.88	63.59	0.26	71.2±1
RM11	2.66	0.99	64.97	0.27	68.4±2
RM14	2.50	1.60	70.30	0.37	65.2±1
RM21	2.31	1.39	67.86	0.28	67.1±1.5
RM24	1.63	1.93	72.44	0.41	52.5±1.5
RM31	2.14	1.57	69.08	0.30	54.3±1
RM34	1.34	2.49	77.27	0.49	48.6±2

Altogether, it can be seen from Fig. 7.6 that the initial flux of the membranes shown a sharp decline and stables after 60 min. The reason for this phenomenon is the membrane compaction, that is, the otherwise open membrane pores close themselves on the application of pressure and become denser and uniform. This results in the reduction of the membrane pore size, which further results in the flux decline. The enhanced porosity due to the addition of the stimuli responsive VCL-TiO_2-AA polymer nanocomposite results in higher membrane flux as compared to the pristine membrane. The steady state flux of the membranes increases from 379.83 L m^{-2} h^{-1} (RM0) to 1939.55 L m^{-2} h^{-1} (RM34).

7.3.4.2 Pure water flux and hydraulic permeability of the modified PSF membranes

The flux profile of the membranes were analysed by measuring the pure water flux (PWF) of the membrane at different transmembrane pressures (0-250 kPa). Figure 7.7 shows the results regarding the PWF of the membranes. The figure shows that the addition of stimuli

responsive VCL-TiO_2-AA polymer nanocomposite to the membranes results in the enhancement of the PWF. For example, the PWF at 250 kPa for membrane RM34 comes out to be 597.78 L/m^2h in comparison to 214.54 L/m^2h for membrane RM0, which is 178.63% higher. Also, the PWF increases linearly with simultaneous increase in the transmembrane pressure.

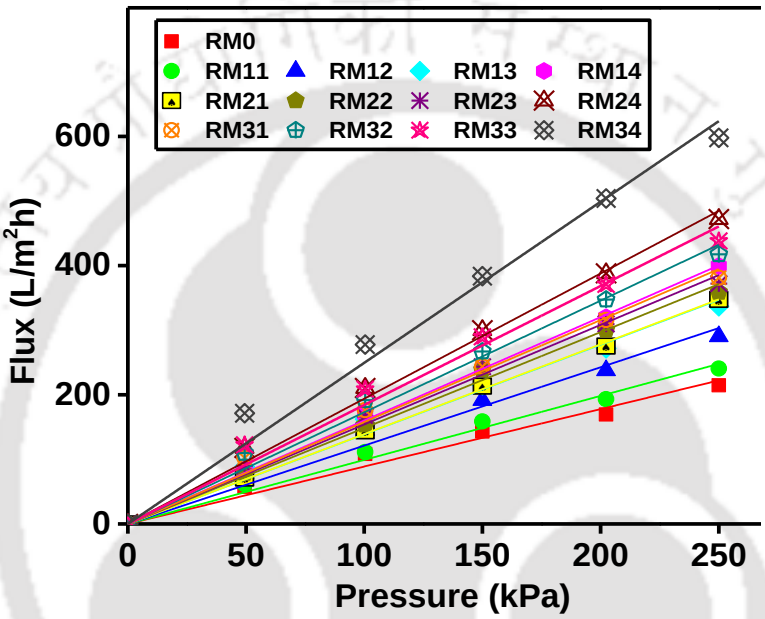

Figure 7.7 Pure water flux profile of the membranes with respect to pressure

The P_m of the membranes follows the same fashion as PWF, that is, the P_m also show increment in its value with the addition of stimuli responsive VCL-TiO_2-AA polymer nanocomposite as shown in Fig. 7.7. The P_m of membrane RM0 as calculated by using Eqn. 2 came out to be 0.88 L/m^2h kPa and increases to 2.49 L/m^2h kPa for membrane RM34. The P_m values are tabulated in Table 7.3 for all the membranes. These results validate the use of the stimuli responsive VCL-TiO_2-AA polymer nanocomposite for the formation of uniform pores and enhanced membrane hydrophilicity.

7.3.4.3 Membrane porosity, equilibrium water content, and hydrophilicity study of the modified PSF membranes

The membrane porosity dictate the EWC of a membrane. Since, the EWC is dependent on the membrane porosity as it value depends on the water uptake capability of a membrane and that depends on the membrane porosity. Furthermore, both these membrane parameters define the membranes separation and selection properties. Thereby, making them important attributes of the membranes. The tabulated results for both membrane porosity and EWC in Table 7.3 shows that the stimuli responsive VCL-TiO_2-AA polymer nanocomposite enhances the membrane porosity as well as EWC. The membrane porosity rises from 0.26 (RM0) to 0.49 (RM34) and the EWC enhances from 63.59 (RM0) to 77.27 (RM34). This increase in the membrane porosity and EWC can be described in terms of thermodynamic and kinetic changes. The addition of stimuli responsive VCL-TiO_2-AA polymer nanocomposite increases the viscosity of the membranes, which brings two specific changes to the thermodynamics and kinetics of the system. The thermodynamics of the system increases and causes decrease in the miscibility of non-solvent with the casting solution causing instantaneous demixing. On the other hand, it causes hindrance to the kinetics of the system opposing the phase separation resulting in increase of the viscosity, causing delayed demixing [23].

The membrane hydrophilicity is responsible for the membrane antifouling performance. Higher the hydrophilicity of a membrane higher will be its antifouling performance. Thereby, the prepared membranes were analysed for their hydrophilicity by measuring their SWCA. The SWCA of the membranes is presented in Table 7.3. The results of the SWCA analysis shows that the addition of stimuli responsive VCL-TiO_2-AA polymer nanocomposite helps in decreasing the SWCA of the membranes. The SWCA for

membrane RM0 is 71.2° and it decreases to 48.6° for RM34. This is due to the fact that the nanocomposite contains hydrophilic entities, which makes the membranes of hydrophilic nature. This ensures that the membranes will be of good antifouling nature, which is further confirmed by the antifouling analysis of the membranes in the succeeding sections.

7.3.5 pH- and thermo-responsive permeability studies of the modified PSF membranes

The pH- and thermos-responsive dependent flux profiles of the membranes are shown in Figs. 7.8 and 7.9, respectively. The figure depicts that the nascent membrane shows no change in its flux profile with pH and temperature changes.

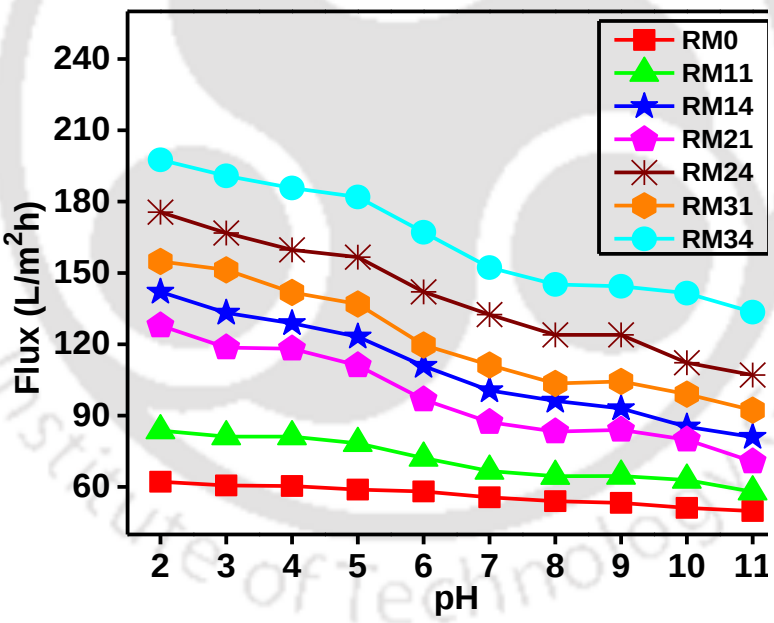

Figure 7.8 Pure water flux of membranes as a function of pH

On the other hand, the membranes modified with the VCL-TiO_2-AA polymer nanocomposite shows significant changes with pH and temperature. It can be seen from the figure that the flux of the modified membranes increases with decreasing pH and decreases with increasing pH. This is due to the ionization of the PAA (pKa value = 4.4-4.9) used in

the nanocomposite. Furthermore, the protonation and deprotonation of PAA results in its expansion and shrinkage under different pH conditions. For instance, the carboxylic acid, present in PAA, at pH higher than the pKa value of PAA deprotonates. The deprotonation of the carboxylic acid results in the formation of carboxylate ions, which results in the increase of the overall nanocomposite charge density. Further, the increase in the charge density of the nanocomposite results in the expansion of the PAA units, thereby blocking the membrane pores. Increasing the pH further, the membrane flux tend to loss more due to the electro viscous effect. The electro viscous effect, a physical phenomenon, shows when a narrow capillary or charged surface allows the passage of an electrolyte across them [107]. The membranes as well as the permeate at pH higher than 7 carries negative charge, therefore, repulsion between the two takes place. This repulsion increases more with further increase in the pH value and results in lower permeation. However, under acidic conditions the PAA gets protonated and shrinks resulting in increase of the membrane pore size. This enhances the membrane flux under acidic conditions. The pH based hydraulic permeability can be best explained on the basis of the Hagen-Poiseuille equation [108]. According to this equation, membrane pure water flux is directly proportional to the fourth power of membrane pore radius. Furthermore, the addition of the VCL-TiO_2-AA polymer nanocomposite shows significant change in the membranes pH based flux profile as it can be seen from the figure that the higher the nanocomposite higher is the change. For example, on changing the pH from 11 to 2 the membrane flux for RM11 and RM14 changed from 57.94 L/m^2h to 83.69 L/m^2h and 81.00 L/m^2h to 142.01 L/m^2h; for RM21 and RM24 it changes from 70.65 L/m^2h to 127.88 L/m^2h and 107.04 L/m^2h to 175.56 L/m^2h; and for membranes RM31 and RM34 it changes from 92.28 L/m^2h to 154.86 L/m^2h and 133.50 L/m^2h to 197.59 L/m^2h. As mentioned earlier, this is due to the addition of the additive

VCL-TiO_2-AA polymer nanocomposite, which results in the increase of the electro viscous effect with increasing pH.

Similarly, the membranes thermoresponsive behaviour was analysed by measuring the water flux for the membranes at 25°C and 40°C. The Fig. 7.9 shows that the membrane flux changes in response to a temperature change. This can be explained on the basis of the PVCL confirmation at these temperatures.

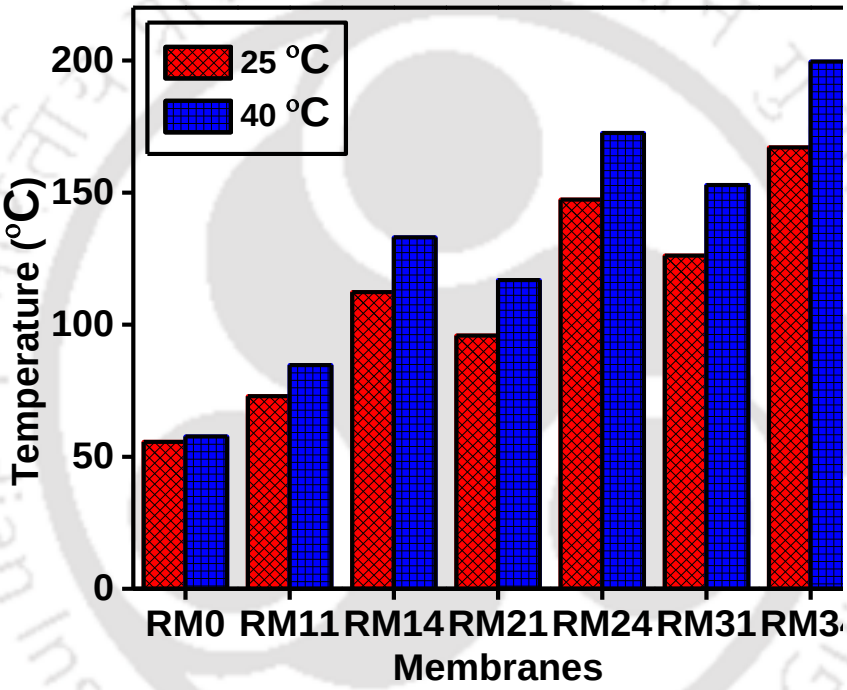

Figure 7.9 Pure water flux of membranes as a function of temperature

The lower critical solution temperature (LCST) of VCL is 35°C. Therefore, it swells by retaining a globular form and shrinks by having a coiled form at temperatures below and above its LCST, respectively [109]. This results in the change of the membrane pore size in response to a temperature change, below and above LCST of VCL. Furthermore, the increase in the amount of the VCL-TiO_2-AA polymer nanocomposite in the membranes shows better flux profile for the membranes as compared to the membranes having less amount of the nanocomposite as the flux of membranes RM11 (84.69 L/m^2h), RM21

(116.88 L/m^{2}h), and RM31 (152.86 L/m^{2}h) is lower than their counterpart membranes RM14 (133.01 L/m^{2}h), RM24 (172.56 L/m^{2}h), and RM34 (199.59 L/m^{2}h) at 40°C. This analysis confirms that the VCL-TiO_2-AA polymer nanocomposite modified membranes are thermoresponsive. Also, the VCL-TiO_2-AA polymer nanocomposite is having a positive effect on the membranes flux profile due to its hydrophilic nature.

7.3.6 Antifouling studies of the modified PSF membranes

The membrane antifouling studies were carried out with HA permeation at 300 kPa and the results are shown in Fig. 7.10. The results shows that F_{W1} is higher compared to F_{HA}, reason being the adsorption of HA molecules on the membrane surface resulting in the partial blocking of the membrane pores. However, the hydraulic washings gives better F_{W2}. This is due to the fact that the hydraulic washing given at 40°C made the polymer nanocomposite to shrink due to the presence of VCL component. This results in the degradation of the adsorbed HA layer over the membrane surface. The subsequent hydraulic washing at 25°C made the VCL chains of the polymer nanocomposite to stretch, which further damages the adsorbed HA layer. This shows that the polymer nanocomposite enhances the hydraulic cleaning efficiency. Thereby, confirming that there is no need of membranes cleaning by traditional chemical methods. This helps in sustaining both the membranes efficiency as well as life time.

The study data was also used to calculate the flux recovery ratio (FRR), which is a measure of the antifouling efficiency of membranes. Membranes with better antifouling nature shows higher FRR values. The obtained FRR values for the membranes are shown in Fig. 7.11. It can be seen from the figure that the membrane RM0 shows the least FRR

value of 96.43%. The FRR values increases for the membranes containing the VCL-TiO_2-AA polymer nanocomposite and membrane RM34 gives the highest FRR value of 98.93%.

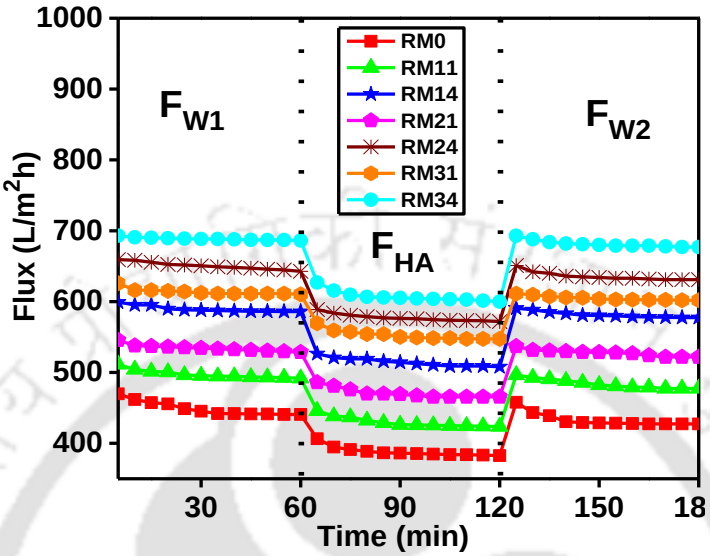

Figure 7.10 Membrane antifouling flux profile

This is due to the fact that the hydrophilic nanocomposite decreases the interactions between the membrane surface and HA molecules. Additionally, this study confirms that the thermoresponsive behaviour of the membranes helps in the removal of the adsorbed HA molecules from the membrane surface by simple hydraulic washings.

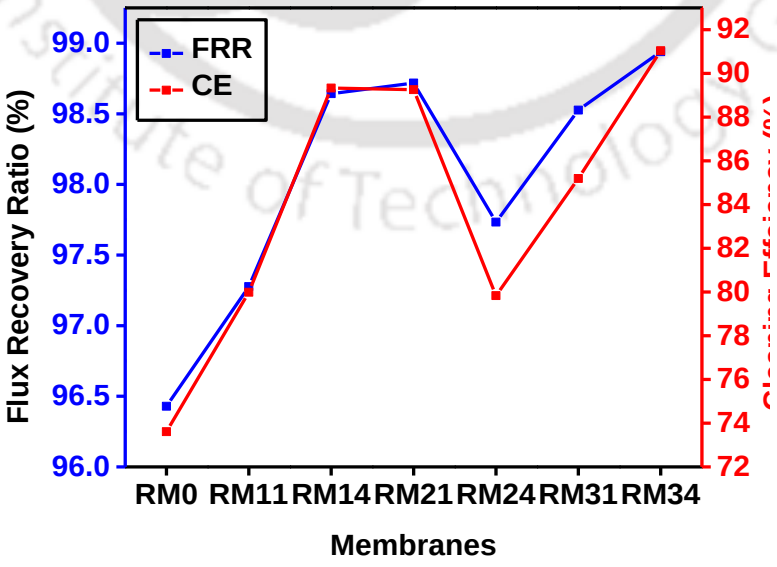

Fig. 7.11. Flux recovery ratio (a) and cleaning efficiency (b) of the membranes

Figure 7.12 shows the membranes total fouling (R_t), reversible fouling (R_r), and irreversible fouling (R_{ir}).

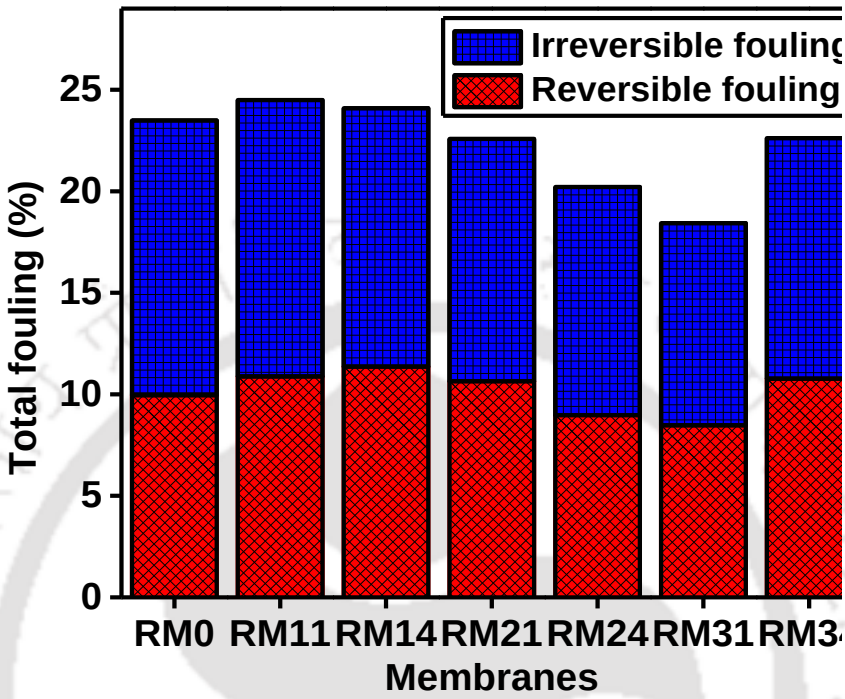

Figure 7.12 Reversible, irreversible, and total fouling of the membranes

The fouling analysis shows that both the reversible as well as irreversible fouling is low in case of membranes modified with the VCL-TiO_2-AA polymer nanocomposite as compared to the nascent membrane (RM0). In addition, the total fouling is also higher for the pristine membrane RM0. This further confirms that the neat membrane RM0 is more prone to fouling. It can be seen from the figure that the membranes with higher amounts of the VCL-TiO_2-AA polymer nanocomposite shows decreasing ratio of reversible and irreversible fouling, which is lowest for the RM34 membrane. Again, the reason is the presence of hydrophilic entities in the VCL-TiO_2-AA polymer nanocomposite. The presence of these hydrophilic groups restricts the adsorption of the foulants over the membrane surface and helps in improving the antifouling performance of the membranes.

The HA rejection was presented in Fig. 7.13. The HA rejection was quiet similar in all the VCL-TiO_2-AA polymer nanocomposite modified membranes.

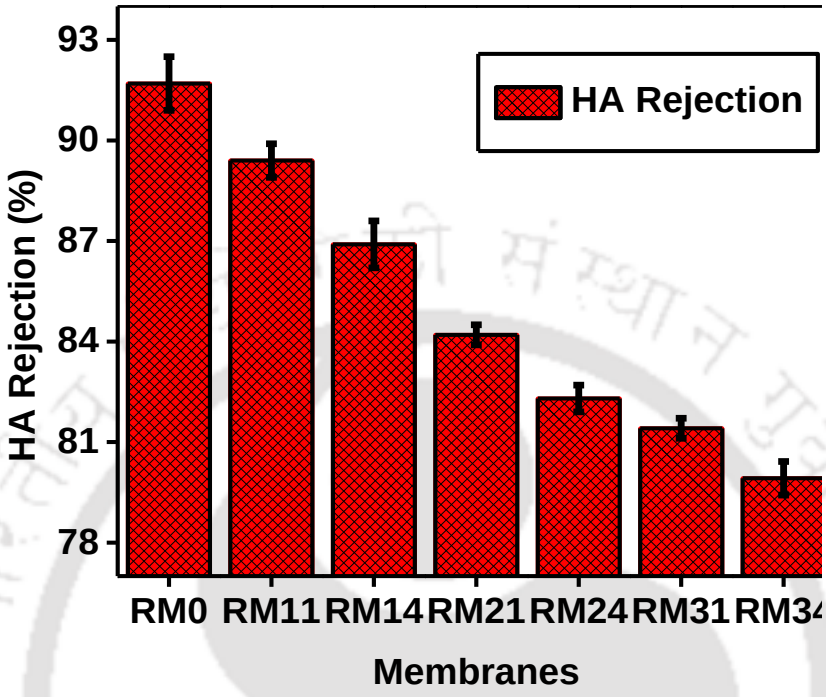

Figure 7.13 HA rejection profile of the membranes

However, the highest HA rejection was shown by RM0 (91.7%) and lowest by RM34 (79.92%). This is due to the fact of the HA molecular structure [106]. The HA molecules tend to form a mesh like gel layer by intra cross linking. Thereby, the membranes can easily reject this mesh like structure. Additionally, the stimuli responsive polymer nanocomposite also plays an important role in HA rejection. Since, a change in pH of the feed can bring notable changes in the confirmation of the nanocomposite. Therefore, the pH of the feed in the present experiment also define the HA rejection. The experiment was carried out at neutral pH, therefore, the electrostatic repulsions between the membranes and HA molecules are less. Also, at neutral pH the membrane pore size is higher as compared to basic conditions due to the swelling of the stimuli responsive VCL-TiO_2-AA polymer nanocomposite additive as explained previously in section 7.3.6.

7.3.7 Photocatalytic dye removal using modified PSF membranes

The dye removal results are shown in Fig. 7.14 for dark and UV light conditions, respectively, at basic, neutral, and acidic pH. The dye removal using modified PSF membranes follow both adsorption as well as photocatalytic paths. The figure shows that under both the dark as well as UV light conditions maximum dye removal taken place at basic pH and minimum at acidic pH. The maximum MB dye removal obtained under dark and UV light conditions is 39.92% and 93.47% for membrane RM34, respectively at basic pH. Furthermore, the MB dye removal recorded for membrane RM34 under dark and UV light conditions are 26.07% and 47.74%, respectively at acidic pH. This is due to the difference of charge present on the membranes as well as dyes at basic pH and similarity of charge at acidic pH. The membranes carries a negative charge under basic conditions and the dye a positive. Conversely, under basic pH conditions the membrane carries a positive charge. Under dark conditions, adsorption is the main mechanism of dye removal. The dye molecules adsorbed on the membrane surface under the influence of charge present on the membrane surface and dye molecules. As explained previously, under basic conditions the membrane and dye molecules carries opposite charge and thus attracts each other and thus shows higher dye removal. On the contrary, the membranes and dye molecules both carry similar charge in acidic conditions which results in the occurrence of repulsive forces among them, thereby, decreasing the overall dye removal. The results from the Fig. 7.14, confirms this as the maximum dye removal can be seen under basic conditions and minimum in case of acidic conditions. Furthermore, the membranes containing high amount of the VCL-TiO_2-AA polymer nanocomposite shows higher dye removal. This is due to the fact that there are more number of sites available for the adsorption of the dye in comparison to the membranes containing low amounts of the additive.

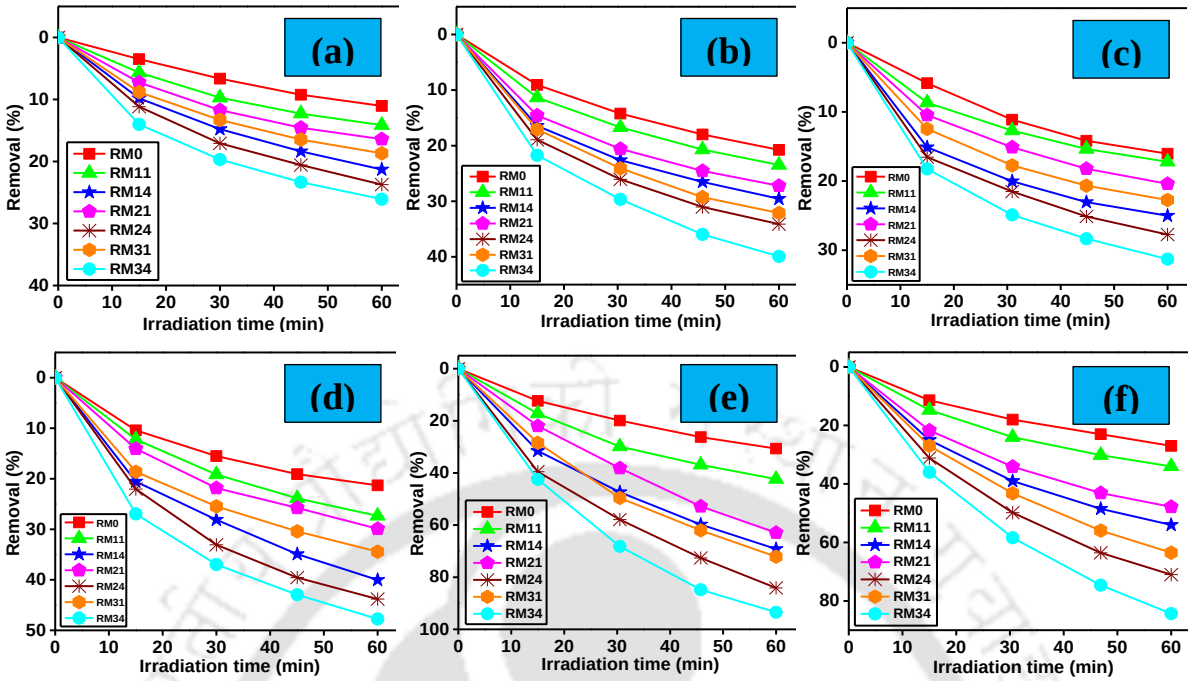

Figure 7.14. Photocatalytic removal of MB dye under different conditions, Dark: (a) acidic, (b) basic, (c) neutral; and UV light: (d) acidic, (e) basic, (f) neutral

The dye removal under UV light conditions, follows two paths viz. adsorption and photocatalysis. Therefore, the dye removal is higher compared to under dark conditions. Firstly, the dye molecules adsorb on the membrane surface under the influence of the charge present on them. As explained earlier, that the membranes and dye molecules are oppositely charged under basic conditions and carries similar charge under acidic conditions. Therefore, the dye molecules have high tendency to adsorb on the membranes under basic conditions as compared to acidic conditions. The opposite charges helps in attracting the dye molecules towards the membranes, where adsorption along with photocatalysis takes place. Thereby, the rate of photocatalysis is higher in case of basic conditions in comparison to acidic conditions. Thus, under basic conditions higher dye removal is achieved as can be seen from Fig. 7.14. The TiO_2 based VCL-TiO_2-AA polymer nanocomposite photocatalyst gets excited below 380 nm wavelength. The electrons reach the conduction band from the valence band due to the excitation caused by the photons.

This results in the occurrence of holes in the valence band. The hydroxyl radicals produced as a result of the reaction between photoexcited holes and water or hydroxide ions assists in the dye removal. This synergy between adsorption and photocatalysis helps in higher dye removal compared to only adsorption. Also, presence of more number of sites for dye adsorption under acidic conditions results in higher photocatalytic removal of the dye.

7.4 Summary

Polysulfone ultrafiltration membranes were successfully modified by using stimuli responsive VCL-TiO_2-AA polymer nanocomposite. The membranes shows positive pH, temperature, and photocatalytic response as can be seen from the pH and temperature studies of the modified membranes. The photocatalytic activity of the membranes was confirmed by the removal of MB dye under different pH and light conditions, namely acidic, basic, and neutral. The membranes shows highest dye removal under basic and UV light conditions. Furthermore, the stimuli responsive polymer nanocomposite additive also have positive effects on the PWF, P_m, SWCA, and antifouling properties of the membranes. The membranes have shown F_{RR} values of 96.43% and 98.93% for membranes RM0 and RM34, respectively. This confirms that the prepared membranes are significantly antifouling in nature.

Chapter 8
Conclusion, summary, and scope of future work

This chapter includes three sections, namely conclusions, summary, and future scope. The first section conclusions, discusses the inferences drawn from various studies presented in this thesis. Summary, the second section of the chapter presents a brief about all the chapters of this thesis. The last section of the chapter discusses about the options available for further studies in the field.

8.1. Conclusions

The presented work deals with the synthesis and characterization of antifouling ultrafiltration polymeric membranes with applications in environmental and biological fields. The work presents various types of membranes synthesized by using five different types of membrane modifying agents or additives, namely non solvent soluble polymers (poly(2-acrylamido-2-methyl-1-propanesulfonic acid) (AMPS) and methoxy poly(ethylene glycol) (mPEG)), carbon nanotubes synthesised from fly ash, Cu_2O photocatalyst and stimuli responsive polymer nanocomposite. The additives used are mostly synthesized and characterized by using different standard characterization techniques, such as FESEM-EDX, FTIR, and XRD. Also, the membranes modified with these additives were characterized for their morphological and permeation characteristics by using characterization techniques, like FESEM, AFM, LLDP, and ATR-FTIR as well as in terms of porosity, equilibrium water content. The membrane ultrafiltration analysis was carried out with BSA (model protein) and HA (model foulant). The ultrafiltration of BSA and HA also helped in analysing the antifouling nature of all of the synthesized membranes. The major conclusions of different studies are presented below.

Role of poly(2-acrylamido-2-methyl-1-propanesulfonic acid) in the modification of polysulfone membranes for ultrafiltration (Refer Chapter 3):

- The FESEM images shows that all the membranes have asymmetric structure.
- The study shows that the membrane MR4 containing 4 wt. % of AMPS shown the highest membrane porosity, EWC, P_m, BSA flux, and least fouling.
- The membrane MR4 shows significant changes in EWC, porosity, hydrophilicity, CF and permeability of 228.65%, 2,316.66%, 26.96%, 43.89% and 209.2%, respectively in comparison to membrane MR0 (Refer Table 3.3).
- All of the modified membranes shows higher BSA and HA flux in comparison to the nascent membrane.
- The modified membranes shown significant antifouling nature compared to the nascent membrane.
- The RSM used to obtain optimum conditions for the BSA flux and separation experiments were successfully validated experimentally.

Evaluation of mPEG effect on the hydrophilicity and antifouling nature of the PVDF-co-HFP flat sheet polymeric membranes for humic acid removal (Refer Chapter 4):

The results of the study shows that with addition of the additive mPEG in different molecular weights from 550 to 5000 Da following observations can be made:

- The additives are firmly embedded in the membrane matrix (Refer Figure 4.1).
- The morphological analysis of the membranes shows that the sublayer of the membrane P3 comprises of a dense structure with comparatively less macrovoids and more porous

top surface than P1 (Refer sections 4.5.2 and 4.5.3.1). Also, the membrane porosity, P_m, PWF, and EWC were significantly increased. (Refer Table 4.2).

- The static water contact angle analysis confirms that the additive also improves the hydrophilicity of the membranes as the SWCA decreases from 71.32° (P1) to 59.45° (P3).
- The additive is also able to make significant improvements in the BSA and HA rejection as well as flux. Membrane P3 shows highest BSA and HA rejection of 95% and 99% at neutral pH (Refer Figure 4.7). Furthermore, the pH of the aqueous solutions is also vital as at pH 4.7 (IP of BSA) BSA flux was the highest and least at pH 10. (Refer section 4.5.3.6).
- The antifouling nature of the membranes was also modified with increase in the molecular weight of the additive. The Total fouling (F_t) value decreases with molecular weight of mPEG (Refer Figure 4.8).

Flyash based carbon nanotubes modified hydrophilic and antifouling ultrafiltration polysulfone membranes (Refer Chapter 5):

The results of the study shows that by using flyash CNTs in the membranes:

- The morphological studies with FESEM and AFM states that the flyash CNTs modified membranes are asymmetric and their surface roughness decreases with addition of flyash CNTs in higher amounts.
- The LLDP analysis of the membranes shows that the membrane CM_0 is having the highest mean pore radius of 2.82 nm and membrane CM_5 with the least mean pore radius of 2.72 nm.

- The membrane shows hydrophilic nature as the SWCA decreases from 73.4° (CM_0) to 46.2° (CM_9). This confirms the antifouling capabilities of the membranes, which can be seen from the ultrafiltration studies of the membranes (Refer Figure 5.13).
- Modified membrane CM_5 shown better BSA rejection as compared to other membranes. This is due to its less pore size but the membrane shows better BSA flux, which is due to its better antifouling capabilities. (Refer Figure 5.13 and 5.14).
- The fouling studies also states that the flyash CNTs modified membranes are antifouling in nature as the F_t value decreases with increasing amount of the flyash CNTs in the membranes (Refer Figure 5.15).

Cu_2O photocatalyst modified polysulfone mixed matrix ultrafiltration membrane for pharmaceutical removal (Refer Chapter 6):

This study discusses about the effects of the Cu_2O photocatalyst on the PSF UF membrane and on the basis of the obtained results the following inferences were made:

- FESEM micrographs shows that the additive have positive effects on pore formation and the finger like structures shortens with the addition of the additive in the membranes (Refer Figure 6.3).
- The PWF, P_m, and hydrophilicity were all seen to be enhanced with the increase in the additives wt% and these values of these membrane parameters increased by 379.92%, 416.66 % and 36.64 %, respectively for membrane RY4 in comparison to membrane RY0.
- The addition of the Cu_2O photocatalyst to the membranes shows positive effect on the antifouling nature of the membranes. Membrane RY4 shows 69.46% increase in the F_{RR} value in comparison to the membrane RY0. (Refer Figure 6.9 (a)).

- The Cu_2O photocatalyst additive in the membranes also induces photocatalytic property. This is confirmed by the positive IBP removal results from aqueous solutions shown by the modified membranes. Membrane RY4 shows 131.8% increase in IBP removal under light and acidic conditions compared to the nascent membrane RY0 (Refer Figure 6.10).

pH and thermo-responsive mixed matrix polysulfone ultrafiltration membrane for photocatalytic dye removal (Refer Chapter 7):

Effects of wt % of stimuli responsive VCL-TiO_2-AA polymer nanocomposite on membrane morphology, permeability, hydrophilicity, HA fouling, and dye removal were studied and based on that following conclusion were made:

- Top surface FESEM micrographs shows that the stimuli responsive VCL-TiO_2-AA polymer nanocomposite enhances the pore formation in the membranes, hence the porosity as well as pore size distribution increases (Refer Figure 7.3 (a)).
- Cross sectional FESEM micrographs shows modified membrane have asymmetric structures containing a dense, selective top layer and porous sublayer. (Refer Figure 7.3 (b)).
- SWCA measurement confirms the increase in the hydrophilic nature of the modified membranes compared to nascent membranes as the SWCA decreased from 71.2˚to48.6˚ for membrane RM34 compared to nascent membrane RM0 (Refer Table 7.3).
- Modified membranes shows that the additive induces pH and thermo sensitivity (Refer Figures 7.9 and 7.10).
- The antifouling nature of the modified membranes is also enhanced as can be seen from the HA flux studies. The modified membrane RM34 shows 23.6% increase in the CE value as compared to the nascent RM0 membrane (Refer Figures 7.11 and 7.12).

- The modified membranes also show photocatalytic characteristics as evident from the results of the photocatalytic dye removal results of the membranes (Refer Figure 7.15).

8.2. Summary

The antifouling behaviour of all the prepared membranes is compared and summarised in Table 8.1. Modified membranes were compared on the basis of total fouling, and BSA and HA rejection. In case of membranes from chapter 8, the bracketed data shows the values by normal hydraulic cleaning.

Table 8.1: Comparative analysis of all the prepared membranes

Membrane composition	Type of additives	Membrane name	Water contact angle (°)	Total fouling (normalized)	BSA rejection (%))	HA rejection (%)
As in Table 3.1 of Chapter 3	Non solvent additives	MR0	68.23 ± 1.0	0.95	99.41	Nil
		MR1	62.63 ± 2.0	0.82	99	Nil
		MR2	57.28 ± 1.0	0.76	99	Nil
		MR3	53.14 ± 1.5	0.75	98	Nil
		MR4	49.83 ± 2.0	0.74	97	100
As in Table 4.1 of Chapter 4	Non solvent additives	P1	71.32 ± 1	0.73	88	Nil
		P2	65.41 ± 1	0.72	93	Nil
		P3	59.45 ± 2	0.70	95	99
As in Table 5.1 of Chapter 5	Flyash based CNTs	CM_0	73.4 ± 1	0.69	61.73	Nil
		CM_1	67.8 ± 1	0.54	76.03	Nil
		CM_3	62.3 ± 2	0.51	82.50	Nil
		CM_5	54.5 ± 1	0.50	84.11	Nil
		CM_7	50.6 ± 2	0.46	79.44	Nil
		CM_9	46.2 ± 2	0.41	73.95	Nil
As in Table 6.1 of Chapter 6	Cu_2O photocatalyst	RY0	71.5 ± 1.8	0.77	87.7	Nil
		RY1	65.4 ± 1.5	0.71	83.4	Nil
		RY2	56.7 ± 1.9	0.61	79.9	Nil
		RY3	51.2 ± 1.7	0.52	77.2	Nil
		RY4	45.3 ± 1.6	0.37	74.3	Nil

As in Table 7.2 of Chapter 7	Stimuli responsive polymer nanocomposite	RM0	71.2±1	0.23	Nil	91.7
		RM11	68.4±2	0.24	Nil	89.4
		RM14	65.2±1	0.24	Nil	86.9
		RM21	67.1±1.5	0.22	Nil	84.2
		RM24	52.5±1.5	0.20	Nil	82.3
		RM31	54.3±1	0.18	Nil	81.4
		RM34	48.6±2	0.22	Nil	79.9

Table 8.1 shows that all of the prepared membranes are antifouling in nature confirmed by their hydrophilicity (SWCA measurements) and protein (BSA) or foulant (HA) rejections. The table shows that membranes MR4, P3, CM_9, RY4, and RM34 have the best antifouling characteristic features compared to other membranes. The membranes shows total fouling in the range of 0.22 to 0.74. The hydrophilic additives used for the modification of these membranes results in the increased hydrophilicity, which results into quite similar SWCA for all of these membranes that is ≈47°, except membrane P3, which is having 59.45° but it still shows better antifouling nature. Also, all of these membranes shows BSA rejection of more than 70%, which is a good sign for their application in various environmental and biological fields.

8.3. Recommendations on future directions

This section discusses about the future scope of the polymeric membranes highlighting the new areas of research especially in the preparation and applicability of polymeric membranes to various commercial and industrial problems. Following are some of the important areas of research that can be taken up for further studies as an extension of the present work.

- The role of AMPS is mainly studied on the membrane performance, therefore, the role of AMPS on the phase inversion and mechanism of membrane formation can be studied for the preparation of a membrane with enhanced membrane flux and rejection effect.

- mPEG 5000 provided better result than other molecular weights of mPEG, so the effect of different wt% of PEGME 5000 on membranes PWF, BSA flux, and fouling behaviour can be studied.
- Flyash CNTs modified with a stimuli responsive copolymer could be studied for better performing membranes in terms of their application and antifouling nature.
- Metal oxide photocatalysts modified with poly(N-vinylcaprolactam-co-acrylic acid) can be studied for better antifouling nature and response to external stimuli.
- Dual sensitivity of the membranes modified with VCL-TiO_2-AA can be studied simultaneously, that is together at different pH and temperature. For example, at pH 2 and 40℃, pH 11 and 40℃, pH 2 and 25℃, pH 11 and 25℃.
- Use of prepared membranes for UF experiments and antifouling behaviour in other modes of operations, such as cross-flow to obtain more realistic idea about their performance in industrial applications.
- Fouling modelling of the prepared membranes using different pore blocking models and combined blocking models.

References

1. R. Singh and M. K. Purkait, membrane technology in separation science, first edition, CRC Press, 2018.
2. K. Nath, Membrane separation process, Prentice Hall of India, 2008.
3. B. K. Dutta, Principles of mass transfer and separation processes, Prentice Hall of India, 2007.
4. M. Mulder, Basic principles of membrane technology, Springer, 2007.
5. M. K. Purkait, M. K. Sinha, P. Mondal, and R. Singh, Stimuli responsive polymeric membranes: smart polymeric membranes, first edition, Elsevier, 2018.
6. B. K. Nandi, M. Rahaman, R. Singh, and M. K. Purkait, Microfiltration membranes: fabrication and application, In S. Sridhar, Membrane technology: an approach towards sustainable solutions in water, health, energy and the environment, first edition, CRC Press, 2018, Chapter 9, Pages 190-209.
7. W. J. Koros, Y. H. Ma, and T. Shimidzu, Terminology for membranes and membrane processes; IUPAC recommendations, Journal of Membrane Science 120 (1996) 149–159.
8. R. Singh and M. K. Purkait, Microfiltration membranes, In A. F. Ismail, M. A. Rahman, M. H. D. Othman, and T. Matsuura (Eds.), Membrane separation principles and applications, first edition, Elsevier, Chapter 4, 2019, 111-146.
9. M. K. Sinha and M. K. Purkait, Preparation and characterization of novel pegylated hydrophilic pH responsive polysulfone ultrafiltration membrane, Journal of Membrane Science 464 (2014) 20–32.
10. N. A. Hashim, F. Liu, and K. Li, A simplified method for preparation of hydrophilic PVDF membranes from an amphiphilic graft copolymer, Journal of Membrane Science 345 (2009) 134–141.

11. X. Ma, Y. Su, Q. Sun, Y. Wang, and Z. Jiang, Enhancing the antifouling property of polyethersulfone ultrafiltration membranes through surface adsorption-crosslinking of poly(vinyl alcohol), Journal of Membrane Science 300 (2007) 71–78.
12. M. Hu, Q. Yang, and Z. Xu, Enhancing the hydrophilicity of polypropylene microporous membranes by the grafting of 2-hydroxyethyl methacrylate via a synergistic effect of photoinitiators, Journal of Membrane Science 285 (2006) 196–205.
13. N. K. Saha, M. Balakrishnan, and M. Ulbricht, Fouling control in sugarcane juice ultrafiltration with surface modified polysulfone and polyethersulfone membranes, Desalination 249 (2009) 1124–1131.
14. W. Zhao, Y. Su, C. Li, Q. Shi, X. Ning, and Z. Jiang, Fabrication of antifouling polyethersulfone ultrafiltration membranes using Pluronic F127 as both surface modifier and pore-forming agent, Journal of Membrane Science 318 (2008) 405–412.
15. M. K. Sinha and M. K. Purkait, Preparation of fouling resistant PSF flat sheet UF membrane using amphiphilic polyurethane macromolecules, Desalination 355 (2015) 155–168.
16. C. A. Mecha and V. L. Pillay, Development and evaluation of woven fabric microfiltration membranes impregnated with silver nanoparticles for potable water treatment, Journal of Membrane Science 458 (2014) 149–156.
17. Q. An, W. Sun, Q. Zha, Y. Ji, and C. Gao, Study on a novel nanofiltration membrane prepared by interfacial polymerization with zwitterionic amine monomers, Journal of Membrane Science 431 (2013) 171–179.
18. F. Zhang, W. Zhang, Y. Yu, B. Deng, J. Li, and J. Jin, Sol-gel preparation of PAA-g-PVDF TiO_2 nanocomposite hollow fiber membranes with extremely high water flux and improved antifouling property, Journal of Membrane Science 432 (2013) 25–32.

19. B. Chakrabarty, A. K. Ghoshal, and M. K. Purkait, Effect of molecular weight of PEG on membrane morphology and transport properties, Journal of Membrane Science 309 (2008) 209–221.
20. S. R. Panda and S. De, Role of polyethylene glycol with different solvents for tailor-made polysulfone membranes, Journal of Polymer Research 20 (2013)179.
21. B. Jung, J. K. Yoon, B. Kim, H. –W. Rhee, Effect of molecular weight of polymeric additives on formation, permeation properties and hypochlorite treatment of asymmetric polyacrylonitrile membranes, Journal of Membrane Science 243 (2004) 45–57.
22. R. M. Boom, I. M. Wienk, T. V. D. Boomgaard, and C. A. Smolders, Microstructures in phase inversion membranes. Part 2. The role of a polymeric additive, Journal of Membrane Science 73 (1992) 277-292.
23. M. K. Sinha and M. K. Purkait, Increase in hydrophilicity of polysulfone membrane using polyethylene glycol methyl ether, Journal of Membrane Science 437 (2013) 7-16.
24. B. Chakrabarty, A. K. Ghoshal, and M. K. Purkait, Preparation, characterization and performance studies of polysulfone membranes using PVP as an additive, Journal of Membrane Science 315 (2008) 36–47.
25. C. Xu, W. Huang, X. Lu, D. Yan, S. Chen, and H. Huang, Preparation of PVDF porous membranes by using PVDF-g-PVP powder as an additive and their antifouling property, Radiation Physics and Chemistry 81 (2012) 1763–1769.
26. A. S. Hoffman, Hydrogels for biomedical applications, Advanced Drug Delivery Reviews 64 (2012) 18–23.
27. H. Ju, B. D. McCloskey, A. C. Sagle, V. A. Kusuma, and B. D. Freeman, Preparation and characterization of crosslinked poly(ethylene glycol) diacrylate hydrogels as fouling-resistant membrane coating materials, Journal of Membrane Science 330 (2009) 180–188.

28. A. Lucas and J. R. Harris, Ancient Egyptian materials and industries, New York Dover Publications, (1998) ISBN 0-486-40446-3.

29. M. Ahmaruzzaman, A review on the utilization of fly ash, Progress in Energy and Combustion Science 36 (3) (2010) 327–363.

30. R. H. Baughman, A. Zakhidov, and W. Heer, Carbon nanotubes--the route toward applications, Science 297 (5582) (2002) 787–92.

31. R. Asahi, T. Morikawa, T. Ohwaki, K. Aoki, and Y. Taga, Visible-light photocatalysis in nitrogen-doped titanium oxides, Science 293 (2001) 269–271.

32. C. Xu, L. Cao, G. Su, W. Liu, H. Liu, Y. Yu, and X. Qu, Preparation of ZnO/Cu_2O compound photocatalyst and application in treating organic dyes, Journal of Hazardous Materials 176 (2010) 807–813.

33. J. Yu, S. Zhuang, X. Xu, W. Zhu, B. Feng, and J. Hu, Photogenerated electron reservoir in hetero-p–n CuO–ZnO nanocomposite device for visible-light-driven photocatalytic reduction of aqueous Cr(VI), Journal of Material Chemistry A 3 (2015) 1199–1207.

34. M. Mishra and D.Chun, α-Fe_2O_3 as a photocatalytic material: A review, Applied Catalysis A 498 (2015) 126–141.

35. C. Kittel, Introduction to solid state physics, 8th ed., Wiley, New York, 2004.

36. Z. Zhang, S. Zhang, S. Liu, M. Wang, G. Fu, L. He, Y. Yang, and S. Fang, Electrochemical aptasensor based on one-step synthesis of Cu_2O@aptamer nanospheres for sensitive thrombin detection, Sensors and Actuators B: Chemical 220 (2015) 184–191.

37. J. J. M. Vequizo, C. Zhang, and M. Ichimura, Fabrication of Cu_2O/Fe–O heterojunction solar cells by electrodeposition, Thin Solid Films 597 (2015) 83–87.

38. H. A. Al-Jawhari, A review of recent advances in transparent p-type Cu_2O-based thin film transistors, Materials Science in Semiconductor Processing 40 (2015) 241–252.

39. D. J. Choi, J. Kim, H. Seong, M. Jang, and Y. Kim, The formation of Cu_2O nanoparticles in polyimide using Cu electrodes via chemical curing, and their application in flexible polymer memory devices, Organic Electronics 27 (2015) 65-71.

40. V. S. K. Yadav and M. K. Purkait, Electrochemical studies for CO_2 reduction using synthesized Co_3O_4 (Anode) and Cu_2O (Cathode) as electrocatalysts, Energy Fuels 29 (2015) 6670−6677.

41. Y. Luo, Q. Huang, B. Li, L. Dong, M. Fan, and F. Zhang, Synthesis and characterization of Cu_2O–modified Bi_2O_3 nanospheres with enhanced visible light photocatalytic activity, Applied Surface Science 357 (2015) 1072−1079.

42. H. R. Buser, T. Poiger, and M. D. Muller, Occurrence and environmental behavior of the chiral pharmaceutical drug ibuprofen in surface waters and in wastewater, Environmental Science and Technology 33 (1999) 2529−2535.

43. F. Mendez-Arriaga, M. I. Maldonado, J. Gimenez, S. Esplugas, and S. Malato, Abatement of ibuprofen by solar photocatalysis process: enhancement and scale up, Catalysis Today 144 (2009) 112−116.

44. T. A. Ternes, N. Herrmann, M. Bonerz, T. Knacker, H. Siegrist, and A. Joss, A rapid method to measure the solid-water distribution coefficient (Kd) for pharmaceuticals and musk fragrances in sewage sludge, Water Research 38 (2004) 4075−4084.

45. A. R. Bakr and M. S. Rahaman, Electrochemical efficacy of a carboxylated multiwalled carbon nanotube filter for the removal of ibuprofen from aqueous solutions under acidic conditions, Chemosphere 153 (2016) 508-520.

46. Y. Qian, L. Chi, W. Zhoua, Z. Yu, Z. Zhang, Z. Zhang, and Z. Jiang, Fabrication of TiO_2-modified polytetrafluoroethylene ultrafiltration membranes via plasma-enhanced surface graft pretreatment, Applied Surface Science 360 (2016) 749–757.

47. R. Singh, V.S.K. Yadav, and M. K. Purkait, Cu_2O photocatalyst modified antifouling polysulfone mixed matrix membrane for ultrafiltration of protein and visible light driven photocatalytic pharmaceutical removal, Separation and Purification Technology 212 (2019) 191–204.

48. R. Singh and M. K. Purkait, Role of poly(2-acrylamido-2-methyl-1-propanesulfonic acid) in the modification of polysulfone membranes for ultrafiltration, Journal of Applied Polymer Science 134 (37) (2017) 45290.

49. R. Singh and M. K. Purkait, Evaluation of mPEG effect on the hydrophilicity and antifouling nature of the PVDF-co-HFP flat sheet polymeric membranes for humic acid removal, Journal of Water Process Engineering 14 (2016) 9–18.

50. G. Capannelli, I. Becchi, A. Bottino, P. Moretti, and S. Munari, in: K. K. Unger, J. Rouquesol, and K. S. W. Sing (Eds.), Characterization of porous solids, Elsevier, Amsterdam, Holland, (1988), 283-294.

51. A. J. Burggraaf and L. Cot, Fundamentals of inorganic membrane science and technology, Elsevier, 1996.

52. S. P. Sutera and R. Skalak, The history of Poiseuille's law, Annual Review of Fluid Mechanics 25 (1993) 1-19.

53. B. J. Kirby, Micro- and nanoscale fluid mechanics: transport in microfluidic devices, Cambridge University Press, 2010.

54. A. T. Hubbard, The handbook of surface imaging and visualization, CRC Press, 1995.

55. F. L. Huang, Q. Q. Wang, Q. F. Wei, W. D. Gao, H. Y. Shou, and S. D. Jiang, Dynamic wettability and contact angles of poly(vinylidene fluoride) nanofiber membranes grafted with acrylic acid, eXPRESS Polymer Letters 4 (9) (2010) 551–558.

56. N. Q. Arancon, C. A. Edwards, S. Lee, and R. Byrne, Effects of humic acids from vermicomposts on plant growth, European Journal of Soil Biology 42 (2006) S65–S69.

57. D. C. Montgomery, Design and analysis of experiments, 5th ed., Wiley, New York, 2001.

58. A. J. Reuvers and C. A. Smolders, Formation of membranes by means of immersion precipitation - Part II. the mechanism of formation of membranes prepared from the system cellulose acetate-acetone-water, Journal of Membrane Science 34 (1987) 67-86.

59. K. J. Kim, A. G. Fane, and C. J. D. Fell, Quantitative microscopic study of surface characteristics of ultrafiltration membranes, Journal of Membrane Science 54 (1990) 89-102.

60. I. M. Wienk, R. M. Boom, M. A. M. Beerlage, A. M. W. Bulte, C. A. Smolders, and H. Strathmann, Recent advances in the formation of phase inversion membranes made from amorphous or semi-crystalline polymers, Journal of Membrane Science 113 (1996) 361-371.

61. C. H. Loh, R. Wang, L. Shi, and A. G. Fane, Fabrication of high performance polyethersulfone UF hollow fiber membranes using amphiphilic Pluronic block copolymers as pore-forming additives, Journal of Membrane Science 380 (2011) 114–123.

62. A.G. Fane, C. J. D. Fell and A. G. Waters, The relationship between membrane surface pore characteristics and flux for ultrafiltration membranes, Journal of Membrane Science 9 (1981) 245-262.

63. C. Feng, R. Wang, B. Shi, G. Li, and Y. Wu, Factors affecting pore structure and performance of poly(vinylidenefluoride-co-hexafluoro propylene) asymmetric porous membrane, Journal of Membrane Science 277 (2006) 55–64.

64. D.A. Musale and S. S. Kulkarni, Relative rates of protein transmission through poly(acrylonitrile) based ultrafiltration membranes, Journal of Membrane Science 136 (1997) 13-23.

65. R. S. Kumar, G. Arthanareeswaran, D. Paul, J. H. Kweon, Effective removal of humic acid using xanthan gum incorporated polyethersulfone membranes, Ecotoxicology and Environmental Safety 121 (2015) 223-228.

66. H. K. Melvin, A. H. Sabran, C. P. Leo, A. L. Ahmad, A. Z. Abdullah, Photocatalysts in polysulfone membrane for the removal of humic acid: the effects of pvp and pva on membrane morphology, separation performance and catalytic hindrance, J. Membr. Sci. Res.2 (2) (2016) 95-101.

67. A. Mehrparvar, A. Rahimpour, and M. Jahanshahi, Modified ultrafiltration membranes for humic acid removal, Journal of the Taiwan Institute of Chemical Engineers 45 (2014) 275–282.

68. Q. Zhang, G. Rao, J. Rogers, C. Zhao, L. Liu, and Y. Li, Novel anti-fouling Fe_2O_3/TiO_2 nanowire membranes for humic acid removal from water, Chemical Engineering Journal 271 (2015) 180–187.

69. A. L. Ahmad, A. A. Abdulkarim, S. Ismail, and B. S. Ooi, Preparation and characterisation of PES-ZnO mixed matrix membranes for humic acid removal, Desalination and Water Treatment 54 (2015) 3257-3268.

70. F. S. Dehkordi, M.Pakizeh, and M. N. Mahboub, Properties and ultrafiltration efficiency of cellulose acetate/organically modified Mt (CA/OMMt) nanocomposite membrane for humic acid removal, Applied Clay Science 105–106 (2015) 178–185.

71. P. Kanagaraj, A. Nagendran, D. Rana, T. Matsuura, Separation of macromolecular proteins and removal of humic acid by cellulose acetate modified UF membranes, International Journal of Biological Macromolecules 89 (2016) 81–88.

72. T. Arumugham, N. J. Kaleekkal, D. Rana, M. Doraiswamy, Separation of oil/water emulsions using nano MgO anchored hybrid ultrafiltration membranes for environmental abatement, Journal of Applied Polymer Science 133 (2016) 42848.

73. L. L. Hwang, J. C. Chen, and M. Y. Wey, The properties and filtration efficiency of activated carbon polymer composite membranes for the removal of humic acid, Desalination 313 (2013) 166–175.

74. R. V. Kumar, I. G. Moorthy, and G. Pugazhenthi, Modelling and optimization of critical parameters by hybrid RSM-GA for the separation of BSA using a tubular configured MFI-type zeolite microfiltration membrane, RSC Advances 5 (2015) 87645-87659.

75. K. J. Kuhn, B. Hahn, V. Percec, and M. W. Urban, Structural and quantitative analysis of surface modified poly(vinylidene fluoride) films using ATR FT-IR spectroscopy, Applied Spectroscopy 41 (5) (1987) 843-847.

76. L. Shi, R. Wang, Y. Cao, D. T. Liang, and J. H. Tay, Effect of additives on the fabrication of poly (vinylidene fluoride-co-hexafluropropylene) (PVDF-HFP) asymmetric microporous hollow fiber membranes, Journal of Membrane Science 315 (2008) 195–204.

77. C. A. Smolders, A. J. Reuvers, R. M. Boom, and I. M. Wienk, Microstructures in phase-inversion membranes. Part 1: Formation of Macrovoids, Journal of Membrane Science 73 (1992) 259-275.

78. M. A. Frommer and R. M. Messalem, Mechanism of membrane formation. VI. Convective flows and large void formation during membrane precipitation, Industrial & Engineering Chemistry Product Research and Development 12 (1973) 328-333.

79. R. Matz, The structure of cellulose acetate membranes. 1. The development of porous structures in anisotropic membranes, Desalination 10 (1972) 1-15.

80. S. P. Nunes and T. Inoue, Evidence for spinodal decomposition and nucleation and growth mechanisms during membrane formation, Journal of Membrane Science 111 (1996) 93-103.

81. H. Strathmann, K. Kock, P. Amar, and W. Baker, The formation mechanism of symmetric membranes, Desalination 16 (1975) 179-203.

82. T. H. Young and L. W. Chen, A two step mechanism of diffusion-controlled ethylene vinyl alcohol membrane formation, Journal of Membrane Science 57 (1991) 69-81.

83. M. K. Sinha and M. K. Purkait, Use of CS–PAA nanoparticles as an alternative to metal oxide nanoparticles and their effect on fouling mitigation of a PSF ultrafiltration membrane, RSC Advances 5 (2015) 66109–66121.

84. M. T. Moghadam, G. Lesage, T. Mohammadi, J. P. Mericq, J. Mendret, M. Heran, C. Faur, S. Brosillon, M. Hemmati, and F. Naeimpoor, Improved antifouling properties of TiO_2/PVDF nanocomposite membranes in UV-coupled ultrafiltration, Journal of Applied Polymer Science 132 (2015) 41731.

85. J. Zhang, Z. Xu, W. Mai, C. Min, B. Zhou, M. Shan, Y. Li, C. Yang, Z. Wang, and X. Qian, Improved hydrophilicity, permeability, antifouling and mechanical performance of PVDF composite ultrafiltration membranes tailored by oxidized low-dimensional carbon nanomaterials, Journal of Material Chemistry A 1 (2013) 3101–3111.

86. J. Ma, J. Zhao, Z. Ren, and L. Li, Preparation and characterization of PVDF-PFSA flat sheet ultrafiltration membranes, Frontiers of Chemical Science and Engineering 6 (3) (2012) 301–310.

87. P. Y. Zhang, H. Yang, and Z. L. Xu, Preparation of polyvinylidene fluoride (pvdf) membranes via nonsolvent induced phase separation process using a tween 80 and H_2O mixture as an additive, Industrial & Engineering Chemistry Research 51 (2012) 4388−4396.

88. M. K. Sinha and M. K. Purkait, Enhancement of hydrophilicity of poly(vinylidene fluoride-co-hexafluoropropylene) (PVDF-HFP) membrane using various alcohols as nonsolvent additives, Desalination 338 (2014) 106–114.

89. D. C. D. Nath, S. Bandyopadhyay, P. Boughton, A. Yu, D. Blackburn, and C. White, High-strength biodegradable poly(vinyl alcohol)/fly ash composite films, Journal of Applied Polymer Science 117 (1) (2010) 114-121.

90. D. C. D. Nath, S. Bandyopadhyay, J. Campbell, A. Yu, D. Blackburn, and C. White, Surface-coated fly ash reinforced biodegradable poly(vinyl alcohol) composite films: part 2-analysis and characterization, Applied Surface Science 257 (4) (2010) 1216–1221.

91. D. C. D. Nath and V. Sahajwalla, Growth mechanism of carbon nanotubes produced by pyrolysis of a composite film of poly (vinyl alcohol) and fly ash," Applied Physics A 104 (2) (2011) 539–544.

92. V. S. K. Yadav and M. K. Purkait, Electrochemical studies for CO_2 reduction using synthesized Co_3O_4 (Anode) and Cu_2O (Cathode) as electrocatalysts, Energy Fuels 29 (2015) 6670−6677.

93. M. Herrero, P. Benito, F. M. Labajos, and V. Rives, Nanosize cobalt oxide-containing catalysts obtained through microwave-assisted methods, Catalysis Today 128 (2007) 129–137.

94. H. Jing, T. Wen, C. Fan, G. Gao, S. Zhong, and A. Xu, Efficient adsorption/photodegradation of organic pollutants from aqueous systems using Cu_2O nanocrystals as a novel integrated photocatalytic adsorbent, Journal of Material Chemistry A 2 (2014) 14563–14570.

95. H. C. Bidsorkhi, H. Riazi, D. Emadzadeh, M. Ghanbari, T. Matsuura, W. J. Lau, and A. F. Ismail, Preparation and characterization of a novel highly hydrophilic and antifouling polysulfone/nanoporous TiO_2 nanocomposite membrane, Nanotechnology 27 (41) (2016) 415706.

96. H. Wu, J. Mansouri, and V. Chen, Silica nanoparticles as carriers of antifouling ligands for PVDF ultrafiltration membranes, Journal of Membrane Science 433 (2013) 135−151.

97. L. Jiansheng, W. Lianjun, H. Yanxia, L. Xiaodong, and S. Xiuyun, Preparation and characterization of Al2O3 hollow fiber membranes, Journal of Membrane Science 256 (2005) 1−6.

98. V. Vatanpour, S. S. Madaeni, R. Moradian, S. Zinadini, and B. Astinchap, Fabrication and characterization of novel antifouling nanofiltration membrane prepared from oxidized multiwalled carbon nanotube/polyethersulfone nanocomposite, Journal of Membrane Science 375 (2011) 284−294.

99. M. Zahmakıran, S. Özkar, T. Kodaira, and T. Shiomi, A novel, simple, organic free preparation and characterization of water dispersible photoluminescent Cu_2O nanocubes, Materials Letters 63 (2009) 400–402.

100. D. Rana and T. Matsuura, Surface modifications for antifouling membranes, Chemical Reviews 110 (2010) 2448–2471.

101. Q. Li, Q. Bi, H. Lin, L. Bian, and X. Wang, A novel ultrafiltration (UF) membrane with controllable selectivity for protein separation, Journal of Membrane Science 427 (2013) 155–167.

102. J. Madhavan, F. Grieser, and M. A. Kumar, Combined advanced oxidation processes for the synergistic degradation of ibuprofen in aqueous environments, Journal of Hazardous Materials 178 (2010) 202–208.

103. F. Li, Y. Kang, M. Chen, G. Liu, W. Lv, K. Yao, P. Chen, and H. Huang, Photocatalytic degradation and removal mechanism of ibuprofen via monoclinic $BiVO_4$ under simulated solar light, Chemosphere 150 (2016) 139–144.

104. K. K. Paul, R. Ghosh, and P. K. Giri, Mechanism of strong visible light photocatalysis by Ag_2O-nanoparticledecorated monoclinic TiO_2(B) porous nanorods, Nanotechnology 27 (2016) 315703.

105. R. M. Silverstein and F.X. Webster, Spectrometric identification of organic compounds, 6th edition, John Wiley & Sons, Inc. Canada, 1998.

106. M. K. Sinha and M. K. Purkait, Preparation of a novel thermo responsive PSF membrane, with cross linked PVCL-co-PSF copolymer for protein separation and easy cleaning, RSC Advances 5 (2015) 22609–22619.

107. Robert J. Hunter, Zeta potential in colloid science, first edition, Academic Press, London, 1981.

108. Q. Wei, J. Li, B. Qian, B. Fang, and C. Zhao, Preparation, characterization and application of functional polyethersulfone membranes blended with poly(acrylic acid) gels, Journal of Membrane Science 337 (2009) 266–273.

109. A. Pich, A. Tessier, V. Boyko, Y. Lu, and H. P. Adler, Synthesis and characterization of poly (n-vinylcaprolactam) -based microgels exhibiting temperature and ph-sensitive properties, Macromolecules 39 (2006) 7701–7707.

Appendix

A. Error analysis

The errors in experimentally measured quantities and in parameters calculated from those measurements are important in that they determine the accuracy of calculation and predictions using those quantities. There are two types of errors viz. systematic error and random error. Systematic errors are the results of faulty assumptions or improper experimental measuring techniques. In this work, care was taken in eliminating systematic errors by appropriately designing the experiments and adopting qualified methods for analysis of the data. On the other hand, random errors result from variation in the precision of measuring parameters and the slight variations that occur in successive measurements made by the same observer under nearly identical conditions. Random errors cannot be eliminated. The focus of the error analysis presented in this section is on the random errors.

In most of the experiments performed in this work, the quantities that are measured directly are concentrations and permeate flow rates which are used to determine the rejection (%) and permeate flux respectively.

A.1. Error in measurement of BSA concentration in permeate

BSA concentration in the aqueous phase was determined by measuring the absorbance value at a specific wavelength in the UV-Vis spectrophotometer. A calibration curve was prepared by taking the absorbance values against the corresponding known values of concentrations of BSA as discussed in section 2.3.8 of Chapter 2. From Fig. 2.3, which is the calibration curve between absorbance and concentration of BSA, it is seen that the standard deviation of the predicted value from actual value of concentration is 0.9995. Thus, every measurement of BSA concentration in permeation is associated with an error of 0.05 % whose effect on rejection values of BSA can be ignored.

A.2. Error in the measurement of permeate flux

The errors in the values of permeate flux are related to the errors in the measurements used to calculate those values. In this section, statistical analysis is used for estimation of the uncertainty associated with the values of permeate flux. Determination of standard deviation is generally considered to be one of the best methods to estimate the uncertainty which is based on the following method:

If u_1, u_2, ..., u_N are the N results of the measurements of a particular quantity u, then the mean value of u (i.e. $\bar{u}$), is defined by

$$\bar{u} = \frac{u_1 + u_2 + ... + u_N}{N} = \frac{1}{N}\sum_{i=1}^{N} u_i \qquad \text{(A.1)}$$

The uncertainty in the result is usually expressed as "root-mean-squared-deviation", which is denoted as Δu, which is computed using the following Eq. (A.2):

$$\Delta u = \sqrt{\frac{(u_1 - \bar{u})^2 + (u_2 - \bar{u})^2 + ... + (u_N - \bar{u})^2}{N-1}} \qquad \text{(A.2)}$$

In the present work, all the membranes were cleaned thoroughly following each experiment. Besides, before each experiment, performance of all the membranes were checked through pure water flux (PWF) measurement; hence uncertainties involved in the PWF measurements are reported here.

The uncertainties involved in different experimental measurements for (PWF) for membranes P1, P2 and P3 are estimated and shown in Table A.1.

Table A.1. Values of uncertainties estimated in PWF measurements for membranes P1, P2 and P3.

Membranes	Run 1	Run 2	Run 3	$\bar{u}$	Δu	Uncertainties (%)
P1	468.59	472.24	465.56	468.79	9.34	1.99
P2	748.45	750.5	746.96	749.97	19.81	2.64
P3	927.27	930.54	925.65	929.82	19.57	2.10